MICRO ELECTRET POWER GENERATORS

Thesis by

Justin Boland

In Partial Fulfillment of the Requirements

for the Degree of

Doctor of Philosophy

CALIFORNIA INSTITUTE OF TECHNOLOGY

Pasadena, California

2005

(Defended May 24, 2005)

ACKNOWLEDGEMENTS

I've been fortunate enough to be at the right place at the right time with enough preparation to make more accomplishments than I have time for writing this thesis. The experience has been invaluable to me, and I gained more than I thought possible. I am eternally grateful to Yu-Chong Tai, the Caltech Micromachining Laboratory and the California Institute of Technology for my time here.

Dedication:

For my wife, the first Dr. Boland. So few of our family and friends really understand why we like this stuff and what it is we actually do. No, I am not in school to be an electrician and my wife is not a mechanic!

ABSTRACT

Micro Electret Power Generators

The taming of electricity and its widespread use allows people to see in the dark, to speak to one another instantaneously across the earth, and it allows retrieval of data from instruments sent out of the solar system. It is right to expect that the uses and demand for electricity will continue to grow, and to extend the ability to generate electricity; here two new micromachined devices for converting mechanical energy into electrical energy are presented. Aided by the wealth of micromachining process technology, generators that use an oscillatory motion to modify the physical structure of a capacitor with a built-in electric field provided by a permanent electret have been designed, built, and tested. The electret creates an electric field inside the capacitor structure, which induces mirror charge at some potential. The modification of the capacitor then generates an alternating displacement current through an external circuit, which provides useful electrical power. The electret microphone is a similar well known device for converting pressure waves into electrical signals by varying the distance between two charged capacitive plates. This work explores and proves feasible the ability to use mechanical forces to change the overlapping area of a charged capacitor structure and using mechanical forces to move a liquid into the gap of a charged capacitor structure, changing its permittivity to produce electricity. This work demonstrates 2.5mW of power from a 2cm diameter rotary generator at 12kRPM and 10μw for a 0.1cm^3 linear shaking generator at 60Hz.

TABLE OF CONTENTS

TABLE OF FIGURES

TABLE OF TABLES

CHAPTER 1

I. INTRODUCTION

I came to the California Institute of Technolgy for the purpose of applying my background in physics to real world problems, or as I put it in my statement of purpose on my application, "I want to build cool stuff." I think this thesis is true to that purpose.

I.1. SCOPE OF THESIS

The central focus of this work is the generation of electricity using mechanical forces in combination with permanent electrostatic fields. Electric fields provide a powerful force for doing work, which is inversely proportional to the square of the distance between charged particles. To take advantage of this large force, electrostatic devices must be made with high precision and small dimensions. A wealth of technological knowledge for producing high-precision, micro-scale, electrical and mechanical system exists in the field of micromachining. The work in this thesis was performed in the Caltech Micromachining Laboratory, which provides micromachining equipment and process technology expertise necessary to build small electrostatic devices to generate electricity.

This thesis describes the design, fabrication, and testing of devices which utilize an oscillatory motion to modify the physical structure of a capacitor with a built-in electric field provided by a permanent electret. An electret is used as the source of an electric field inside the capacitor structure, which induces mirror charge at some potential difference on the capacitive plates. The modification of the capacitor then generates an

alternating displacement current through an external circuit, which provides useful electrical power.

Two mechanisms are explored and proven feasible to produce electricity from an electrostatic field in two new power generating devices. First, a device is build that uses a rotational torque to modify the overlapping area of a charged capacitor structure. Second, a vibrational mechanical force is used to shake a fixed capacitor structure that contains an air gap and liquid that can flow into and out of the air gap, which changes the strength of an electric field within the charged capacitor structure. This thesis demonstrates 2.5mW of power generated from a 2cm diameter rotary generator at 12kRPM and 10μw for a 0.1cm^3 linear shaking generator at 60Hz.

I.1.a. ORGANIZATION

This thesis is divided into five chapters: Introduction, Electrets, Variable Area Rotational Electret Power Generator, Liquid Rotor Electret Power Generator, and Conclusions and Future Work.

The Introduction compares electrical power generation techniques. This chapter introduces the concept of "energy harvesting," can be a viable method for providing electrical energy to remote and portable applications. Concise arguments are made for electrostatic power generators, which rely on the phenomenon of "displacement current." Micro electromechanical systems are explained as an invaluable tool for pursuing electrostatic power generators. Finally the source of funding is explained to give context

to the development project followed by the delineation of duties. Although this project is funded as part of a power generation system, the generators described are separate and complete systems worthy of an entire thesis.

Chapter 2 explains "electrets", which provide the electric field used to generate electricity in the generators presented. This chapter provides examples of electret fabrication, as well as the specific micromachining technology used in this work and the unique electron implantation system used in the Caltech Micromachining Laboratory. Measurement techniques used to characterize the electret are then explained. Finally, electrets produced for this work are analyzed, and a new fabrication method for producing superior uniformity is explained and characterized.

Chapter 3 covers the world's first micromachined rotary electret power generator (REPG). Background information is given that sets the stage for applying micromachining techniques to produce the REPG. New theory is development to address the design of this new device. Design and fabrication of several versions of the device are presented as well as the experimental results.

Chapter 4 encompasses the world's first liquid-rotor electret power generator (LEPG). This device originated out of the necessity to improve gap control for a REPG device when proposed liquid bearings were argued against due to their effect on the electric field of the REPG. Simple theory exists for insertion of a dielectric into the gap of a capacitor, but a theoretical model had to be developed to cover the dynamics involved in the use of a system that can be used for power generation. This theory is then used to design and

fabricate LEPG devices. LEPG devices are tested over a wide range of variables, as well as parallel and serial combinations of devices and some non-obvious electrical connections that prove advantageous.

Chapter 5 summarizes the contributions of this work and proposes some future work using the insight gained during this course of study. As with any new area of exploration, a great deal of knowledge is learned but much more awaits the eager researchers who follow.

I.1.b. PROBLEM STATEMENT

It is commonly accepted that the uses and demand for electricity will continue to grow and that new sources of electricity are important to the future of human technological progress. To answer the growing need for electricity, this thesis describes new work in the field of generating electricity from mechanical motion by presenting two novel micromachined power generators.

I.2. ELECTRICITY

Of the four fundamental forces of nature: strong force, electromagnetic force, weak force and gravitational force, the electromagnetic force is the best understood. The origin of the electric force is the negatively charged elementary particle, the electron, which exerts an attractive force towards positively charged protons and a repulsive force towards other negatively charged electrons. Since all stable matter is made of these elementary particles, the electric force dominates most observed interactions between materials.

The magnetic force is a consequence of electrical charge in motion, and consequently the electromagnetic force is simply a unified theory for explaining the physical interactions of electricity and magnetism.

Electric and electricity are the general term associated with stationary and moving electric charges. In the past two centuries, humans have become especially adept at moving electrical charges.

I.2.a. GENERATING ELECTRICITY

Electricity, being the flow of electrical charge, can be a consequence of human action. The first documented case of man made electricity dates back to the ancient Greeks, who witnessed electrical force as a result transferred electrons from rubbing amber. The word electron is thus derived from the Greek word "elektron" meaning amber.

From the writings of Thales of Miletus it appears that Westerners knew as long ago as 600 B.C. that amber becomes charged by rubbing. There was little real progress until the English scientist William Gilbert in 1600 described the electrification of many substances and coined the term electricity from the Greek word for amber. As a result, Gilbert is called the father of modern electricity. In 1660 Otto von Guericke invented a crude machine for producing static electricity. It was a ball of sulfur, rotated by a crank with one hand and rubbed with the other. Successors, such as Francis Hauksbee, made improvements that provided experimenters with a ready source of static electricity. Today's highly developed descendant of these early machines is the Van de Graaf generator, which is sometimes used as a particle accelerator. Robert Boyle realized that attraction and repulsion were mutual and that electric force was transmitted through a vacuum (c.1675). Stephen Gray distinguished between conductors and nonconductors (1729). C. F. Du Fay recognized two kinds of electricity, which Benjamin Franklin and Ebenezer Kinnersley of Philadelphia later named positive and negative.

Insert I-1. Brief history of electricity [1-4]

Remarkable advances in human understanding of electricity began occurring in the 18th century around the time Benjamin Franklin harnessed lightning, which is simply the discharge from triboelectrically generated charge in clouds. Leyden jars were used to show capture of electricity. Work by Ampere, Maxwell, and others have led to well understood laws of electricity that were used to develop electromagnetic power generators (electrostatic power generators already existed). Edison pioneered a generation and distribution system along with greatly improved light bulbs, which cemented the need for electricity in the home.

I.2.a.i. TRIBOELECTRICITY

The generation of electricity from rubbing two dissimilar things together is known as "triboelectricity," which is the first source of man-made electricity. Everyone has seen examples of triboelectricity in the form of lightning, which is caused by charge transfer between air and water. Children generate triboelectricity by dragging their shoes on carpet to build up a charge that allows them to shock a friend. This method of generating electricity is simply the conversion of mechanical energy to electrical energy through friction. This motion causes electrons to be transferred from one material to another, causing an excess of electrons on one material and a deficiency of electrons on the other.

While this is the oldest form of electricity, it is still the least understood. Modern theses on triboelectricity still fail to lead to reliable laws that can quantify or predict the outcome of a triboelectric event. The unpredictability of triboelectricity prevents it from being widely used as a source for electrical energy.

I.2.a.ii. PHOTOVOLTAIC GENERATION

In 1906, Albert Einstein published one specific paper on the photoelectric effect that later won him the Nobel prize in physics. The photoelectric effect theory unifies the observations that light acts as wave and also as particle. This theory explains the mechanism by which light generates electrons on the surface of metals. Later, this same effect would be used to convert light into useful amounts of electricity for use in calculators, street signs, and even remotely piloted Mars exploration vehicles. Using the

energy from the sunshine or indoor lighting as a power source is a convenient way to generate electrical power.

I.2.a.iii. CHEMICAL GENERATION

The battery is probably the most recognized device for producing electrical energy. The battery is a chemical system that generates electricity as the byproduct of a chemical reaction. Chemical generation of electricity is limited to the quantity of chemicals in a system, but is well known as an effective method to store a large amount of useful energy in a small, portable space that can easily be converted to electrical energy.

I.2.a.iv. ELECTROMAGNETIC GENERATION

Thomas Edison and George Westinghouse are responsible for bringing large quantities of electrical energy into the homes and businesses of the world, which was accomplished by a complicated distribution system and simple electromagnetic power generators. These machines are optimized to exploit the electromotive force generated by a changing magnetic field on a wire, an effect first documented by André Marie Ampère. The typical electromagnetic power generator converts rotational mechanical energy, which can be supplied by chemical-mechanical energy in the case of a combustion-vehicle, thermal-mechanical energy in the case of wind driven a turbine, human-mechanical in the case of a generator mounted to a bicycle wheel, or gravity fed as in the case of hydroelectric dams. While effective and well understood, electromagnetic power

generators do not scale well to very small dimensions due to the need for many coils of wire and the difficulty in maintaining strong magnetic dipoles in small magnets.

I.2.a.v. ELECTROSTATIC GENERATION

Electrical power generation is the production of a useful electrical current at some voltage. Typically, AC current is produced via a varying magnetic field and collecting electrical current from loops of wire. Electrical current can also be generated by a chemical reaction, photoelectric effect, triboelectric effect, quantum-thermal effect, or in the case of this work by the influence of a purely electric field.

	Electromagnetic	Electrostatic induction	Electret	Variable capacitance
Fabrication	Micro coil & permanent magnet	Simple	Simple	Simple
External circuit	None	High-frequency circuit	None	Voltage source
Voltage	∝ speed	Constant	~ Constant	Constant
Current	∝ speed	∝ speed	∝ speed	∝ speed
Power	∝ speed^2	∝ speed	∝ speed	∝ speed
Working temperature	< Curie point	-	< Glass transition temperature	-
Note	Large rotational speed required	MIT μGT		Low efficiency

Table I-2. Comparisons of power conversion techniques.

Common alternating current (AC) found in private homes and public buildings provided by national power grids is used for operating all manner of electrical devices, the most

common being lights and motors. Machines waste kinetic energy in the form of vibration. AC electricity commonly has a frequency of 60 Hz. When a motor is operated at 60 Hz it will inevitably produce vibrations at this drive frequency and multiples of the drive frequency. Figure I-1 describes the measured vibrations of a simple microwave oven with a fundamental mode around 120Hz and roughly a $\frac{1}{\omega^2}$ displacement[5]. The obvious question, then, is "can wasted vibrations be reclaimed for some other use?"
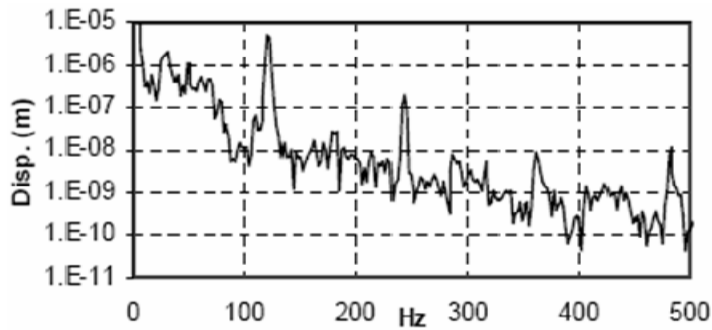
Figure I-1 Measured vibrations from a microwave oven

I.2.b. ALTERNATIVE ENERGY

Since the majority of grid electricity is generated by electromagnetic generators through burning of fossil fuels, any other power generation technique is considered "alternative energy". Harnessing the light, wind, flowing water, thermal gradients, and renewable fuels to produce electricity are all example of alternative energy. Likewise, these sources are all renewable since they all can be replenished on a timescale that is short compared to a human lifespan. Interestingly, all of these sources are derived from the energy released from nuclear fusion within the sun.

A form of alternative energy that is not renewable is nuclear fission since the source of this energy, radioactive elements, are changed in a physical manner that is not feasibly reversible within a human lifespan.

I.2.b.i. PORTABLE ALTERNATIVE ENERGY

Since chemical cell batteries are the standard for portable electricity, there is an analog to alternative energy that is called "portable alternative energy." The major disadvantage of alkaline and other non-rechargeable batteries is that they cannot be made to contain more energy without industrial reprocessing. Rechargeable batteries require connection to an energy source to regain their power, and they have a limited number of cycles before the chemistry degrades to the point where industrial reprocessing is also necessary. Batteries are useful because of their large energy density, but they require maintenance.

Demand for power supplies used in portable products in the United State is projected to increase 6.1 percent annually to $10.3 billion in 2008. Batteries are the standard technology for providing portable power, but they have limited lifetimes. The amount of batteries being disposed of in landfills became so great that in 1996 President Clinton signed into law the Mercury-Containing and Rechargeable Battery Management Act in an effort to reduce the toxicity of landfills and incinerator ash that is caused by the heavy metals found in batteries [6]. This act significantly contributes to the recycling of batteries, but it has not curbed the dependence on chemical cells for portable energy. Re-usable batteries all suffer from limitations that prevent them from being cheaper and/or more effective.

Comment [JSB1]: Finish reference

In contrast, solar cells used in calculators and watches provide energy by converting an external energy source, the sun or indoor lighting, to electrical power. Furthermore, solar cells do not degrade noticeably over the lifetime of the device. This alternative approach to providing portable electrical power can eliminate the dependence on batteries and maintenance, which has allowed for new applications, like earth-orbiting satellites, that would not otherwise be possible with chemical cell batteries.

Other small devices can produce electrical energy from kinetic energy from an external source, such as human motion. One example is the Kinetic series of watches by Seiko, which store human motion as electrical energy in a capacitor. This solution eliminates the need for chemical cells and allows for a watch that can run for an indefinite amount of time.

I.3. ENERGY HARVESTING

"Energy Harvesting" is the term used to describe converting wasted ambient energy into useable electrical energy. For example, bridges vibrate as vehicles travel over them, and those vibrations have kinetic energy that could be used for generating electricity. An energy harvester might convert enough of the vibration into electricity to operate a sensor and wireless node to monitor the temperature, stress, or humidity on the bridge and relay the information to listening posts for analysis.

Energy harvesters promote innovation by eliminating conventional power supplies. Devices that convert the vibrations to usable electricity would allow new applications, such as "set and forget" remote sensors that rarely or never need maintenance. Networks of sensors can be dispersed to monitor an area, such as "Smart Dust" [7, 8].

Natural sources of energy are ubiquitous. Solar energy, gravitational energy in the form of ocean waves and hydroelectric dams, and wind energy are already being harvested to produce electricity.
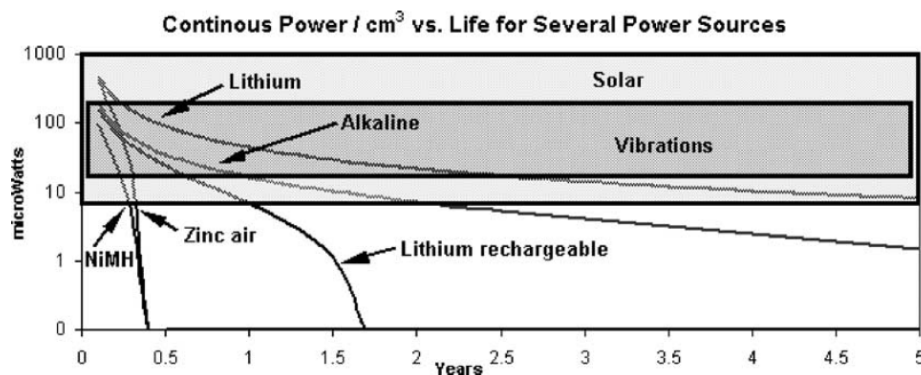
Figure I-2 Electrical power delivered over time from various sources [5].

Harvesting applications must receive some input energy from the environment. Assuming the environmental energy is relatively constant, Figure I-2 clearly shows the advantages of energy harvesting over time. Both solar energy (indoors and outside) and vibrational energy in the environment may fluctuate within the gray ranges shown in Figure I-2, but they never cease as a source of environmental energy.

The growing field of "energy harvesting" is finding, converting, and utilizing small amounts of energy that ordinarily go unnoticed and unexploited. Energy harvesting is the act of taking wasted ambient energy and converting it useful electrical power. Devices that accomplish this are called "energy harvesters" or "power scavengers." One common example of this is the solar powered calculator.

I.3.a. ENERGY HARVESTING METHODS

Power Density ($\mu W/cm^3$)	Over one year	Over 10 years	Over 100 years
Solar* (Direct Sun)	10000	10000	10000
Solar* (indoor)	6	6	6
Thermoelectric(DT=10°C)	15	15	15
Vibration (Piezoelectric)	100	100	100
Vibration (Electrostatic)	50	50	50
Vibration (Electret)	1000	1000	1000
Biomotion Energy (inside shoe)	330	330	330
Batteries (Lithium)	45	4.5	0.45
Hydrocarbon (micro heat engine)	330	33	3.3
Fuel Cells (Methanol, theoretical)	280	28	2.8

Table I-3. Power density of various electrical power generators.

* Flux density measured in ($\mu W/cm2$)

As can be seen in Table I-3, energy can be captured from the environment and does not need to be stored in chemical form. When compared with Figure I-2, it is obvious that stored energy is insufficient for devices that are designed to operate independently over long periods of time. The solar power figure is for irradiance, which is the amount of light energy incident on a surface per time.

Power source	$(\mu W)/cm^3$	$(Joules)/cm^3$	$(\mu W)/cm^3/yr$	Storage needed?	Regulation?	Available?
Primary battery	N/A	2,880	90	No	No	Yes
Secondary battery	N/A	1,080	34	N/A	No	Yes
Micro fuel cell	N/A	3,500	110	Maybe	Maybe	No
Ultracapacitor	N/A	50–100	1.6–3.2	No	Yes	Yes
Heat engine	1×10^6	3,346	106	Yes	Yes	No
Radioactive (63Ni)	0.52	1,640	0.52	Yes	Yes	No
Solar (outside)	15,000*	N/A	N/A	Usually	Maybe	Yes
Solar (inside)	10*	N/A	N/A	Usually	Maybe	Yes
Temperature	40*†	N/A	N/A	Usually	Maybe	Soon
Human power	330	N/A	N/A	Yes	Yes	No
Air flow	380‡	N/A	N/A	Yes	Yes	No
Pressure variation	17§	N/A	N/A	Yes	Yes	No
Vibrations	375	N/A	N/A	Yes	Yes	No
LEPG	100	N/A	N/A	Yes	Yes	No

* Measured in power per square centimeter, rather than power per cubic centimeter.

† Demonstrated from a 5ºC temperature differential.

‡ Assumes an air velocity of 5 m/s and 5% conversion efficiency.

§ Based *on* 1 cm³ closed volume of helium undergoing a 10ºC change once a day.

Table I-4. Survey of power sources [9, 10]

The advantages of using stored chemical energy is that the power available is well known and the power density is much larger than a power harvesting solution, as can be seen in Table I-4. A primary battery with an energy density of 2,880 Joules/cm3 can deliver power up to Watt range for a few seconds, while the energy scavengers can only deliver as much power as they can convert during that time, which is in the microwatt range. The disparities between power density and energy density drive the development of chemical cells toward greater lifetime and energy harvesters towards greater power delivery.

I.3.b. SURVEY OF KINETIC ENERGY HARVESTING DEVICES

Preceding this work are many examples of energy harvesting devices. Many of these devices are built using micromachining tools, while other devices are just small. The physical principles that govern each device are very different, and now the scope will be narrowed to better explore the area of interest. Specifically, the focus of this thesis is on converting raw kinetic energy into electrical energy.

I.3.b.i. ALTERNATIVE DEFINITION: POWER SCAVENGING

Power scavenging is the art of harvesting small amounts of energy from the local environment without significantly affecting the original environment. Power scavengers are a subset of energy harvesters where the available ambient energy converted is small compared to the total energy available so that the presence of the device is not noticed. The distinction of a device being a "power scavenger" becomes relevant depending on the end application.

One example of a power scavenger is a kinetic energy harvester mounted in a wristwatch. The addition of a power scavenger to the wristwatch should not require any changes to the original environment (how much someone shakes their wrist) in order for the harvester to operate properly. The harvester must also have small mass and volume such that its presence can go unnoticed. With these expectations, it is obvious that the harvester is not expected to convert all or even most of the available energy to electrical power because doing so would interfere with the ability to move the wrist.

I.3.b.ii. FIGURES OF MERIT

Energy conversion devices convert one form of energy to another, and the typical measure of the success of the device is the efficiency: the ratio of the output power to the input power. The second law of thermodynamics can be used to prove that the output power can never be greater than the input power, thus efficiency is always 100% or less. For any device that delivers electricity, the first metric used to characterize it is efficiency.

However, for power scavenging devices the input energy is much less than the available energy. The measure of efficiency ignores the requirements placed on the design of power scavengers, namely that the volume and mass of the generator must be minimized for the scavenger to be an attractive power solution. That is why the most important measure that is used in comparing power scavenger devices is the power output divided by the volume of the generator, or the power density.

I.3.b.ii.1. Linear Energy Harvesters

For linear power generators, much work has been published exploring the ability of different types of power generators to harvest energy from an input force. Typically, linear electromagnetic power generators operate in a resonance mode that is referred to as a velocity-damped resonant-generator (VDRG). Linear electrostatic power generators typically operate in either a nonlinear, coulomb-force parametric-generator (CFPG) mode or a coulomb-damped resonant-generator (CDRG) mode. Generator architectures do not

have operational maximums at the same frequency, volume, mass, or acceleration, which makes comparing them difficult.

For vibration driven power generators, power output has been shown to scale in proportion to the source motion amplitude (Y_0), the driving frequency (ω), and the mass of the device (m) [11-13]. This is not surprising because the kinetic energy (KE) of any resonant system is

$$KE = \frac{1}{2}m\left(Y_0\omega\cos(\omega t)\right)^2 \tag{I.1}$$

while power P is the rate of energy, which is proportional to

$$P \propto Y_0^{\,2}\ \omega^3\ m \tag{I.2}$$

Mitcheson et al shows that it is reasonable to normalize the theoretical power output by the factor in Equation (I.2) for each of the three different types of generator architectures. They plot the normalized power output for the VDRG, CDRG, and CFPG for various normalized amplitudes and driving frequencies, as can be seen in Figure I-3.

Term	Definition	Significance
VDRG	Velocity Damped Resonant Generator	Resonant structure, magnetic field based
CDRG	Coulomb Damped Resonant Generator	Resonant structure, electrostatic based
CFPG	Coulomb Force Parametric Generator	Non-resonant structure, electrostatic based
Y_0	Drive amplitude	It is possible for the structural frame of the generator to move a large distance while the internal portion has little or no relative motion to the frame
Z_l	Maximum internal displacement	The moving element inside the generator has limited motion relative to the structural frame of the generator
ω	Drive frequency	Frequency of oscillation/rotation
ω_n	Resonant frequency	Frequency at which a fixed energy input produces maximum internal displacement
ω_c	ω/ω_n	Ratio of the drive frequency to the resonant frequency. Can be greater or less than 1
m	mass	Total mass of the generator including the frame and the moving portion
P_{LEH}	Power from a LEH device	LEH power is derived from vibrations/impacts
P_{REH}	Power from a REH device	REH power is derived from rotation
N_{LEH}	Figure of merit for a LEH device	$N_{LEH} = \dfrac{P_{LEH}}{Y_0^2 \ \omega^3 \ m \ V}$
N_{REH}	Figure of merit for a REH device	$N_{REH} = \dfrac{P_{REH}}{f^2 \ V}$

Table I-5 Power conversion definitions
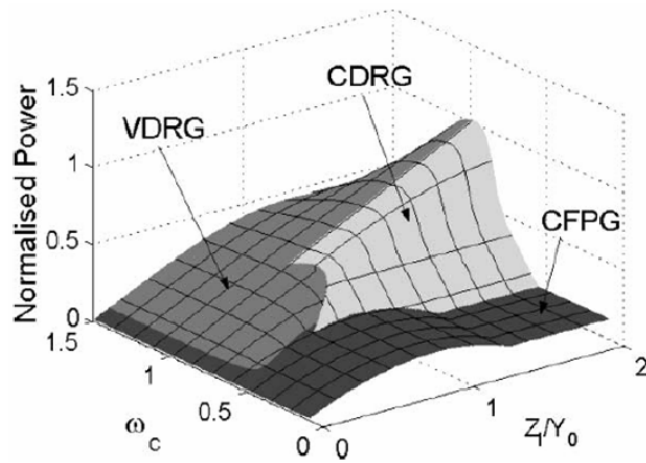
Figure I-3 Generator architecture comparison

Figure I-3 shows the relative strengths and weaknesses of each architecture where ω_c is the ratio of the driving frequency (ω) divided by resonant frequency (ω_n) and Z_l/Y_0 is the ratio of the maximum displacement of the moving element inside the generator with respect to the frame of the generator (Z_l) divided by the drive amplitude (Y_0). It should be noted that both resonant cases are equally efficient at the resonant frequency of the device, while the parametric-generator (CFPG) is best suited for frequencies much below the resonant frequency of the device. Figure I-3 also shows that the CFPG dominates at low Z_l/Y_0 ratios. For power scavenging devices mounted in applications where the driving frequency is not fixed and the drive amplitude is large, as in the case for a wristwatch, the best choice is obviously a CFPG.

In order to compare various linear vibrational energy harvesters on a consistent scale, a new figure of merit is defined that normalizes the output power by the quantity in Equation (I.2) and also divides by the device volume V since this is parameter is relevant to the utility of a power generator. The units of this figure of merit are $\dfrac{1}{Volume}$ or cc^{-1}, where 1cc is roughly the volume of a sugar cube. Thus, linear energy harvesters (LEH) can be compared with the following figure of merit (N_{LEH})

$$N_{LEH} = \frac{P_{LEH}}{Y_0^2\ \omega^3\ m\ V} \tag{I.3}$$

This figure of merit is proportional to the efficiency of the device divided by the volume. It applies to resonant and non-resonant linear energy harvesters alike.

I.3.b.ii.2. Rotational Energy Harvesters

For rotary power generators used as power scavengers, the driving force is also much larger than the kinetic energy converted to electrical power. Seiko's Kinetic power generator uses a counterweight to convert planar shaking motions to rotation. While the same metrics as above could be applied to describe the merits of the generator, it is more convenient to define a figure of merit where the power produced (P_{REH}) is divided by rotational speed squared (f^2) at which it is produced. Power output on a fixed load resistance scales as the square of the speed when the load resistance is less than the load-matched resistance, which is the typical mode of operation when the load resistance is fixed. Again, since these devices are meant to fit into tiny applications, it is also necessary to divide the power generated by the volume of the generator. This is a fair evaluation as long as the driving power remains significantly larger than the power harvested. For rotational energy harvesters (REH)

$$N_{REH} = \frac{P_{REH}}{f^2 \, V} \tag{I.4}$$

The units of this figure of merit are $\dfrac{Power}{Frequency^2 \cdot Volume}$, or more $\mu W \; Hz^{-2} \; cc^{-1}$ which is more appropriate for miniature power generators.

I.3.b.iii. ROTARY ELECTROMAGNETIC POWER GENERATORS

Seiko sells roughly one million watches in its Kinetic series (2001), which are watches that harness kinetic energy to power a watch for humans moving in their environment.

They have developed a tiny electromagnetic generator, using the same physical principles

of large-scale generators.
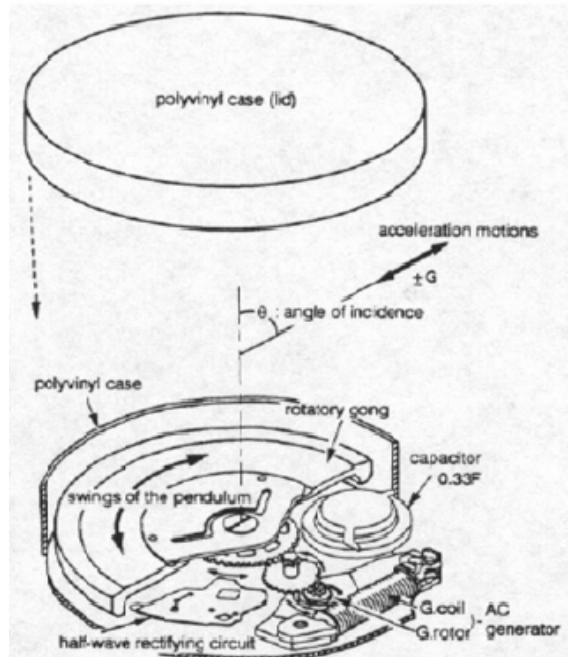
Figure I-4 Diagram of Seiko's Kinetic line of energy harvesting watches.

A bottom view of the watch innards in Figure I-4 shows the rotating pendulum that the

watch encounters.   When the Seiko watch is worn on the wrist, it experiences

accelerations that drive the pendulum, which spins a magnet in a coil via a 1:100 gearing

ratio. This magnet causes alternating magnetic fields to be incident on the generator coil,

which produces an alternating current at low voltage. This current is rectified so it can be

stored on the 0.33 farad capacitor, which is the energy reservoir for the timekeeping

mechanism.
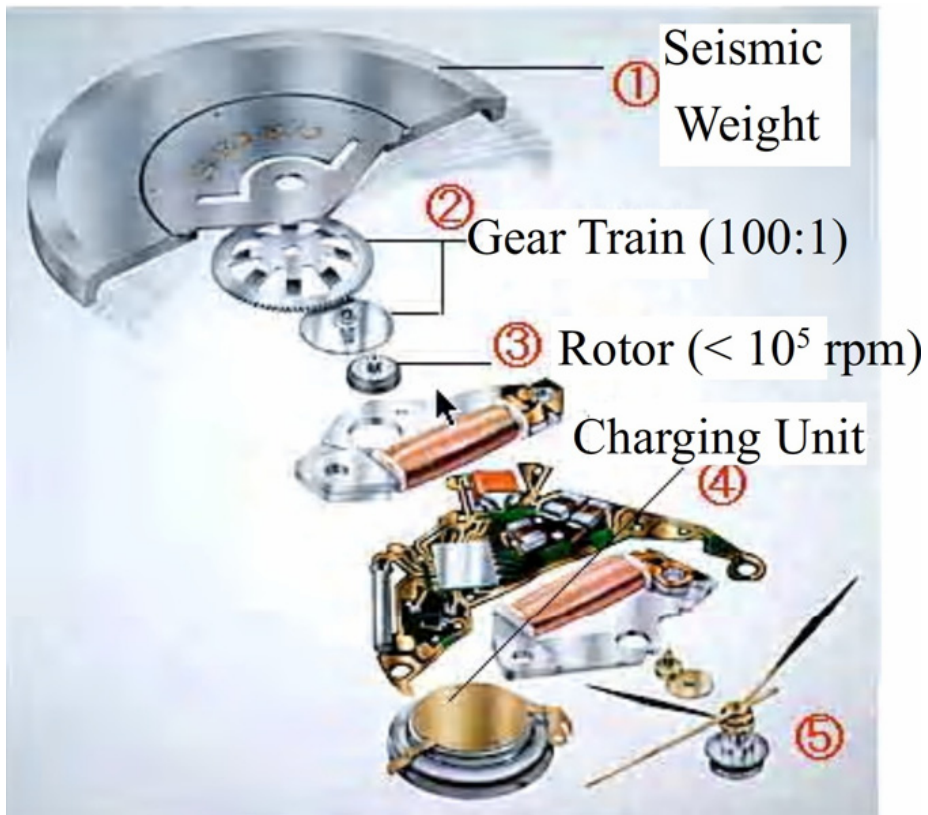
Figure I-5 Exploded Diagram of Seiko's Kinetic line of energy harvesting watches.

The exploded view of Figure I-5 allows the gearing mechanism to be seen clearly, as well as the other systems in the watch. Special care is taken to ensure that the system is optimized, and the end result is a portable, energy harvesting device with a great deal of utility. Seiko claims to produce up to 40μW with this generator.
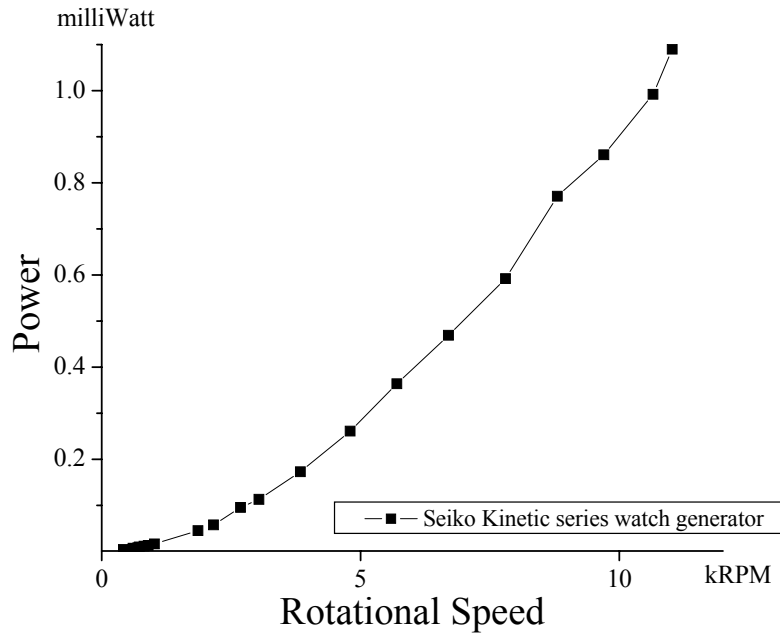
Figure I-6 Lab test of Seiko's Kinetic generator. Speed corresponds to the
relative rotation of the magnet to the coil.

The plot in Figure I-6 shows the RMS power generated by a Seiko generator across a
327Ω load resistor. For the experiment, the gears from the assembly were removed and
the magnet rotor (#3 in Figure I-5) was driven in place directly by an external motor from
600RPM to 11,000RPM. Speed was measured with a stroboscope, while voltage across
the load resistor was measured with a Fluke true RMS multimeter. This test measured
the production of 45μW at 30Hz. The volume the generator occupies is difficult to
measure. Using only the magnet and the coil as the generator volume, the volume is
approximately   1cc.   Then,   the   figure   of   merit   for   the   generator   is
$N_{REH} = 0.05 \ \mu W \ Hz^{-2} \ cc^{-1}$. The low power produced at low speeds is inherent in rotary
electromagnetic generators due to winding losses and internal inductance.

I.3.b.iv. LINEAR ELECTROMAGNETIC POWER GENERATORS

Since MEMS allows for easy design of planar structures, it is no surprise that linear electromagnetic power generators have been well explored. [12, 14]
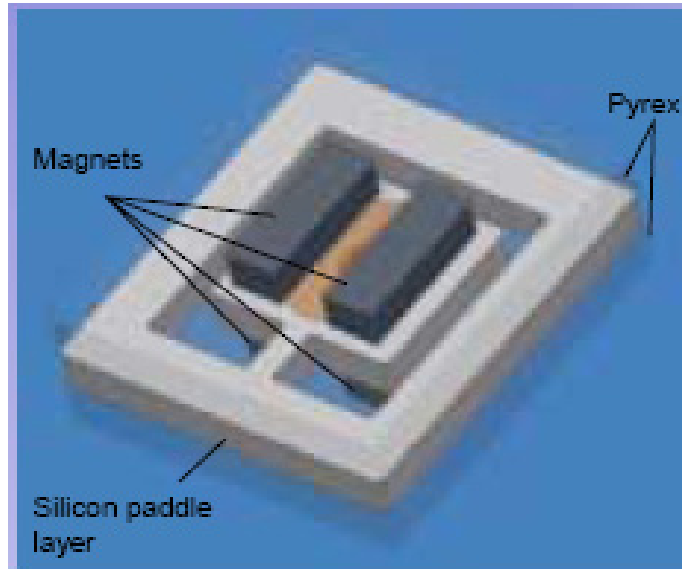
Figure I-7 Linear electromagnetic power generator developed by Perpetuum [15].

The previous linear electromagnetic power generator shown in Figure I-7 was presented at the PowerMEMS 2004 conference.   This device is also fabricated using micromachining processes [15]. This devices produces current by varying a magnetic field on a coil of wire. The magnets are mounted to a resonant structure that captures impulses and/or driven oscillations. The structure is tuned to resonant at 60Hz for use in industrial energy harvesting.

Figure I-8 Perpetuum's 2-terminal power generator package [16].

The packaged, 2-terminal version of this power generator shown in Figure I-8 is roughly 30 cubic centimeters, weighs 50grams, and delivers 4mW at 100Hz (see Figure I-9 for power curve) and an acceleration of 0.4g. Thus, the figure of merit is $N_{LEH} = 3.3 \; cc^{-1}$.
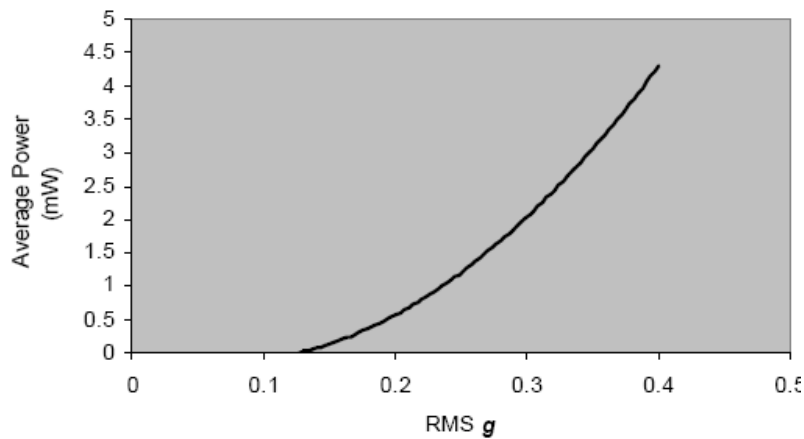
Figure I-9 PMG0100 Evaluation Model [17]

I.3.b.v. PIEZOELECTRIC POWER GENERATORS

The most aggressive development in mechanical energy harvesting devices has used

piezoelectric materials [5, 10, 18-24]. These materials convert a mechanical stress to an

electrical polarization, which can then induce a current in an external circuit.   The

piezoelectric material used is typically lead zirconate titanate (PBT) with a perovskite

crystalline lattice. Any piezoelectric material, such as porous electrets [25-29] or lead

barium titanate [30], can be used providing a compatible machining process exists. The

ability of the material to convert mechanical force to electrical energy is limited by the

efficiency which the piezoelectric material converts force to charge. A typical example

of a piezoelectric cantilever is shown in Figure I-10 [31].
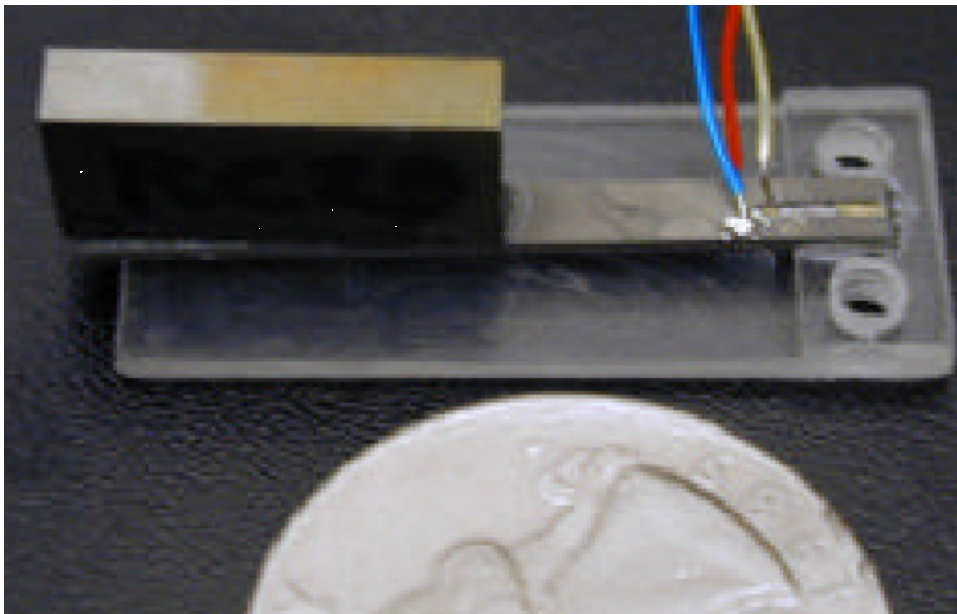
Figure I-10 Piezoelectric cantilever with proof mass for converting vibrations to electricity

Although piezoelectric materials and transducers are well explored, novel piezoelectric generators have recently been presented in literature, such as the piezoelectric windmill presented by Priya et al. [32] in 2005.
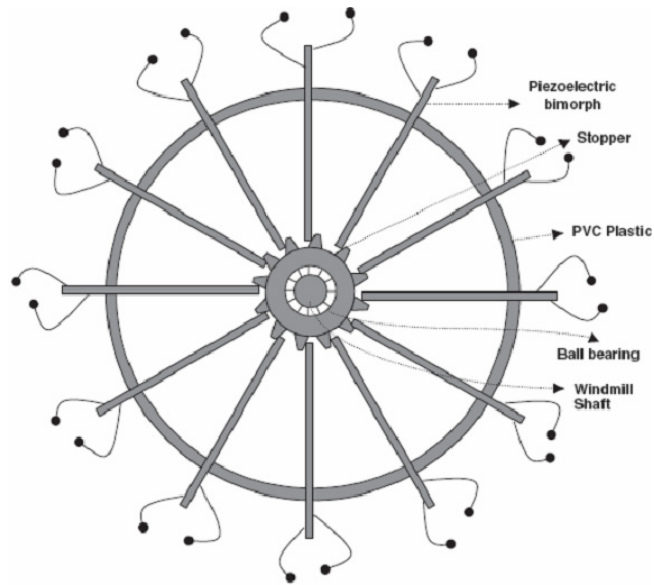
Figure I-11 Schematic for piezoelectric windmill power generator

The generator portion of the piezoelectric windmill is depicted in Figure I-11. The generator is connected to a windmill to provide rotational torque on the windmill shaft shown in Figure I-11. The torque on the shaft causes the connected stoppers to bend the piezoelectric bimorphs, which causes electrical polarization of the bimorphs that can be used as electricity.

I.3.b.vi. CHARGE SHUTTLE

More recently, the coulomb force power generator (CPFG) is being realized as the best microscale non-resonant power generator system [33].   Simple theoretical arguments presented by Mitcheson et al. show that, at low amplitudes, velocity damped resonant generators (VDRG), such as electromagnetic power generators, produce much less power output than CFPGs by the ratio

$$\frac{P_{CFPG}}{P_{VDRG}} = \frac{4\beta}{\pi}$$

(I.5)

Where β is the breakaway factor—the fraction of the maximum acceleration that the mass is able to move relative to the frame. The geometry of such a design can be seen in Figure I-12
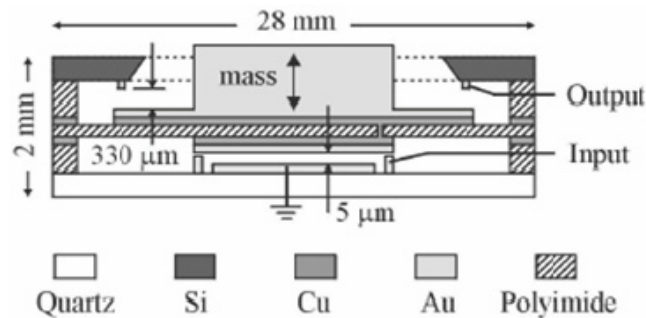
Figure I-12 Cross section of a charge shuttle

This device operates cyclically by charging the mass, applying a force to move the mass from the bottom to the top, and finally harvesting the charge at the output which is now at higher potential. This requires external circuitry as shown in Figure I-13.
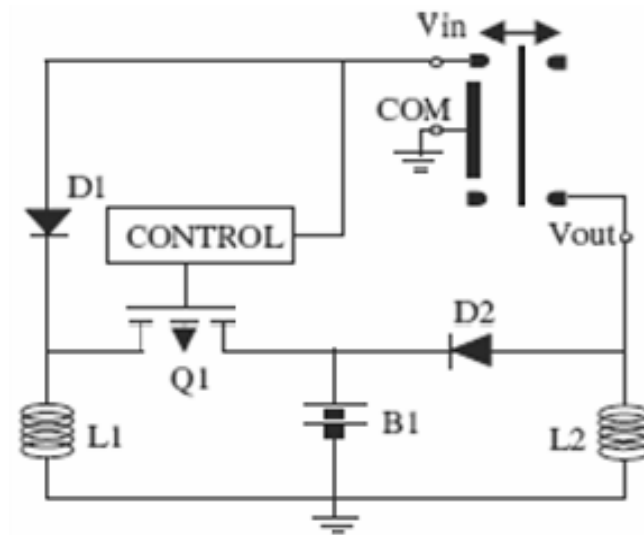
Figure I-13 Drive circuitry for the charge shuttle.

It is reported that this power generator produces 0.3μJ per cycle at 1Hz, 250μm displacement, and a mass of 0.5g. Therefore, $N_{LEH} = 73,000cc^{-1}$, which is most likely a gross exaggeration because the total mass and volume of the device were not explicitly stated. Furthermore, the power that is required to operate the circuitry is not reported, which is most likely much larger that the power generated.

I.3.b.vii. ELECTROSTATIC POWER GENERATORS

The following two cases are variable gap electrostatic power generators that can be easily micromachined [34]. The first case (Figure I-14) is a typical MEMS device in that it is essentially 2-dimensional. It bears strong resemblance to the comb drive electrostatic actuator [35] and the capacitive MEMS accelerometer [36, 37].
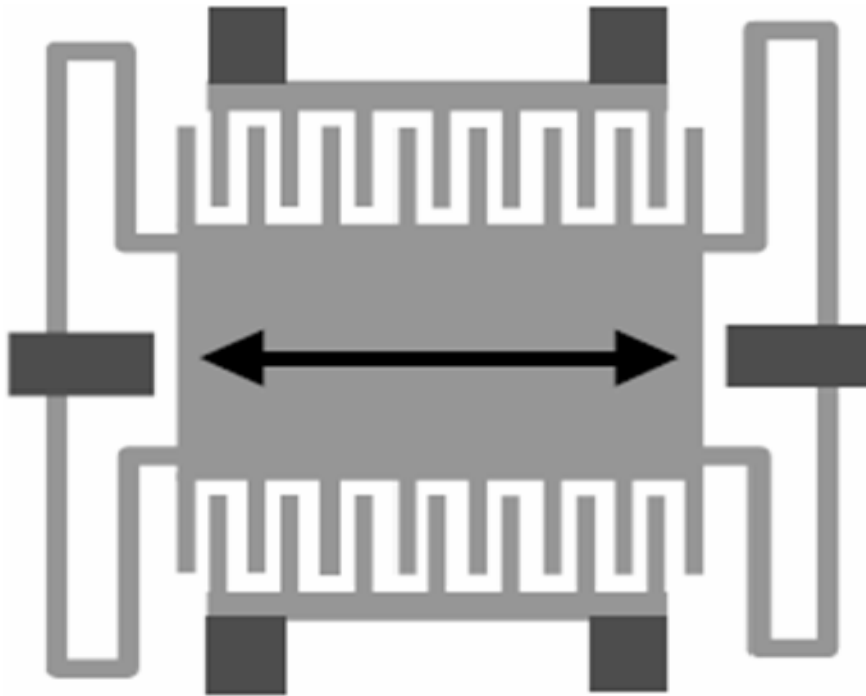
Figure I-14 In-plane variable gap capacitance micromachined power generator

Figure I-15 Out-of-plane variable gap capacitance micromachined power generator

The following was reported for the variable gap generator shown in Figure I-14: power generated = 116μW/cc, mass assumed to be the density of silicon times the moving mass = 0.04g (does not take into account total device mass), frequency = 120Hz, displacement = 5.6μm, which yields $N_{LEH} = 51,000cc^{-1}$. This calculation should be revisited when the total mass of the device is released.

I.4. DISPLACEMENT CURRENT POWER GENERATORS

I.4.a. ORIGIN OF DISPLACEMENT CURRENT

James Clerk Maxwell coined the term "displacement current" to explain the magnetic effects caused by time varying electric fields. Maxwell's generalization of Ampere's Law states

$$\nabla \times B = \varepsilon_0 \mu_0 \frac{\partial E}{\partial t} + \mu_0 J \qquad (I.6)$$

where B is the magnetic field, ε_0 is the permittivity of free space, μ_0 is the permeability of free space, E is the electric field and J is the current density. When $B = 0$, equation (I.6) reduces to

$$J_D = -\varepsilon_0 \frac{\partial E}{\partial t} \qquad (I.7)$$

which is the mathematical definition of displacement current J_D.

I.4.a.i. DISPLACEMENT CURRENT IN A CAPACITOR

Applied to a simple parallel plate air gap capacitor, this construct explains mathematically how current can appear to flow through the inside of a capacitor when no conduction path exists.

Assume the potential across the capacitor is initially zero, that is $V_C\left(t=0^-\right)=0$. In this case, the electric field inside the capacitor is also zero. Now, an external voltage source, V_S, and current limiting resistor is applied across the capacitor plates to make an electric circuit. The voltage difference across the resistor causes instantaneous current to flow through the resistor and into the capacitor defined by Ohm's Law as

$$I\left(t\right)=\frac{V_S-V_C\left(t\right)}{R} \tag{I.8}$$

When the current reaches the top capacitor plate, it is physically stopped because there is no further conduction path. Yet, somehow, the bottom plate of the capacitor sends the same current back around the circuit. So, even though no conduction path exists through the capacitor element, current still flows through the entire circuit.

This effect exists because any charge q on the top plate will create a mirror charge $-q$ on the bottom plate equal in magnitude but opposite in sign. The simple visualization is that charge q the bottom plate is instantaneously repelled by q the top plate and, by conservation of charge, $-q$ is left behind.

From Gauss's law, any charge q on the top plate will establish an electric field inside the capacitor of

$$E(t)=\frac{-q(t)}{2\,A\,\varepsilon_0} \tag{I.9}$$

where A is the area of the capacitor plate. The $-q$ charge on the bottom plate presents an additional electric field of the same magnitude in the same direction as that described in (I.9). Thus, the electric field in the capacitor has changed from $E_C(t=0^-)=0$ to

$$E_C(t) = \frac{-q(t)}{A\,\varepsilon_0} \qquad\qquad (I.10)$$

Charge flowing through the resistor at the rate $I(t) = \frac{\partial q(t)}{\partial t}$, or described as a volume current density into the top plate of the capacitor $J(t) = \frac{I(t)}{A}$, creates an instantaneous time changing electric field inside the capacitor equal to

$$\frac{\partial E_c(t)}{\partial t} = \frac{-J(t)}{\varepsilon_0} \qquad\qquad (I.11)$$

which is equivalent to equation (I.7). The current into the capacitor's top plate is $J(t)$, the displaced current out of the bottom plate of the capacitor is $J(t)$, and now described, and the displacement current J_D describes a fictitious current flowing across the gap in the capacitor to conserve charge.

I.4.b. DISPLACEMENT CURRENT FOR POWER GENERATION

The displacement current effect also applies to the current that flows out of any conductive plate when the electric field on that plate changes with time. If the displacement current and associated voltage is large enough, an external circuit can be

driven by just a metal plate and an impinging time changing electric field. In essence, a displacement current device can be used to generate electrical power. When the electric field is provided by a permanent electric dipole, called an electret, this device is called an electret power generator.

The main elements of the electret power generator are the electret, metal plates, and a mechanism to change the electric field on the plates. The change in capacitance $C(t)$ occurs by changing the distance between the plates $d(t)$, the overlapping area of the capacitor $A(t)$, or the permittivity of the capacitor $\varepsilon(t)$

$$C = \frac{\varepsilon A}{d} \tag{I.12}$$

The electret material inside the generator stores a fixed amount of charge Q, which creates mirror charge on the capacitor plates. The voltage V of the capacitor is

$$V(t) = \frac{Q}{C(t)} \tag{I.13}$$

Then, an external circuit is connected and powered by the voltage of the capacitor. The external circuit, whether a light bulb or sophisticated electronics, is represented as a load R. The power that the generator can supply to the load is simply

$$P = \frac{V^2}{R} \tag{I.14}$$

I.4.b.i. VARIABLE DISTANCE ELECTRET POWER GENERATORS

Changing the distance between two capacitive plates changes the capacitance of the structure originally described in Equation (I.12) by

$$\frac{\partial C(t)}{\partial t} = \frac{\partial}{\partial t}\left(\frac{\varepsilon A}{d}\right) = \frac{-\varepsilon A}{d^2}\frac{\partial d}{\partial t} = C(t)\frac{1}{d}\frac{-\partial d}{\partial t}$$ (I.15)

When some fixed charge is implanted in a thin layer of dielectric inside the capacitor, it will create a voltage on the top and bottom electrodes. An external circuit can be connected to measure the voltage across this capacitor.

If one of the plates is mounted such that pressure waves will cause one of the plates to move, this structure can then be used to measure sound waves. This is the basic operating principle of an electret microphone. This was the topic for the Ph.D. thesis of Wen Hsieh [38] who graduated the Caltech Micromachining Laboratory in 2000. This example of fixed-charge variable capacitance devices in the Caltech Micromachining Laboratory provides precedence for the work in this thesis.

The electret microphone fabricated in the Caltech Micromachining Laboratory was very successful. The voltage output was sufficient for making sensitive acoustical measurements as a sensor device. However, the current output of the electret microphone was not sufficient as a power source.

The one point that should be made about the fixed-charge variable distance capacitor is that it should be possible to design the structure to generate a much larger current for the same energy input. Such a power generator would be optimized to produce maximum

current at the frequency of largest spectral power density. This would imply that it would also have a narrow frequency of interest, and probably have poor performance as a microphone. This type of device was not pursued as a power generator because the maximum capacitance change obtained with this structure is limited to the displacement range a support structure could allow, which would need to be considerably large and flexible to compete with the following designs.

I.4.b.ii. VARIABLE AREA ELECTRET POWER GENERATORS

Changing the overlapping area of a capacitor changes the capacitance describe in Equation (I.12). Ignoring stray fields, capacitance changes linearly with change in area of the capacitor originally described in Equation (I.12) by

$$\frac{\partial C(t)}{\partial t} = \frac{\partial}{\partial t}\left(\frac{\varepsilon A}{d}\right) = \frac{\varepsilon}{d}\frac{\partial A(t)}{\partial t} \qquad (I.16)$$

This linear relationship is much clearer than the microphone case. By placing a thin, charged dielectric on the stationary electrode, a mirror charge is induced. When the overlapping area is zero, all of this charge can be said to reside on the stationary electrode. When the moving electrode overlaps the stationary electrode, charge is induce in it too. The voltage of the two plates will change in time, and this is used to drive an external circuit.

I.4.b.iii. VARIABLE PERMITTIVITY ELECTRET POWER GENERATORS

Finally, the capacitance of Equation (I.12) can be varied by changing the permittivity of a capacitor's air gap. Ignoring stray fields, capacitance changes linearly with change in permittivity of the capacitor originally described in Equation (I.12) by

$$\frac{\partial C(t)}{\partial t} = \frac{\partial}{\partial t}\left(\frac{\varepsilon A}{d}\right) = \frac{A}{d}\frac{\partial \varepsilon(t)}{\partial t} \qquad (I.17)$$

This linear relationship is also fairly clear. A capacitor with an air gap has a changing permittivity caused by the insertion of another dielectric into the capacitor with time. Mirror charge is induced in the electrodes by placing a thin, charged dielectric inside this capacitor without taking up a significant portion of the air gap. When the air gap is completely empty, the capacitor will have an induced voltage of

$$V_0 = \frac{Qd}{\varepsilon_0 A} \qquad (I.18)$$

When a dielectric material occupies the gap completely, the voltage will be described by (I.19)

$$V_{\frac{\lambda}{2}} = \frac{Qd}{k_l \varepsilon_0 A} \qquad (I.19)$$

where $k_l\varepsilon_0$ is the permittivity of the introduced dielectric and $\frac{\lambda}{2}$ represents half a period of cyclic motion. The AC voltage of this generator is will then have an open-circuit peak-to-peak voltage of

$$V_{pp} = \frac{Qd}{\varepsilon_0 A}\left(1 - \frac{1}{k_l}\right)$$ (I.20)

The voltage of the two plates will change in time proportionally to the permittivity of the air gap, and this is used to drive an external circuit.

To extend the ability to generate electricity, two novel micromachined devices for converting mechanical energy into electrical energy using electric fields are presented in this thesis.

I.5. PHYSICAL SCALING

Micro electro mechanical systems (MEMS) is the term used to describe devices whose characteristic dimension is roughly between 0.1×10^{-6} meters and 100×10^{-6} meters. "Micro" is the System International (SI) prefix meaning 1×10^{-6}, and is often written as 1μ, and for measuring distance as 1 μm. Since the characteristic dimension of a device is not always obvious, an alternate denotation for the term MEMS is: any device fabricated using microscale processes; typically such processes are complimentary to or were developed for the production of integrated circuits (IC). Both definitions prove useful and are described in more detail below.

I.5.a. PHYSICS-BASED DEFINITION OF MEMS

Fundamental physics describes the world in terms of dimensions, fields, forces, energies, masses, times, etc. The interactions of these quantities rarely scale linearly. Often, different types of interactions become dominant depending on the magnitude of the

quantities of a system. By knowing which types of interactions dominate, simplifying assumptions can be made to facilitate calculations.

Engineering advances often come in quantities of length: when all other quantities are held constant, increasing or decreasing the lengths in a design often increase the effect of ignored terms in nonlinear fashion, which soon produces undesirable effects. To engineers, the Tacoma Narrows bridge is a tragic example of this effect.

For the layman, it is well known that water runs downhill. However, a droplet of water tossed at wall may stick and appear to defy gravity, whereas a gallon of water tossed at a wall will not. Effects such as surface energy, gravity, temperature, density, and others will have an influence on what size of droplet will stick, but for everyday conditions, the water will not move if the ratio between the volume and the surface area is significantly below a certain quantity. Arbitrarily, this quantity is called λ, which is related to the ratio of the droplet volume to its surface area, as described in Equation (I.21).

$$\lambda = \frac{\frac{4}{3}\pi r^3}{4\pi r^2} \propto r \qquad (I.21)$$

Conversely, the water rolls downhill if the ratio λ is significantly above some amount. It can then be said that in ordinary conditions, λ describes the tendency of a droplet to roll down a wall. Formally, λ is related to inertial energy divided by surface energy. Since λ has units of length, λ is called the "characteristic dimension." If the characteristic dimension is greater than a certain amount, the physics of motion will apply. If the characteristic dimension is much less that this amount, then surface energy

will dominate the droplet. It is not a coincidence that the simple number for determining which physical mechanism will dominate a droplet thrown at a wall is a unit of length. A device can be said to be a micro device if the operating principles require it to have a characteristic dimension less than 100x10-6 meters. Similarly, nano devices operate on physical principles that become significant below 100x10-9 meters. Micro devices are used to exploit a wide variety of physics, but the overwhelming majority of devices take advantage of mechanical or electrical gains at the microscale, which leads to the term micro electro mechanical systems. The terms "MEMS device" and "micro device" are used interchangeably to describe devices that exploit physics of the micro world.

I.5.b. PROCESS-BASED DEFINITION OF MEMS

An alternate derivation of the term "MEMS" can be traced back to the founders of the MEMS field, who created layered 3-dimensional devices using additive and subtractive processes that were commonly available for creating micro-scale integrated circuits. Examples of additive processes are evaporation coating of surfaces with metals or polymers and spin-coating liquids onto flat surfaces. An example of subtractive process would be using heated potassium hydroxide to etch into a silicon region. It is because additive and subtractive processes are commonly measured in microns added or removed, and the dimensions of surface length perpendicular to these processes, that the term "micro" is applied to the final system regardless of the physics of device operation.

Since MEMS is a process and materials driven field, the definition based on the scale of the process is just as valid as the definition based on physical interactions, and the term is used broadly. Often, both definitions apply to the same device.

I.5.c. APPLYING MEMS

Many MEMS devices are designed to interact with the larger scale world. For instance, a MEMS accelerometer mounted in a vehicle can determine when an impact occurs and to what magnitude. The key to this interaction is proper mounting of the accelerometer to the frame of the vehicle so that physical accelerations are transmitted properly. The transferal of large scale mechanical force to a small scale electric field is the operating principle of this device.

MEMS are also the key to observing nanoscale phenomena. An atomic force microscope utilizes a MEMS cantilever with a MEMS-process sharpened tip to trace over and plot the three-dimensional world at 10^{-9} meter (nearly atomic scale) precision. An SEM uses a microscale aperture as a starting point in controlling an electron beam that can detect features with nano precision.

MEMS devices and processes allow new methods of interacting with the world. The Caltech Micromachining Laboratory has all the tools needed build novel devices that exploit the physics of the microscale.

I.6. FUNDING

To understand the origin of this work, it is necessary to explain the context and goals for which it is performed. The project below provides funding in an effort to design and build a more efficient device to convert chemical energy to electricity for use in remote locations. The work described thereafter in this thesis can be considered an independent system.

This project began with a proposal to the United States Department of Defense through the Defense Agency Research Projects Administration (DARPA) to build a Pulsed Chemical-Electret Generator (PCEG), which is a novel MEMS-based electrical power generator consisting of a pulsed chemical-thermal reactor (PCTR) that uses non-pressurized liquid hydrocarbon fuel with no moving parts and an electret generator (EG) capable of providing >kV, >100mW power output. The following description of the High-Voltage Micro Power Generation, Chemical Thermal Reactor, Electret Generator is nearly verbatim from the original Technical Proposal for BAA 01-09 to explain the original motivation behind this project.
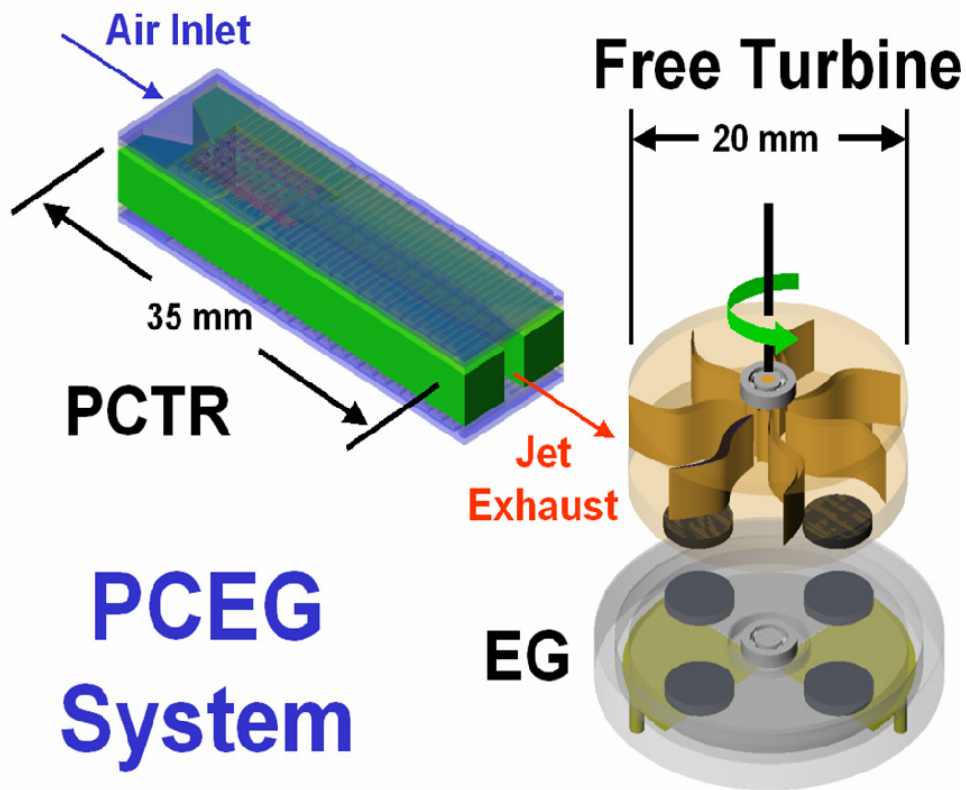
Figure I-16 Pulsed Chemical-Electret Generator system concept

Integrated with many innovative MEMS devices, this unique Pulsed Chemical-Electret Generator can *directly power* micro actuators made of piezoelectric or electrostrictive materials, which are most efficiently driven in the kilovolt range. The proposed micro power generator (MPG) will charge small energy storage devices (super-capacitors and or batteries) intermittently for high power electrical loads and to provide low emission signatures during critical operational periods. Photostructurable ceramic glass material will be used for fabricating high efficiency 3D (non-extruded shape) turbines with high

temperature capabilities. In addition to thermal management, chemical species transport and reactions will be numerically simulated for design optimization. With the following innovative claims, *a unique high voltage MPG will be developed for powering MEMS actuators and sensors*:

1. No moving parts (neither pumps nor valves) and non-pressurized liquid fueled (no pressurized lines and tanks) MEMS pulsed chemical-thermal reactor (PCTR) for high efficiency chemical-to-kinetic energy conversion.

2. Thermal management through fuel evaporation will allow silicon-based materials to be used instead of exotic and process-limited materials such as silicon carbide (SiC).

3. Efficient 3D turbines for kinetic energy coupling from the PCTR reactor jet streams to the electret generator.

4. A new electret generator for delivering kV range output based on a newly developed thin-film Teflon® electret technology.

5. Photostructurable ceramic glass for fabricating high efficiency 3D turbine and high aspect ratio MEMS.

6. Magnetic coupling between turbine and power generator without solid coupling to allow sealing the high rotational velocity generator in vacuum. A 50% energy saving can be achieved by eliminating air drag.

7. Numerical simulations of the pulsating flow-thermal- reacting fields will be used for system and component optimization

The proposed PCTR is a pulsed combustor scalable in size from millimeters-to-centimeters designed to take full advantage of scaling laws to enhance operating efficiency and minimize size (*there are no real direct macro world counterpart*). The heat generated by combustion will evaporate liquid fuel (and oxidizer if not in natural aspirating mode) for the next combustion cycle. The heat-of-vaporization of the fuel is used to control combustion chamber temperature. This novel PCTR is more than a concept; we have already fabricated and performed preliminary tests on a few simple prototypes. The photograph below shows pulsed combustion of a prototype symmetric PCTR in natural aspirating mode at three different phase angles during a pulse cycle. The combustion channel was 8 x 4.5 x 38 mm. Although many technical challenges still exist, feasibility has been demonstrated. In our view, the proposed PCTR offers the benefits of no moving parts (ie, fuel pumps and valves), non-pressurized liquid fuel storage (no pressurized lines, more valves, and pressurized tanks), and the ability to burn widely-available non-processed hydrocarbon fuels (ie, methanol, JP, diesel, and gasoline) while taking full advantage of scaling laws as compared to the current state-of-the-art MPGs.
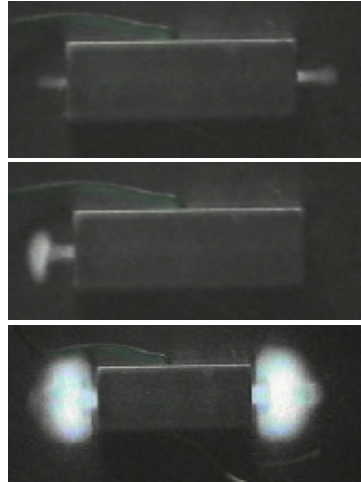
Figure I-17 Pulsed combustion of a prototype symmetric PCTR in natural
aspirating mode at three different phase angles

High-speed jet streams exhausted from the end of the reactor will impinge on turbines to convert linear momentum into rotational motion. A high-voltage electret generator or low-voltage electromagnetic generator (EMG) attached to the turbine axis can provide electric power over a wide voltage range. We propose to develop a totally new type of electret generator. EGs have many obvious advantages over EMGs. First, EGs are fundamentally high-voltage, low-current power generation devices and were not available in the past for high-voltage applications such as piezoelectric transducers and electrostatic/electrostrictive MEMS. Second, with the same power delivery and form factor, the proposed EGs will be structurally simpler and much lighter than conventional EMGs. EGs are capacitive machines while EMGs are inductive devices, thus EGs do not require heavy and inefficient coil windings found in EMGs. Also, power leads that are needed in capacitive EGs can be thin-film metals on lightweight non-conductive substrates such as plastics. The electret for the proposed EG is a newly-available thin-

film Teflon® electret, while EMGs will require heavy permanent magnets. Third, the proposed EGs are fundamentally more efficient than the EMGs due to their simplicity and low mass. The total energy loss in an EMG includes mechanical loss (friction from inertial loads on bearings/commutators and aerodynamic viscous dissipation) and electrical loss (resistive loss in the coil windings). Even if the mechanical energy loss (bearings and aerodynamics) of the proposed EG is assumed to be the same as in EMGs, EGs are more efficient than EMGs because they have minimal resistive losses; they have no coil windings. Serious efforts in developing electret generators in the past never took off mainly because of the lack of good electret technology. Recently, our group has successfully developed a new thin-film Teflon® electret technology based on the new DuPont spin-on Teflon® (AF Series) that became available only a few years ago. In fact, we have demonstrated a working, high-sensitivity electret microphone out of this technology. As a result, the timing is perfect for using the indispensable long-life-time, high-charge-density electret technology for the proposed power generator.

Photocerams are proposed for fabricating the required high-efficiency, high-temperature 3D turbine blades. Photocerams can be patterned using masks with ultraviolet light or by using laser direct-write processing. The latter approach enables three dimensional (3D) patterning with resolution approaching 10 microns. Photocerams have zero porosity, good abraded flexural strength (~ 150Mpa) and are inert to reactive gas chemistry.   In general, ceramic materials are poor thermal conductors (i.e. thermal conductivity for Foturan® glass/ceramic ~1.3- 2.7 W/m.K versus single crystal silicon with 157 W/m.K). Our team member has developed a laser direct-write patterning technique for

microfabrication of true 3D structures in photocerams. Their approach utilizes the best aspects of direct-write and batch-processing techniques. The technique uses a merged-process approach whereby the direct-write step is only used to impregnate the 3D image (3D turbine blades) via a volumetric patterning step. Key aspects are that the resulting microstructures can be either left in a semi-ceramic state or converted to a full ceramic state. The following figure shows an array of semi-ceramic combustion chambers (left picture), two interconnected fluidic microcavities converted to full ceramic state (middle picture) and a coupon where only the center portion has been converted to a full ceramic state (right picture).
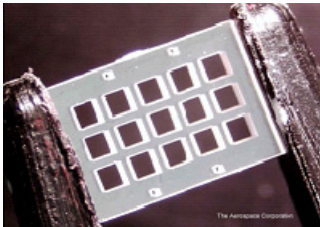
Figure I-18 Semi-ceramic combustion chambers
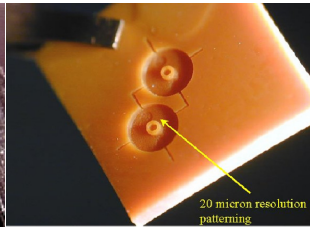
Figure I-19 Two interconnected fluidic microcavities.
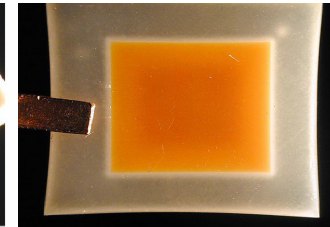
Figure I-20 Coupon.

We have also refined a process for 3D laser direct-write processing of silicon. The process uses a laser-assisted chlorine etch chemistry to remove material at rates of ~100,000 cubic micrometers per second. We propose to use the novel 3D silicon processing capability to fabricate efficient MPG turbines and as a selective area post-process tool to "tailor" microstructure geometries for enhancing MPG efficiency.

The proposed chemical power conversion system uses chemical combustion, heat transfer, fluid dynamics and electrostatics. In addition to imbedded MEMS temperature

and pressure sensors for combustion diagnostics and studies, a computational virtual prototyping tool can provide insight into system operation and aid in the design optimization. We propose to adapt existing multi-disciplinary simulation tools, CFD-ACE+, for computation design and optimization of the complete power generation system.
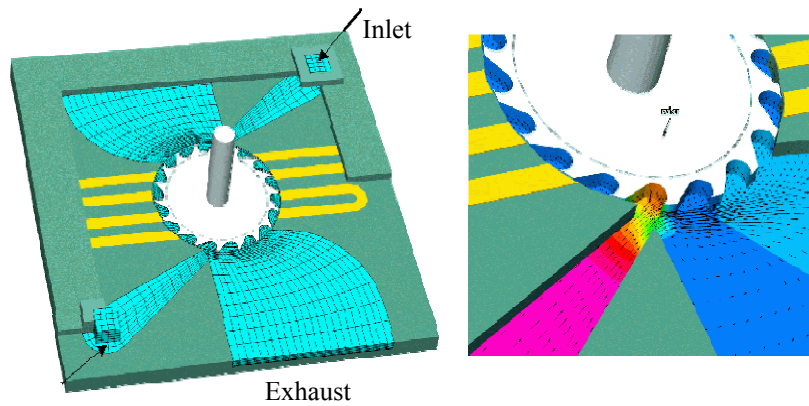
Figure I-21 CFD simulation of a turbine

CFD-ACE+ is an advanced multi-physics, multi-scale computational package, and it has all the essential modules for combustion, combustion instability, turbo machinery, electrostatics and electromagnetism. Chemical power conversion, turbine and electret generator operation can be modeled with these modules. The code can also provide for design optimization. In this study, the existing combustion module will be modified for pulsed combustion with special emphasis on thermal inertia and hence operational frequency. Maximum amplitude and frequency of temperature variation can be found through this process to determine capability of the present concept. From this, energy

utilization and efficiency will be estimated. Comparison and validation against experimental data will be made for the pulsed combustion model; the computed thermal fields will be compared to experimental data. A systematic parametric study will be carried out focusing on system geometry, arrangement of combustor stabilizer, fuel efficiency, effective ventilation, etc. CFD analysis will also be used for micro-turbo-generator design. Combustor nozzle, turbine blade, and turbine geometry will be optimized by the CFD code for efficient conversion of jet flow energy into rotational kinetic energy. Finally, even though the electret generator is not a fluid or thermal device, its performance will be analyzed by the existing electrostatics capability in CFD-ACE+.

Our unique pulsed combustor will energize a novel high-voltage power generator for MEMS sensor and actuator applications. This innovative MPG consists of four major components and will be performed by four groups which have established records in successfully developing numerous MEMS components and systems.

Pulsed chemical-thermal reactor – UCLA

Electret high voltage generator – Caltech

3-D laser fabrication – Aerospace Cooperation

Full system/components simulation – CFDRC

While working on rotational power generation, the concept for a linear power generation system began to take form.
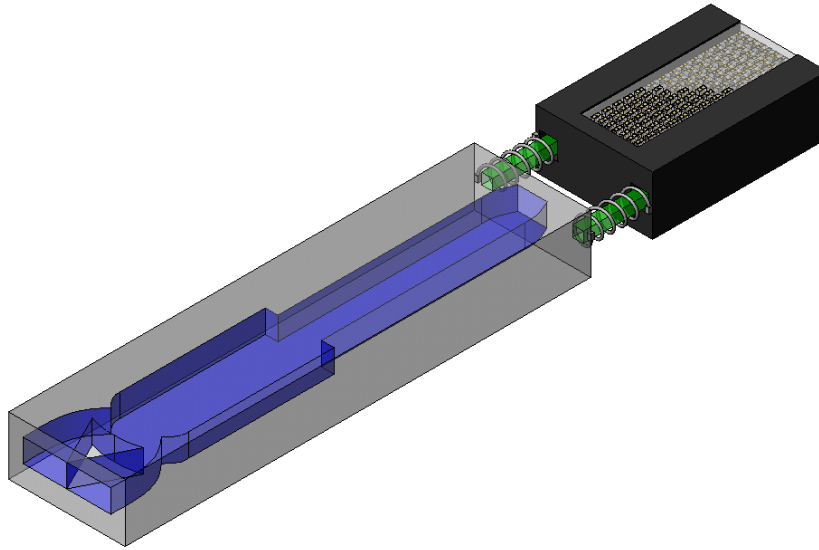
Figure I-22 Proposed new design for pulsed combustor thermal resonator and shaker generator system.

The above cartoon (Figure I-22) is the current concept of a system to generate power from linear vibration. In this case, the PCTR drives a liquid rotor electret generator directly without the use of a turbine. This system is much simpler that the previously described rotational system, and this new concept may prove to have superior efficiency.

Future work will attempt to integrate the electret power generators covered in this work with the PCTR produced by UCLA. For the purposes of this thesis, the system integration work not covered.

CHAPTER 2

II. ELECTRETS

"Electrets" are insulating materials that exhibit a permanent net electrical dipole moment. Figure II-1 shows the magnetic field from the familiar bar-magnet and Figure II-2 depicts the field generated from what could be termed a "bar-electret." Both exhibit a permanent dipole field, where field lines emanate from the top and end at the bottom of the bars. While many parallels can be drawn between the two cases, some relationships are misleading while others are completely false. The magnetic field shown in Figure II-1 has approximately the same shape as the electric potential shown in Figure II-2, however, the electric field is actually shown in Figure II-3.
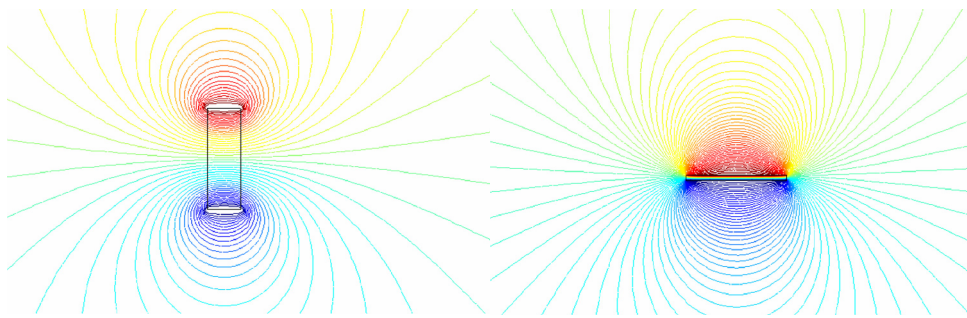
Figure II-1 Contour plot of magnetic field from a bar electret.

Figure II-2 Contour plot of electric potential from a sheet electret
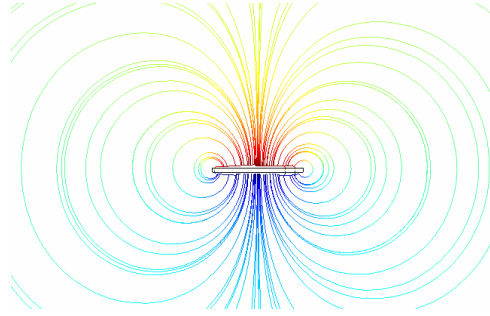
Figure II-3 Streamline plot of electric field from a sheet electret

The magnet and the electret are established by effective sinks and sources, called north and south poles for magnets and positive and negative poles for electrets. These sinks and sources cause a disruption of the neutrality of space and they interact with susceptible materials. In both cases, like poles will repel each other while opposite poles will attract. A material such as iron that exhibits characteristic ferromagnetism, can be attracted to magnetic fields. Iron atoms, which individually may initially be magnetically neutral, are influenced by a magnetic field and spontaneously align themselves to the field. Once the iron is thus polarized, there is an attractive force between the magnet and the iron that depends on the strength of the dipoles.

Water molecules have permanent electric dipole moments caused by the polarized covalent bond between oxygen and hydrogen. In this case, the oxygen atom strongly attracts an electron from each hydrogen atom, which results in a net positive space charge on the hydrogen atoms and a net negative charge on the oxygen. This charge separation creates a net electric dipole.

II.1. ELECTRET CLASSIFICATION

Electret materials exhibit an electric dipole through one or both of the following physical mechanisms: polarization and charge storage. In this thesis, the latter of these effects is exploited for power generation because trapped charge electrets have a longer lifetime and larger electric dipole moment than purely polarized electrets.
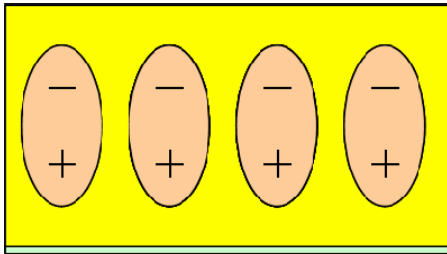
Figure II-4 Heterocharge by polarization
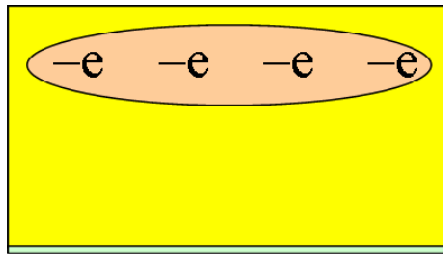
Figure II-5 Homocharge electret with implanted electrons

II.1.a. HETEROCHARGE ELECTRETS

When electrically polar molecules are present in the bulk of the electret and they align to produce a net electric dipole moment, the electret is said to be polarized. Since the dipole has both positive and negative charges, by definition, the electret is termed "heterocharged." This situation can be produced by heating a dielectric and cooling it in an electric field, or it can be the result of implanting positive and negatively charged particles in opposites of a dielectric.

II.1.b. HOMOCHARGE ELECTRETS

Homocharge electrets, as might be expected, involve only one type of charged particle. These charged particles or ions are trapped and stored in the dielectric. It is vital that deep charge traps are available for long-term storage and that the material is highly insulating to prevent charge migration over time [28, 39-41]. Figure II-5 shows electrons implanted into the bulk of the dielectric just below the top surface. Figure II-2 and Figure II-3 were both simulated in FemLab by putting a surface charge on the top of the materials and grounding the underside.

II.2. CHARGING METHODS

There are few different methods to create an electret, but the discussion will focus on methods that are relevant to this thesis.

II.2.a. TRIBOELECTRIC

It was noticed that Teflon chips were slightly charged after dicing. A simple experiment confirmed the charging is due to a phenomenon known as triboelectricity, which involves charge transfer from a liquid to a solid. In the experiment, a Teflon chip with a floating metal layer and a sealing Teflon layer was run under deionized water for 30 seconds (The floating metal layer electret design and process described in Section II.4.a.). The sample was then measured for surface charge density distribution. This measurement takes approximately 10 minutes to perform by hand. Since most of the charge deposited by the triboelectric effect resides on the surface, near-complete decay in charge magnitudes were observed on a timescale less than a few hours. The charge density in Figure II-6 clearly shows the 4-pole pattern. Future studies should be considered to determine whether this charge can be driven-in into the Teflon by applying an electric field during or after triboelectric charging.
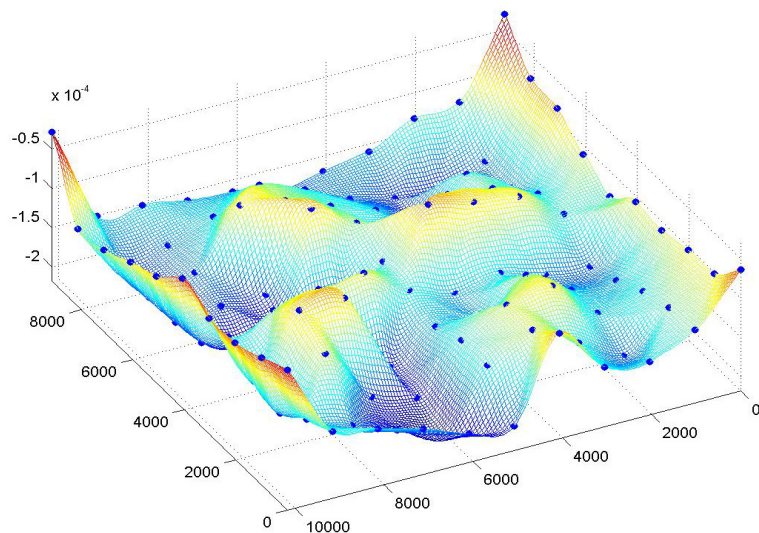
Figure II-6.Triboelectrically charged Teflon chip

The resolution of Figure II-6 is not adequate to discern fine details. The time necessary to make this surface scan by hand is 10 minutes. Doubling the resolution for this scan would take 40 minutes to complete, and such a long and tedious scan is sure to increase operator error. A simple solution to this problem is to add a computer controlled x-y stage and read in the voltages using a GPIB device, which has since been implemented.

II.2.b. BACK LIGHTED THYRATRON FOR ELECTRON BEAM IMPLANTATION

The back lighted thyratron (BLT) consists of a vacuum chamber partially pressurized with helium gas and a high-voltage copper thyratron assembly driven by an external UV flashlamp [42]. The thyratron assembly, also called a psuedospark device in literature [43], consists of two capacitor plates separated by an insulator with a hole through the center of the assembly. By applying 1-25kV across the capacitor plates, a large electric

field builds up inside the empty region. The field can be kept from breaking down on its own by choosing proper voltages and pressures in accordance with the Paschen curve. The proper operation point is at a helium pressure of 100-600mTorr and a voltage of 1-25kV.

When the thyratron is at the proper voltage and pressure, the UV flashlamp is pulsed, causing the copper inside the assembly produces electrons via the photoelectric effect. These electrons cause an avalanche effect as they are accelerated towards ground, creating a high density pocket of electrons. Once the pocket of electrons escapes the thyratron region, the electric field is no longer sufficient to maintain the avalanche. The process is repeatable in the time it takes to recharge the flashlamp, about 5 seconds. The result is a controlled, high density, pulsed, electron beam.

Care must be taken such that the applied voltage for a given helium concentration does not break down and generate plasma on its own. Although the majority of electrons produced by continuous plasma do not have significant electron implantation energy, a large transient pulse is generated at the start which is undesirable because the electron dose cannot be controlled. Implanting more electrons into the Teflon causes electric field breakdown inside the bulk of the material, which leads to lower total charge densities.

The pressure-voltage relationship for self-sparked and induced breakdown form a set of Paschen curves. Between the two curves is the desirable operating range of the BLT, roughly centered on 430 mTorr and 11kV.

The high density pocket of electrons formed by the psuedospark forms a pulsed beam that is accelerated towards the ground plane. The beam spreads as it travels through space due to electron-electron repulsion. The cross-section of the electron beam is captured by a Teflon dielectric placed on the ground plane, which records the spatial distribution of charge. Figure II-7 is a plot of the spatial charge density, which appears as a 2-D Gaussian in the transverse directions. At higher voltages, the Gaussian is concentrated and the electrons have more kinetic energy.
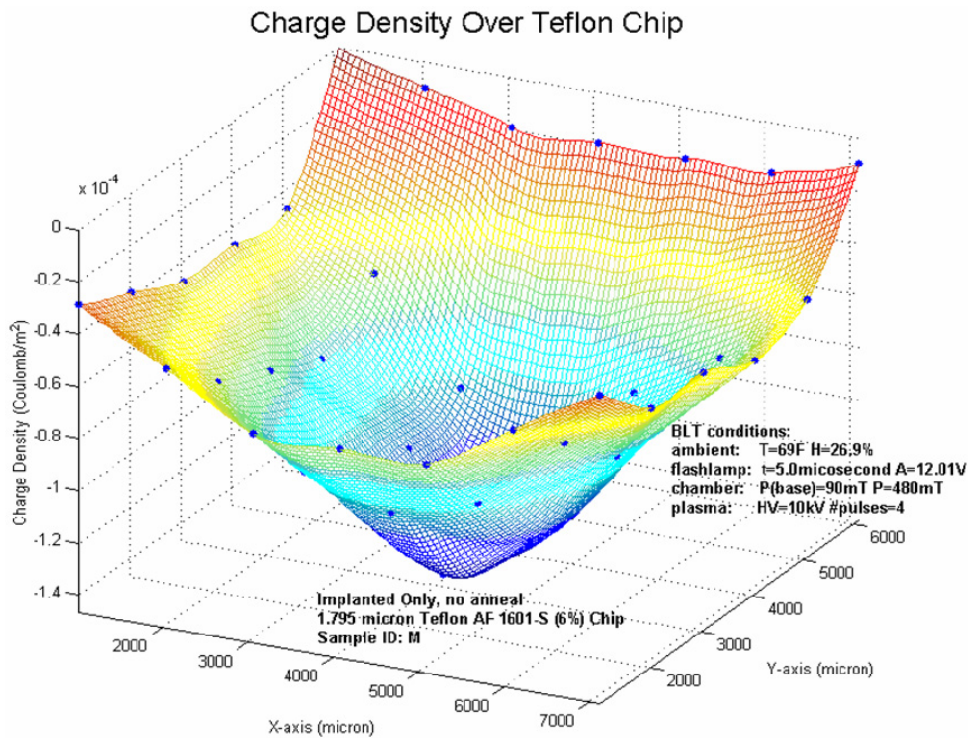
Figure II-7 Charge density of implanted Teflon using the back lighted thyratron

The use of a BLT as an electron source is unique to the Caltech Micromachining Laboratory. It is utilized because of the high density of electrons, the speed of the electron implantation process, and the large acceleration voltage that allows electrons to be stored in deep traps where they will be stable for hundreds of years. Useful theoretical development on the lifetime of implanted charge can be found elsewhere[44].

Also critical to the storage of charge is the electron implantation depth. The electrons must be located within the bulk of the dielectric material, or else they can easily be lost to surface conduction and humidity.
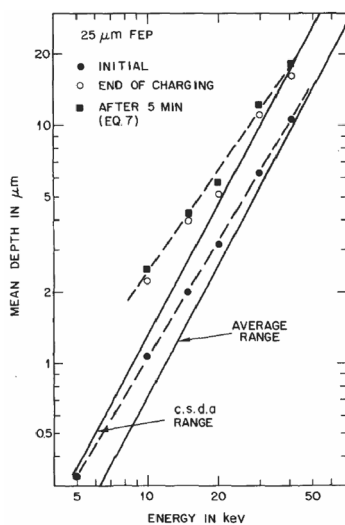
Figure II-8 Mean charge depth for corona charged FEP Teflon

The electron implantation depth can be estimated by Monte Carlo simulation [45-49]. Figure II-8 was derived by the aluminum range divided through by the densities of the polymers. This is very helpful for shallow electron implantation depths because depth sounding techniques do no have sufficient resolution to take the necessary measurements.

II.3. Measurement Techniques

To know how strong an electret is, the field that emanates from the material must be quantified. Quantifying the electric field allows for calculation of the implanted charge, which is the physical source of the electric dipole.

II.3.a. Charge Density

Almost every method to measure the charge within an electret begins by placing the electret on a ground plane and then measuring the ground referenced voltage induced on a probe above the electret surface.

The electric field above or below an infinite, two-dimensional plane with uniform surface charge density $\sigma \left[\text{Coulomb} \middle/ \text{meter}^2 \right]$ surrounded by a dielectric of permittivity $k_{dielectric} \varepsilon_0 \left[\text{Farad} \middle/ \text{meter} \right]$ can be found using Gauss' Law to be

$$ E = \frac{\sigma}{2\, k_{dielectric}\; \varepsilon_0} \qquad (\text{II.1}) $$

When this charge plane is placed a distance d above an infinite ground plane, the voltage of the charged plane is simply

$$ V = \frac{\sigma}{2\, k_{dielectric}\; \varepsilon_0} d \qquad (\text{II.2}) $$

A probe placed on or above the electret surface will experience the electric field due to charge implanted in an electric and/or due to polarization of the electret. Subsequently, a

voltage will appear on that probe. It is commonly assumed that the charge implanted in the electret resides on the top surface of a dielectric of thickness τ, so that the implanted charge density can be calculated by rearranging Equation (II.2) to get

$$\sigma = \frac{V \ 2 \ k_{dielectric} \ \varepsilon_0}{\tau} \qquad\qquad (\text{II.3})$$

Charge densities are calculated by taking surface voltage measurements with a Monroe Electronics isoprobe Model 244 with a high resolution 1024AEH probe. The probe is mounted on an x-y-z stage to allow precise measurements of the effective surface charge.
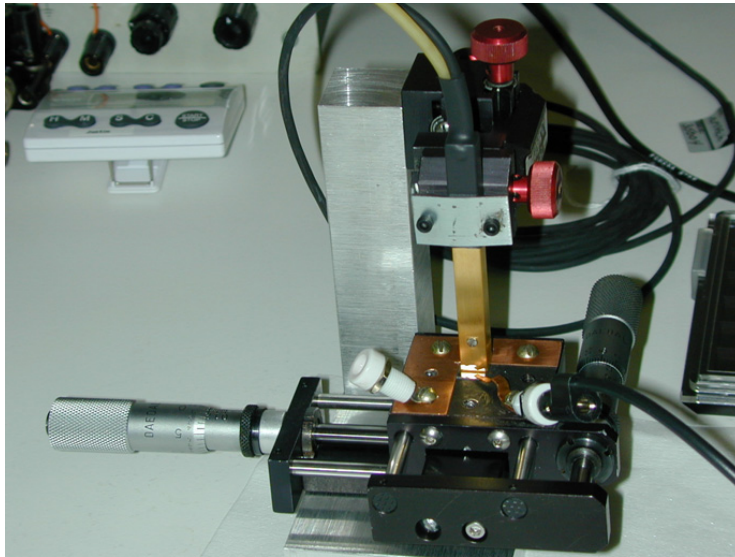
Figure II-9 Isoprobe mounted on X-Y micropositioner

Minimum observed resolution in x and in y was 254μm, although the resolution of the stage was 25.4μm in x-axis and 10μm in the y-axis. The rotary electret generator that is explained in Chapter 3 relies on an electric field that is patterned in the x-y plane, and

therefore the effective surface charge densities in x-y only need to be defined the dielectric thickness and the voltage of the surface. Making an infinite plane approximation, the isoprobe is sufficient for quantifying the charge implanted.

II.3.a.i. ERROR IN DEPTH OF CHARGE

It is important to note that the distance between the charge layer and the ground plane must be assumed. Figure II-8 shows that electrons implanted into an electret with an energy of 10keV will penetrate to an average depth of roughly 1μm. Without taking this into account, using τ =100μm instead of 99μm will produce an error in charge density of roughly 1%. However, the calculated charge is lower by 25% for an electret with τ =5μm and a charge layer that is 1μm below the surface.

The measurement of depth of the implanted charge represents a critical obstacle in measuring charge densities accurately. However, the resolution of charge sounding techniques is 1μm, which is not precise enough to locate charge implanted with 10keV energy.

II.3.a.ii. LATERAL RESOLUTION OF CHARGE

Assuming the implanted charge density can be approximated to a single depth, the patterned electric field from the electrets rarely extend laterally enough, as evidenced by Figure II-6 and Figure II-7, to satisfy the infinite plane assumption used to derive Equation (II.1).
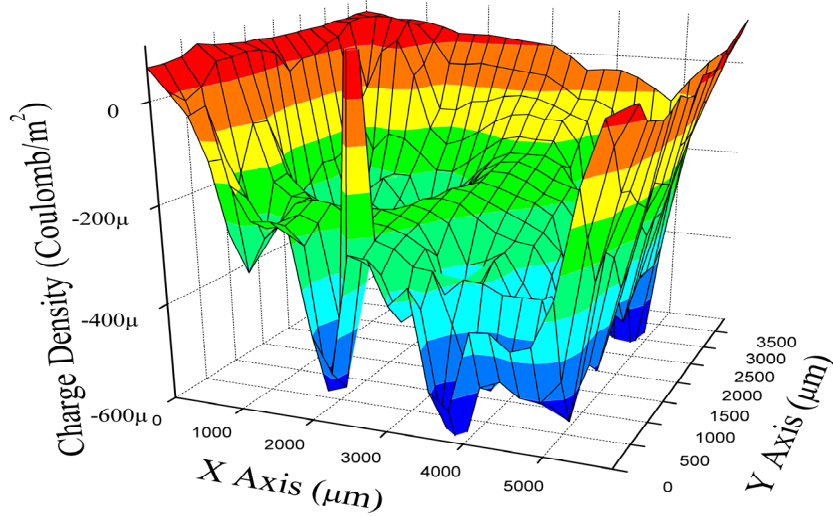
Figure II-10 Charge density measurement used to determine minimum distance between data points.

The variation of voltage over the surfaces shown in Figure II-6 and Figure II-7 begs the question, "What is the lateral resolution of the isoprobe?" The lateral resolution is defined by the spot size of the tool, which geometrically depends on the height above the surface during the measurement and the physical aperture of the probe. By taking voltage measurements over the surface every 100μm in the X-axis and 250μm in the Y-axis, a detailed plot of the surface voltage can be made.

Standard Deviation vs. Spacing of measurements
Average Charge Density vs. Spacing of measurements
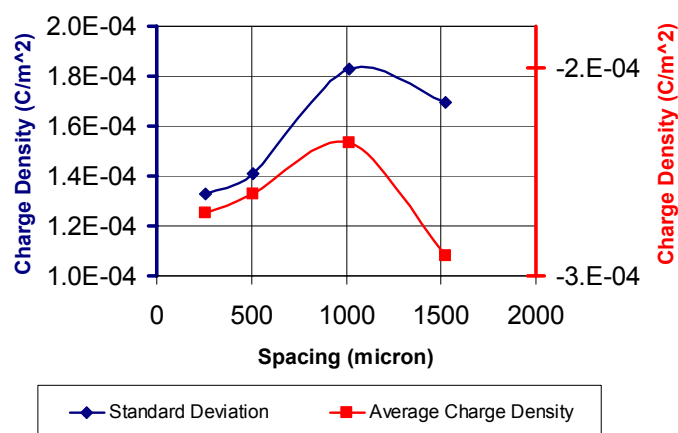
Figure II-11 Average charge density and standard deviation when dropping data points from dataset used to produce Figure II-10.

By statistically comparing neighboring data points from the scan of Figure II-10, it was determined that a measurement spacing of 1mm would allow both average measurement of charge and high contrast as shown in Figure II-12.

II.3.b. DEPTH SOUNDING TECHNIQUES

Laser induced pressure pulses and thermal pulses are often used to measure the depth of charge distributions in electrets. Recently, better engineering techniques allowed Mellinger et al. to produce three-dimensional measurements of space charge with vertical resolution of 0.5μm and lateral resolution as small as 38μm [50].
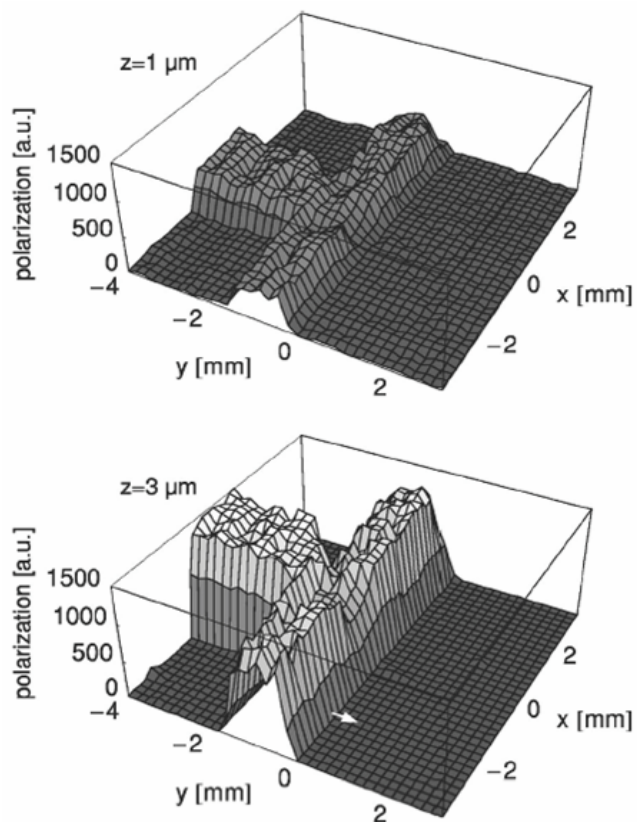
Figure II-13 Polarization map of a 11 µm thick PVDF film poled with a T-shaped electrode. At z=1µm (top graph), the polarization is significantly lower than in the bulk. The arrow indicates the direction of the high-resolution scan [ibid].

Their measurement of a 7mm x 7mm electret sample using this method and lowering lateral resolution to 200µm takes 3.5hours to complete. This may prove to be a nice tool to evaluate the characteristics of an electron implantation beam or, if the beam is already well characterized, a tool to evaluate different electret materials and how pre- and post-processing affects electrets.

II.4. UNIFORMITY

The power generators that will be described rely on a large electric field to generate power. When the back lighted thyratron implants change in a spatial Gaussian distribution, steps must be taken to produce a more uniform distribution with large electric field. After attempting some simple beam optics, a second idea came to mind that uses the insight gained from the Monte Carlo graph in Figure II-8.

II.4.a. FLOATING METAL LAYER ELECTRET

Electron beam implantation is a well-studied method for implanting electrons within dielectrics. Beam writing can be performed by raster scanning over a dielectric; it takes considerable time to implant a sufficient number of electrons while occupying an expensive machine for a menial task using this method. In contrast, a BLT provides a pulsed electron source with very large electron doses within ~100ns. Electron implantation with the BLT produces a Gaussian distribution over the surface of the electret, as in Figure II-7, which is not desirable for providing a uniform electret. To alleviate this problem, a metal layer is deposited on top of a thick dielectric layer, patterned to be electrically floating, and then sealed with a thin dielectric layer [51]. The floating metal layer provides a reference voltage and therefore an electric field non-uniformity of less than 1% of the surface as seen in

Figure II-14. The electrically floating metal layer is patterned into a circle. Charge outside the metal circle is approximately equal to the Gaussian case of Figure II-7.
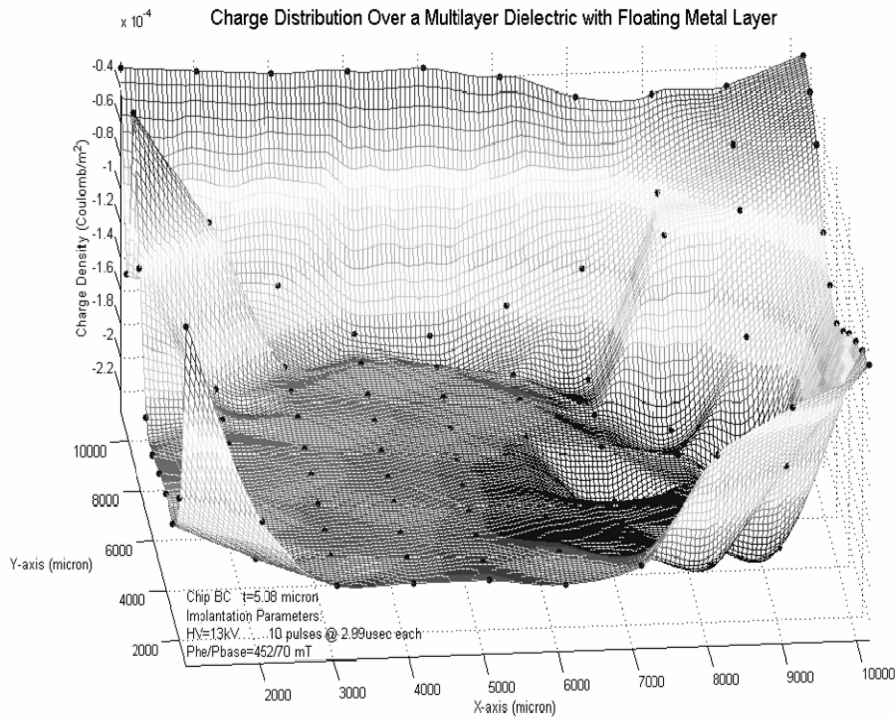
Figure II-14 Charge implanted in a chip with floating metal layer.

II.4.a.i. FLOATING METAL LAYER PROCESS

The floating metal layer electret is an entirely new structure, invented and implemented for this thesis. The typical process is to thermally evaporate a 500Å layer of aluminum on top of a 4μm to 10μm thick dielectric layer of Teflon AF, pattern the metal to be electrically floating, and then seal the metal with a 400nm thin dielectric layer of Teflon AF. After the final bake of the top layer of Teflon AF, charge can be implanted as previously described.

Teflon

SiO_2
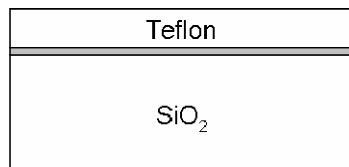
Step 1. Spin thick Teflon AF layer on metallized wafer and bake fully

Teflon

SiO_2
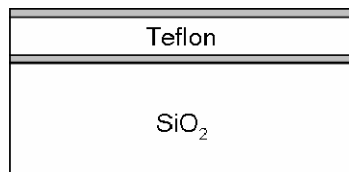
Step 2. Evaporate 500Å aluminum on top of thick Teflon

PR

Teflon

SiO_2
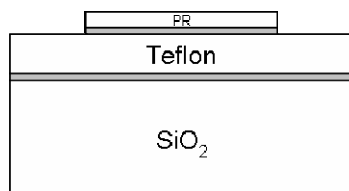
Step 3. Spin thin photoresist on top of aluminum layer, develop, etch aluminum

Teflon

SiO_2
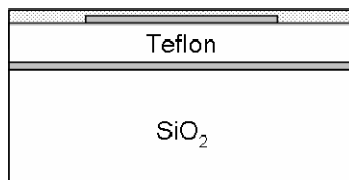
Step 4. Remove photoresist with O_2 plasma, spin 400nm thin sealing layer of Teflon AF

Table II-1 Process flow for floating metal layer electret

Some difficulties of this process are stress between layers and catastrophic breakdown through the dielectric. It may be possible to fix the first problem with the second. A catastrophic breakdown from the floating metal layer to ground can cause too much current to flow in plane within the floating metal layer. When the metal is cracked, the rush of charge may burn up thin sections of metal, which would prevent further charge decay towards ground. Lower surface potentials were consistently observed in non-cracked layers than in cracked layers after electron implantation.

II.5. CONCLUSIONS

Previous work in charging micromachined electrets was improved for uniformity by the micromachined floating metal electret. Spatial resolution of charge density was realized by use of a 2-axis X-Y stage with Z-adjustment for use with the isoprobe, which was a necessary improvement over past techniques due to the large area that must be charged and the variation that existed over the area. Process was also extended to include thicker electret materials, which allows for higher surface voltages.

CHAPTER 3

III. VARIABLE AREA ROTATIONAL ELECTRET POWER GENERATOR

Knowing that changing the overlapping area of a capacitor can cause a displacement current, the MEMS toolbox is searched for a method to solve a problem that has not been solved before. The goal is to efficiently generate power using only electrostatics.

III.1. INTRODUCTION

Electret generators (EG) are a relatively undeveloped class of power generators. An electret generator differs from an electromagnetic generator in that the electromotive force is purely electrostatic with no use of magnetic fields. An electret generator also differs from a purely electrostatic generator, sometimes called a charge pump, in that no control circuitry is needed to provide an initial electric field or accumulation of electrons on the charge shuttle of the purely electrostatic generator. A third class of electrostatic power generator uses a temporarily induced dipole moment in a dielectric, which is similar to an alternator in that both require power to set up a temporary field that is subsequently used for power generation. The main advantages that can be exploited in using an electret are that the electric field is more practical and useful on the microscale than the magnetic field, the processing of electrets is compatible with CMOS technology in contrast to magnets, and the permanent dipole of an electret eliminates any overhead required by other devices to generate power.

III.1.a. RELATED WORKS

Rotational electret power generator theory and experiment was first reported by Jefimenko [52] and later refined by Tada [53], although Sessler [45] suggests that concept may go back to Nazarov in 1954 [54]. A crude, macro-scale electret generator with a radius of 45mm was studied by Tada [55]. Maximum reported power output from Tada's (non-micro) electret generator was an uninspiring 1.02mW, which does not compare favorably with electromagnetic generators of similar scale.
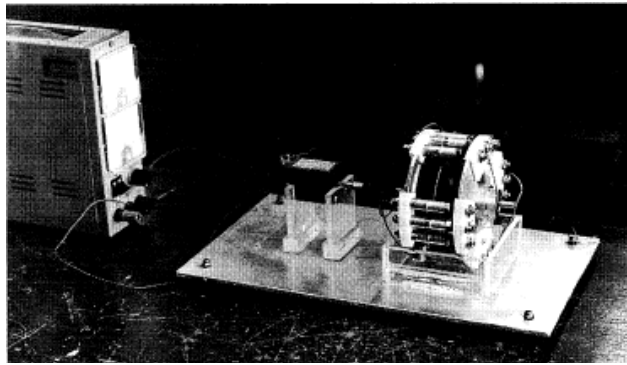
Figure III-1 First electret power generator. Tada (1992)

The key to increasing power output of this technology is better precision, which micromachining excels at producing. An optimized micromachined power generator can produce power much greater than 10mW using considerably smaller overall device dimensions than the 90mm diameter device previously mentioned. However, micromachining requires a compatible electret technology and development of a full process flow to build the entire device.

III.1.b. MICROMACHINING ELECTRETS

As an electret, Teflon can contain charge densities of -5×10^{-4} C/m2 with a theoretical lifetime of hundreds of years (supported by accelerated testing) [44]. Previous work on micro electret microphones in the Caltech Micromachining Laboratory used Teflon AF 1601-S because it is a spin-on dielectric compatible with MEMS process with good charge storage characteristics. For power generators, processing capabilities were extended to allow for multiple spins of this material and also patterning using photoresist and oxygen plasma.

Once Teflon is deposited and patterned, it must undergo a polarization or charge implantation process to become an electret. Multiple methods exist to give the Teflon a dipole moment as explained in *Chapter 2*. Here, a back lighted thyratron (BLT) [42] is utilized because of the high density of electrons, the speed of the implantation process, and the large acceleration voltage that allows electrons to be stored in deep traps where they will be stable for hundreds of years.

III.2. Theoretical Development

The theories of Jefimenko and Tada are more complex than necessary for this problem. A more practical linearized theory can easily be derived as explained below.

Beginning with the infinite plane approximation, which assumes that the width of the electrodes is large compared to the distance between them, a linearized theory is derived to describe a rotational electret power generator that acts as a fixed-charge, variable capacitance device. The geometry used in this derivation is that of Figure III-2 and Figure III-3.
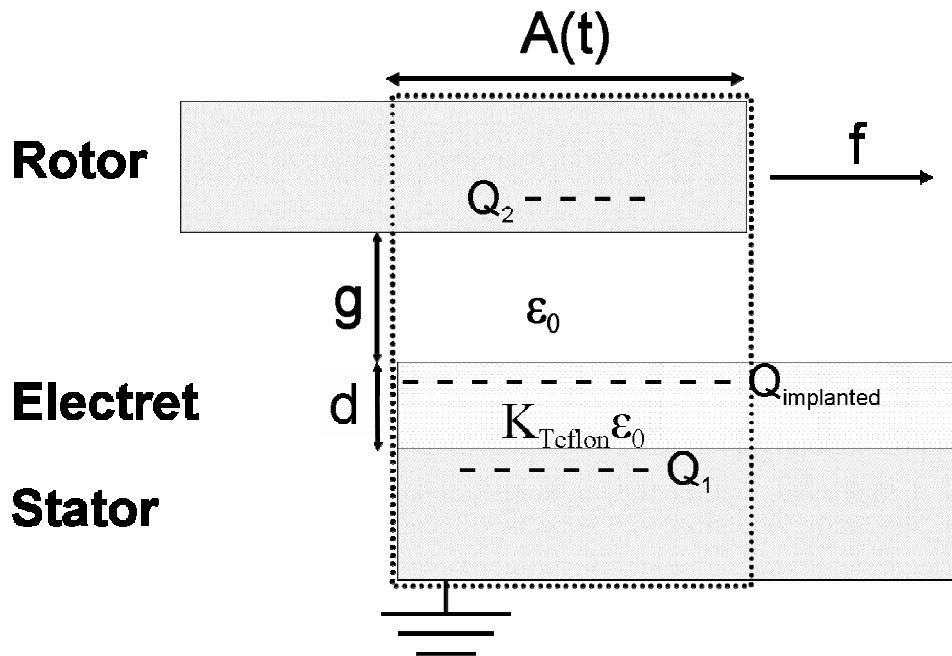
Figure III-2. Schematic of electret generator (cross-section view).
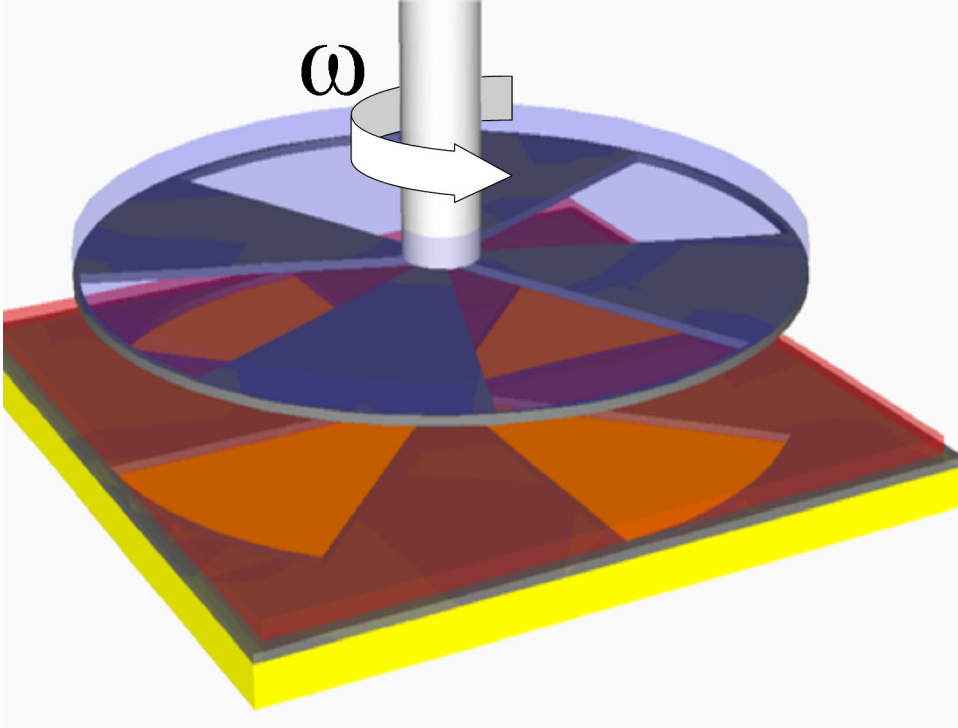
Figure III-3. Perspective view of electret generator showing a 4-pole rotor and stator.

Charge is assumed to exist just below the surface of the Teflon with a uniform spatial density σ. $Q_{Teflon}(t)$ is the charge implanted into the Teflon and only residing in the capacitor configuration defined by the overlapping area of the top and bottom plates. Therefore,

$$Q_{Teflon}(t) = \sigma A(t) \qquad \text{(III.1)}$$

where $A(t)$ is the area of the overlapping top and bottom plates. The area function will not be defined at this point to keep the derivation perfectly generalizable for different geometries, which has already proven useful for the seismic electret generator [56].

Conservation of charge in the dotted region of Figure III-2 implies

$$Q_{Teflon}(t) = Q_1(t) + Q_2(t) \qquad \text{(III.2)}$$

Then, $Q_1(t)$ and $Q_2(t)$ are the induced mirror charges on the top and bottom plate due to the charge implanted in the Teflon.

The equivalent circuit model of Figure III-4 is derived from the conceptual model of Figure III-2.
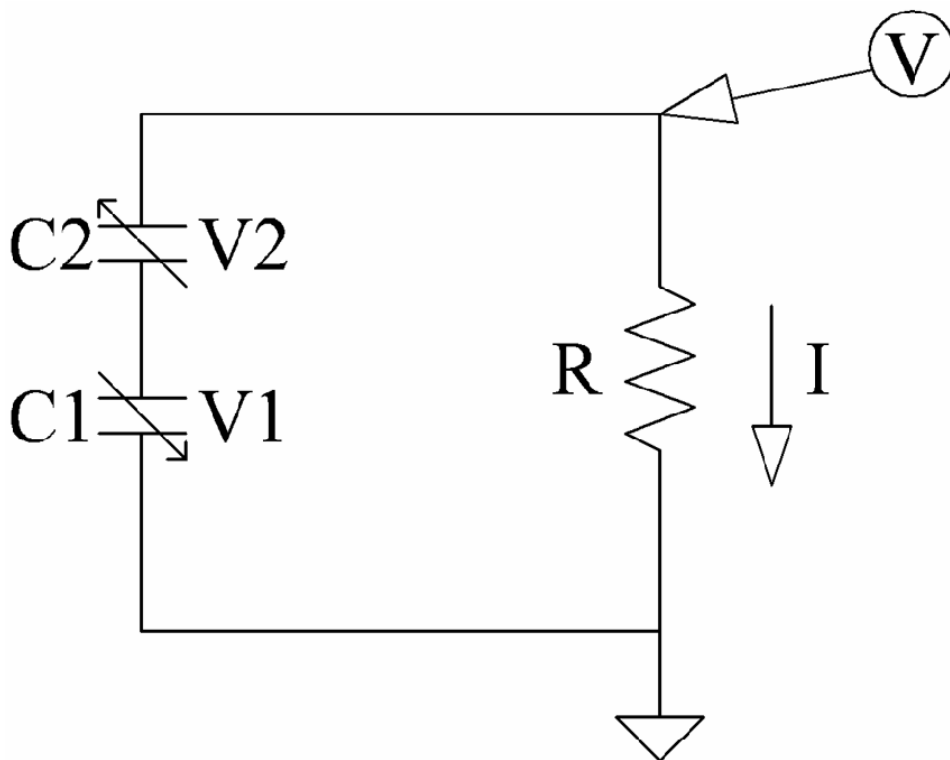
Figure III-4 Equivalent circuit for variable area electret power generator.

The capacitance of the overlapping capacitors is defined by

$$C_1(t) = \frac{k_{teflon}\varepsilon_0}{d} A(t) \tag{III.3}$$

$$C_2(t) = \frac{\varepsilon_0}{g} A(t) \tag{III.4}$$

illustrates how Kirchhoff's Voltage Law can be used to solve for the output voltage of the generator

$$V(t) = \frac{-Q_1(t)}{C_1(t)} + \frac{Q_2(t)}{C_2(t)} \tag{III.5}$$

Substitution of equations (III.2) and then (III.1) to eliminate Q1(t) and QTeflon(t) from equation (III.5) and subsequent collecting of terms yields

$$V(t) = \left(\frac{-d}{k_{teflon}\varepsilon_0}\right)\sigma + \left(\frac{d}{k_{teflon}\varepsilon_0} + \frac{g}{\varepsilon_0}\right)\frac{Q_2(t)}{A(t)} \tag{III.6}$$

Examining Figure III-4, the current through the load resistor is defined as

$$V(t) = IR = -\frac{\partial Q_2(t)}{\partial t} R \tag{III.7}$$

Combining equations (III.6) and (III.7) gives a linear, first order ordinary differential equation:

$$\frac{\partial Q_2(t)}{\partial t} + \left(\frac{d}{K_{teflon}\varepsilon_0} + \frac{g}{\varepsilon_0}\right)\frac{1}{R\, A(t)}Q_2(t) = \left(\frac{1}{R}\right)\left(\frac{d}{K_{teflon}\varepsilon_0}\right)\sigma \tag{III.8}$$

The analytical solution to equation (III.8) is obtained by the well known integrating factor

technique [57]

The function $A(t)$ is purposefully left undefined up till now, which gives the freedom to

choose $A(t)$ to describe many different phenomena. The most obvious choice for $A(t)$

is to describe the steady state power generated by a rotational power generator, which

will be shown momentarily. Another choice for $A(t)$ could allow derivation of an

equation describing the transient properties of the rotational power generator, which has

never been reported. Other types of electret power generators can also be described, such

as a moving mass on springs with a horizontally patterned geometry. Any function

describing the change in overlapping area with time can be used with similar result,

although functions where area does not change linearly with time can complicate the

simple integral at the end of this derivation.

For a rotational geometry and constant rotational speed, $A(t)$, the overlapping area

shown in the dotted box of Figure III-2, is defined by the following:

$$A(t) = \begin{cases} \dfrac{n\pi\, r^2 f}{2}t & t:0<t<\dfrac{1}{2nf} \\[4mm] -\dfrac{n\,\pi\, r^2 f}{2}t & t:\dfrac{1}{2nf}<t<\dfrac{1}{nf} \end{cases} \quad \text{for} \qquad\qquad \text{(III.9)}$$

From Figure III-3, n is the number of poles, r is the radius of the generator, and t is the

time. Examining the symmetry of the generator geometry, the steady state electrical

output is expected to have a periodicity of $\dfrac{1}{nf}$, which is the rotational period divided by

the number of poles. Now that $A(t)$ is defined, it is possible to solve for the current

flowing through the resistor

$$I(t) = \dfrac{-\sigma \dfrac{d}{\varepsilon_0}}{R + \dfrac{1}{n\,\pi\,r^2\,f}\left(\dfrac{d}{K_{teflon}\,\varepsilon_0} + \dfrac{g}{\varepsilon_0}\right)} \qquad \text{(III.10)}$$

and

$$P(t) = I^2(t)\,R \qquad \text{(III.11)}$$

for this purely resistive load. Setting $\dfrac{\partial P}{\partial R}=0$, maximum power is then achieved when the

load resistance is

$$R_{optimal} = \dfrac{1}{n\,\pi\,r^2\,f}\left(\dfrac{d}{K_{teflon}\,\varepsilon_0} + \dfrac{g}{\varepsilon_0}\right) \qquad \text{(III.12)}$$

This gives a load-matched power equation

$$P_{optimal} = \dfrac{\sigma^2\,n\,\pi\,r^2\,f}{\dfrac{4\,k_{teflon}\,\varepsilon_0}{d}\left(1+\dfrac{k_{teflon}\,g}{d}\right)} \qquad \text{(III.13)}$$

This result shows that maximum power occurs when σ, n, r, f, and d are maximized.

Also, k_{Teflon} and g should be minimized to yield maximum power. Each quantity can be

improved, however, secondary relationships between variables do exist and limit maximization efforts, as explained below.

III.3. DESIGN AND FABRICATION

Product design benefits from iterative design cycles, and the evolution of the rotational electret power generators involved many different processes to get to where it is today. A general device design will be explained followed by some specific examples of process flows.

III.3.a. DESIGN OPTIMIZATION

The following table lists the constraints that effect the design of the generator. Some of the constraints are due to material limitations, some are defined design parameters, and other are due to governing physics. Design is iterative because improving some parameters will affect other design parameters. It is important to understand the relationships between design parameters before beginning the actual design.

Variable	Increase or decrease?	State of the art	Limitations	Other relationships
σ	Increase	$5 \times 10^{-4} C/m^2$	Breakdown field	σ decreases as d increases
n	Increase	128	Lithography, infinite plane approximation	$\frac{\pi r}{n} > 10 \ (d+g)$ or infinite plane approximation fails
r	Increase	1cm	Size limitation, gap control	Design constraint
f	Increase	20kRPM	Bearings	Design specifies 100kRPM
d	Increase	10μm	Processing techniques	σ decreases as d increases
k_{Teflon}	Decrease	1.93	Already lowest known dielectric	Affects σ and lifetime of charge
g	Decrease	80μm	Bearings, angular alignment	$g < \dfrac{d}{K_{teflon}}$ or gap will dominate power generation

Table III-1 REPG parameters for optimization

III.3.a.i. CHARGE DENSITY

Charge density, σ, should be increased without limit. Unfortunately, charge is limited by the dielectric strength of the material and the trapping ability. In the case of Teflon AF 1601-S, the limit for E_{max} is 20V/μm.

III.3.a.ii. DIELECTRIC CONSTANT

Power output increases with decreasing dielectric constant, k_{Teflon}, which is why Teflon AF with dielectric constant of 1.93 is chosen. Teflon is the optimal dielectric since it has

the lowest dielectric constant of any known material. Choosing a different dielectric, such as oxide, material may allow storage of more charge but the lifetime of the charge will be significantly reduced. Only gasses and vacuum have better permittivity, and they can be included into the Teflon to lower its effective permittivity.

III.3.a.iii. GAP SPACING

Gap spacing, g, should be minimized. Setting $g = \dfrac{d}{k_{Teflon}}$ allows Equation (III.13) to be rewritten as

$$P_{optimal} = \frac{\sigma^2 \, n \, \pi \, r^2 \, f}{8 \, \varepsilon_0 \, g} \qquad \text{(III.14)}$$

While setting $g \, \Box \, \dfrac{d}{k_{Teflon}}$ gives

$$P_{optimal} = \frac{\sigma^2 \, n \, \pi \, r^2 \, f}{\dfrac{4 \, k_{teflon} \, \varepsilon_0}{d}} \qquad \text{(III.15)}$$

Therefore, every effort should be made to decrease gap spacing. Decreasing gap spacing also has a positive effect on the maximum number of poles, which is described in Section III.3.a.iv. However, gap control is found to be the most difficult part of the rotary electret power generator, so the first criterion that $g = \dfrac{d}{k_{Teflon}}$ is the most difficult to satisfy.

III.3.a.iv. NUMBER OF POLES

The number of poles, n, should be as high as possible as long as the back-end circuitry (light bulb or rectification and/or regulation circuitry) works well at the output frequency of the generator. In the case of $n = 128$ and $f = 100kRPM$, the frequency of the electrical output would be $f_{output} = 213kHz$, which may cause problems if external capacitance is not well controlled.

The real limit of n is more likely to be the stray electric fields. If the electrode area is confined to where the infinite plane approximation holds, then A is constrained by n, d, and g.
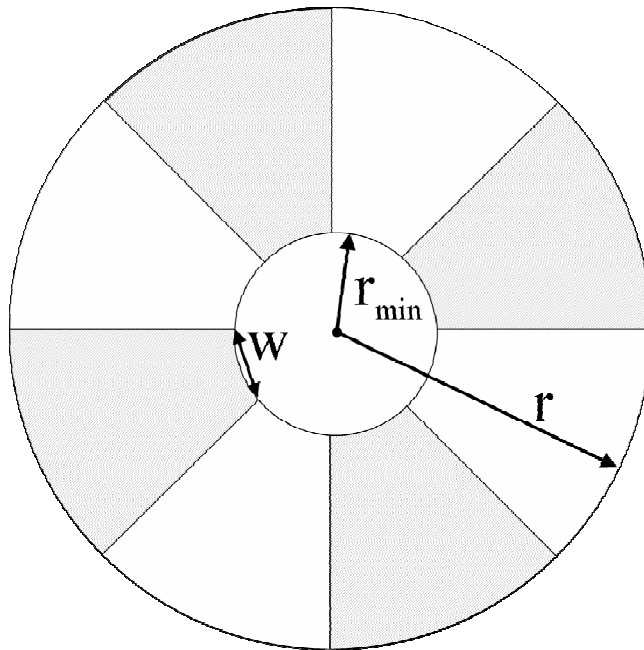
Figure III-5 Used to find the critical width w from gap distance

To neglect the fringing field, the smallest dimension within 90% of the active generator area must be ten times larger than the gap distance. This point is demonstrated using values comparable to the first generator. Since 90% of the effective area of an $r = 5\text{mm}$ generator is outside $r = 1.58\text{mm}$, the shortest dimension w (see Figure III-5) is found to be 1.2mm by using the number of poles, $n = 4$, and the law of cosines. Assuming w must be ten times larger than g and it was previously stated that $g = \dfrac{d}{k_{Teflon}}$, then w need only be 22.5µm for a 9µm dielectric thickness. If g really was as easy to control, the condition would certainly be met. By using this argument, it is expected to see good performance in generators with a few hundred poles.

III.3.b. FABRICATION CONSIDERATIONS

The geometry of Figure III-3 was chosen for the electret power generator to accommodate a rotational input and allow for layered, 2-dimensional fabrication processes that are standard in the Caltech Micromachining Laboratory. The rotor and stator are fabricated independently and then mounted in a testbed. The layered fabrication allows for extremely flat surfaces to be obtained, which is necessary to obtain minimum gap distance to produce maximum power output.

The rotor consists of a substrate to provide mechanical support and a patterned metal electrode. The stator consists of a substrate, patterned metal, and an electret material. By symmetry, it does not matter if the rotor or stator is rotated while the other piece is held still.

An external circuit is electrically connected between the electrodes of the rotor and stator. This circuit minimally consists of a load resistor to allow current to flow between the electrodes and measure the power transferred to the resistor; however, future work will replace the resistor with rectifying and conditioning circuitry to produce electrical power for specific applications.

To prevent the rotor and stator from having physical contact with each other, a gap distance must be maintained by some mechanism. A gap is necessary to prevent wear to the electret material. Furthermore, physical contact between the rotor and stator will lower the efficiency of the generator when energy is lost due to friction. The preferred method to maintain gap distance is with bearings that allow relative rotation and electrical connection to the rotor. For this reason, air bearings are not used despite some favorable characteristics.

An external rotation must be applied to the rotor. For this, the rotor is connected to an axle that is connected to a motor. Electromagnetic coupling may be used in the future to reduce unwanted radial and axial vibrations caused by physical coupling.

When assembled, the rotor and stator should face each other with the normal to the surfaces being antiparallel. The centers of the rotor and stator should also align. Finally, the gap distance should be as small as possible according to Equation (III.13). Any deviation in these will cause a loss in power generation.

III.3.b.i. TEFLON PROCESSING

In previous processing [58, 59], it was determined that a 1.2μm Teflon layer can be spun-on a flat wafer if the Teflon solution is 6% solids and 94% Fluorinert FC-75, as supplied by Dupont. This thin film initially has a rough surface on the order of +/-25% of the film thickness. A long prebake at 330°C for 15 minutes is necessary to allow the surface to reflow to lower the roughness. Baking at this temperature also has the added effect of removing all solvent, which is a necessary step when spinning multiple layers of Teflon. Failing to remove all solvent will prevent subsequent Teflon films from adhering to the surface.

Applying HMDS vapor for 3 minutes to the fully baked, spun-on Teflon modifies its naturally hydrophobic nature enough for photoresist to be spun on top of the Teflon. Further trials proved that spinning Teflon on fully baked Teflon is also possible with use of HMDS. The adhesion between Teflon layers appears to be very good, and often was better than adhesion between thermally evaporated aluminum and a thermally oxidized silicon substrate. In the case of a floating metal layer, adhesion between the aluminum that was evaporated on top of Teflon is sufficient unless any part of the Teflon-aluminum interface is exposed to solvents. Thus, floating metal layers must be sealed before wet dicing or other wet etch steps occur.

DuPont also supplies an 18% solids version of the Teflon AF 1600-S, but this solution is too viscous for conventional spin coating. A 7.4% solids mixture is made by mixing the 18% solids version of Teflon with Fluorinert FC-40. This solution produces spun-on

films 9μm thick at 500RPM. Fluorinert FC-40 has similar electrical characteristics to Fluorinert FC-75, but FC-40 has a kinematic viscosity 2.75 times higher than FC-75. Furthermore, the 1.2μm film had height fluctuations greater than +/-25% while the 9μm film had variations less than 1%. The main disadvantage of FC-40 is its higher boiling point, which means higher temperatures and longer bake times are required to drive off all solvent from the thicker Teflon film.

Fluorinert Liquid	FC-87	FC-72	FC-84	FC-77	FC-104	FC-75	FC-3283	FC-40
Average Molecular Weight	290	340	388	415	435	420	521	650
Typical Boiling Point, °C	30	56	80	97	101	102	128	155
PourPoint, °C	-101	-90	-95	-95	-65	-88	-50	-57
Density, g/cm³	1.63	1.68	1.73	1.78	1.77	1.77	1.82	1.87
Density, -54°C g/cm³	1.84	1.90	1.93	1.97	1.96	1.96	□	□
Kinematic Viscosity, cs	0.4	0.4	0.55	0.8	0.8	0.8	0.75	2.2

Figure III-6 Table of different Fluorinert solvents, which are used to dilute Teflon AF 1601-S

III.3.c. REPG VERSION 1.0

The first design had rotors with a radius of 4mm and stators with a radius of 5mm. Design size was chosen to maximize available area on a $1cm^2$ chip, which is the area available using the stepper to pattern the substrates. The rotor is only 4mm in radius so that electrical contact to the ground layer of the stator is possible with silver paste. Since only regions where the rotor and stator overlap result in the production of electricity, for all practical purposes, r_{eff} = 4mm.

The number of poles in these experiments, n = 4, was chosen to compare with results found in literature. In Tada's work [55, 60], the number of poles remains low due to the method of making them, namely cutting by hand. It is preferable to use MEMS lithography, which is capable of producing linewidths smaller than 10μm and far exceeding the assumptions that fringing fields can be neglected. This limit will be explored later.

Teflon thickness for REPG v1.0 was 9μm, and in contrast to Tada's setup, was on the stator instead of the rotor. This configuration was chosen for the ability to test different electret thicknesses and charge densities without having to remount the rotor.

The process flow of a rotor and stator with dielectric is shown in Figure III-7. Rotors and stators for electret generators have a matching number of poles and similar electrode geometry.

Rotors   *Stators*

Evaporate 2000Å aluminum   Evaporate 2000Å aluminum

Pattern aluminum   Pattern aluminum

                                              Spin coat 9μm Teflon AF 1601-S

Dice rotors
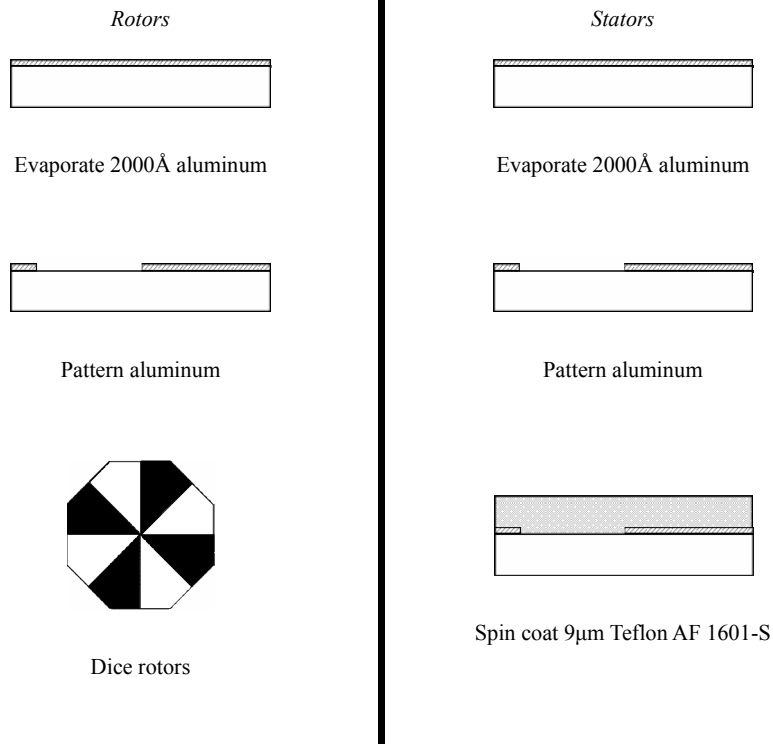
Figure III-7 Process flow for first version of REPG

For the rotor, 2000Å aluminum was evaporated onto a quartz wafer and then patterned. The wafer was then diced, and one die was diced into an octagonal shape to closer approximate a circular rotor. The rotor is glued to a metal axle on a testbed, and is electrically connected to the axle with silver paste. The rotor should be mounted with its plane normal aligned to the long axis of the rotating axle or else the planes of the rotor and stator cannot be parallel during rotation. The rotational plane misalignment angle is the angle between the rotor's normal and the rotational axis and will be discussed further in Section III.4.b.ii.

Stators are produced by first evaporating 2000Å aluminum onto a quartz wafer. The aluminum layer is patterned and then the wafer is diced into 1cm x 1cm squares. Then a thick layer of Teflon AF 1601-S is spun on individual stators and baked. After baking, the Teflon is implanted with electrons from the back-lighted thyratron. Finally, a small piece of Teflon is removed with a razor blade from a corner of the stator for electrical connection by silver past and a wire. The stator is mounted to a 5-axis micropositioner on the testbed.

Figure III-8 REPG V1.0 mounted on testbed version 1. Photo taken before rotor and stator are aligned.
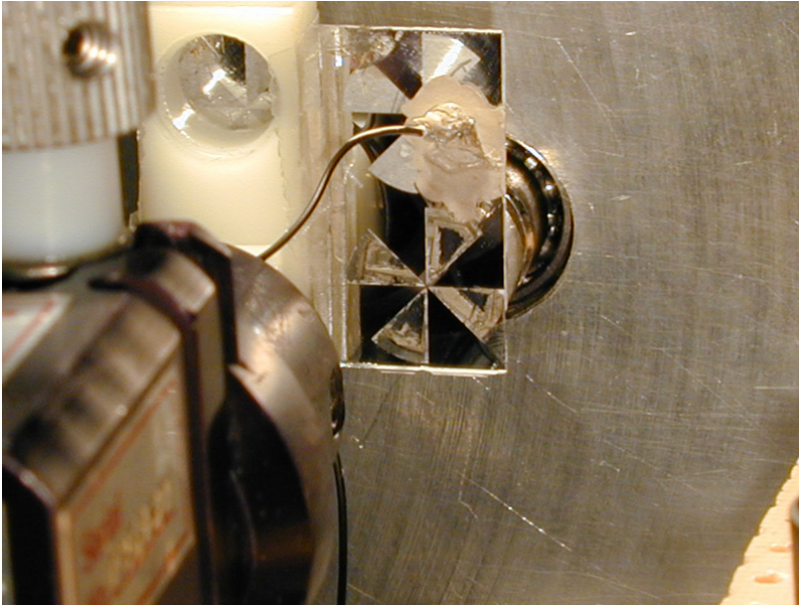
Figure III-9 REPG V1.0 mounted on testbed version 1. Photo taken after rotor and stator are aligned.

III.3.d. REPG Version 2.0

The second REPG design included bulk-etched cavities for producing thick electrets on silicon while maintaining the excellent planarity of the silicon wafer. By spinning consecutive layers, it was determined that Teflon can be spin-coated up to about 10μm thick before cracking. However, by first etching a 40μm deep vertical cavity into silicon using a deep reactive ion etcher (DRIE) running standard Bosch process, it is possible to pour liquid Teflon AF into the cavities and build up a 40μm thick Teflon layer that could later be implanted with charge. This is the bulk-etched electret, which is patented along with the electret power generators. The process for creating these cavities is the following:

1. Bare ground plane etched in silicon

2. Liquid Telfon AF 6% poured on surface

3. Air dry and bake for 30 min at 100 degrees

4. Plastic reflow, 20 min at 350 degrees on a hotplate

5. Scrape off excess
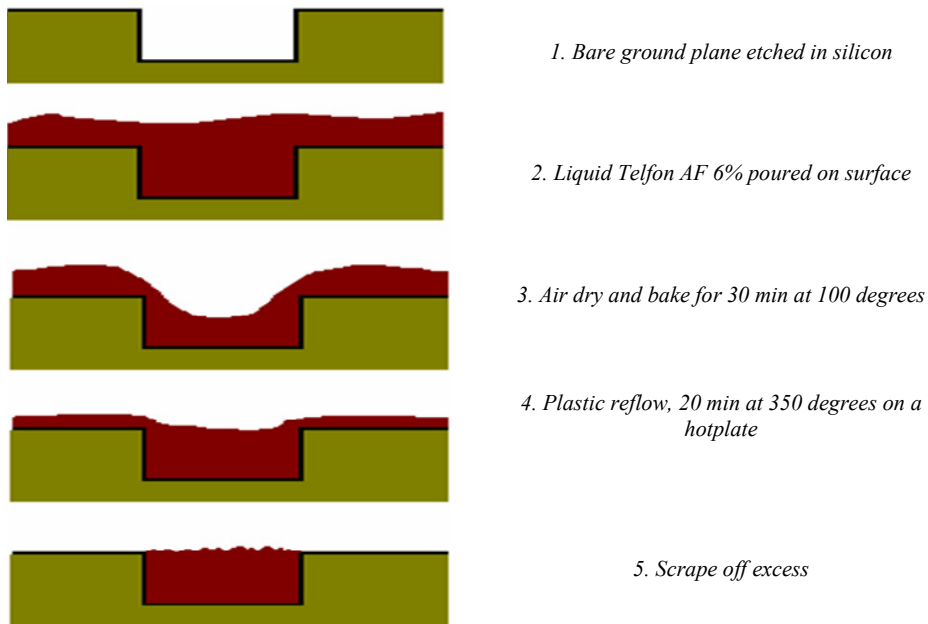
Figure III-10 Process flow for bulk-etched electrets

The process of Figure III-10 begins by using standard lithography to define the location of the trenches in a photoresist mask. The photoresist then serves as a physical etch barrier when the silicon wafer is exposed to the anisotropic, inductively coupled SF6 plasma etch of the deep reactive ion etcher (DRIE) in what is called the standard Bosch process. The Bosch process is advantageous because it provides for 90° sidewalls, which allows for fine patterning of an electret structure. The Bosch etch process is used to etch 40μm deep trenches. Then the photoresist is stripped and the wafer cleaned. The last part of step 1 is the thermal evaporation of 2000Å of aluminum onto the surface in a 5μTorr vacuum, which provides the ground plane for the electret. Steps 2 though 5 are shown in

Figure III-10, and basically require a patient graduate student (or undergraduate student in the case of Svanhild Simonson) to perform the operations by hand.

As can be seen in Figure III-11, the thick layer of Teflon AF is cracked after step 3, which is caused by the large volume change as roughly 94% of the liquid evaporates and only 6% is left behind. Figure III-12 demonstrates that reflowing of Teflon AF in step 4 is possible.
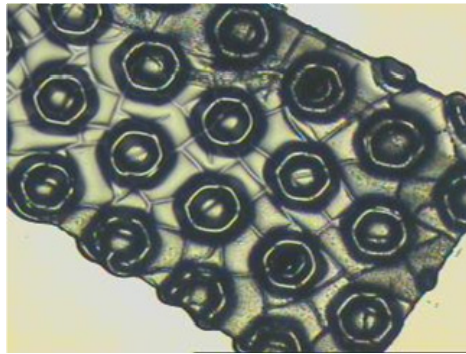
Figure III-11 Bulk-etched Teflon with anchors before reflow step.
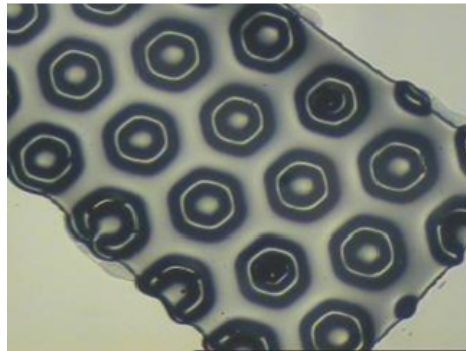
Figure III-12 Bulk-etched Teflon with anchors after reflow step.

The features inside the channels are anchors to prevent the Teflon from delaminating from the silicon during step 5. The adhesion mechanism of Teflon to a substrate is purely mechanical and not chemical. Therefore, small, deep trenches can be etched into the silicon substrate prior to the cavity etch of step 1, which provides greater opportunities for the reflowed Teflon to mechanically latch onto the substrate. The final improvement of this process was to perform an extended, isotropic etch of these small deep cavities to provide a lock structure for the Teflon to hold onto the substrate. This improvement was subsequently applied to parylene and was more thoroughly explored in the Caltech Micromachining Laboratory by Matthieu Liger.

This electret can also be improved by using the floating metal layer process afterwards.

III.3.e. REPG VERSION 3.0

The purpose of this design was to explore the power generated by larger rotors and stators as well as to increase the number of poles of the devices. This design had rotors with a radius of 10mm and stators with a radius of 10mm. Lithography for this design was performed with a Kasper 2100 contact aligner instead of the stepper. The process follows exactly as before with the exception of using the different exposure system.

The number of poles was varied from $n = 4$ to 256. Although the rotors and stators were produced, the full range of experiments were not performed because the angular misalignment was too large and the gap control not precise enough to compare power generated with the number of poles.

III.3.f. REPG Version 4.0, 5.0 / Prototype Version 1.0, 2.0

The goal of the next designs was to eliminate the need for an external testbed. The next design had rotors with a radius of 4.9mm and stators with a radius of 4.9mm, which was chosen to be compatible with lithography on the stepper. The stepper was used for its superior alignment abilities, which would be needed for this version.   Process is significantly more complicated than previous versions, and requires multiple lithography steps as well as new etching and deposition techniques.
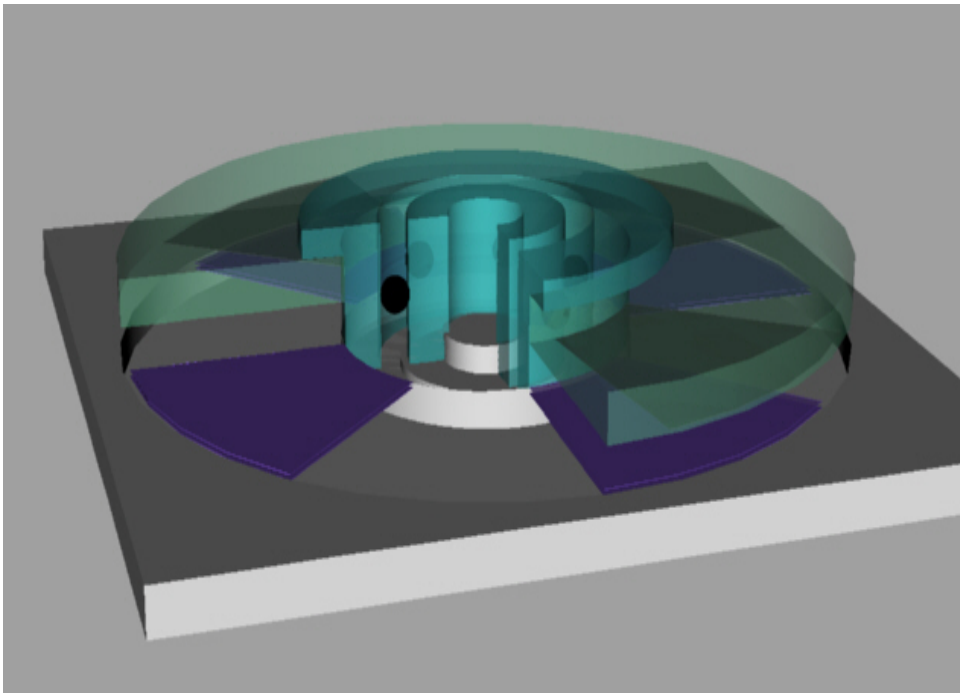
Figure III-13 REPG version 4.0. Cutaway view of final assembled device including bearings.

A cutaway of the final proposed device can be seen in Figure III-13. A commercially available flanged ABEC 9 bearing was used in the design to provide structural support

for the rotor as well as an electrical connection to the rotor electrode. Process for this device was accomplished with a delay mask technique for successive anisotropic etches using the DRIE running standard Bosch process.

While machining the rotors and stators, the design requirement was modified so that the radius of the rotors and stators was 10mm. This could allow for greater power production and it more closely matches the design requirements of the DARPA grant discussed in Section I.6.
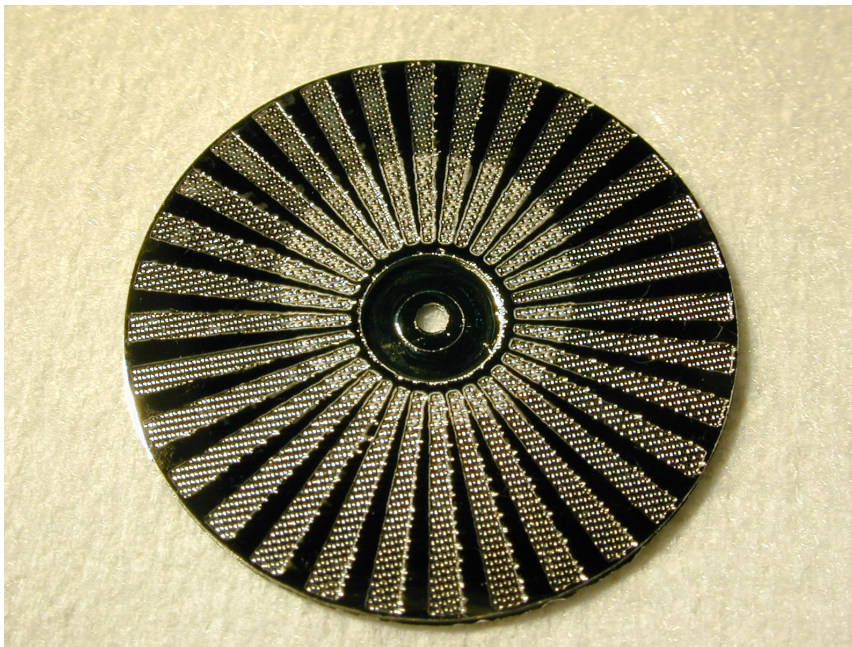
Figure III-14 Stator for REPG version 5.0. This design incorporated the use of bulk-etched cavities.

Although some final devices were produced (Figure III-14), it was determined that the angular free angle of the bearings was too great to maintain adequate gap control. No successful test was ever performed using these devices.

III.4. EXPERIMENTAL RESULTS

III.4.a. CHARGE

Charge densities are measured with a Monroe Electronics isoprobe Model 244 with a high resolution 1024AEH probe as described in Section II.3.a. The majority of samples displayed charge densities of -5×10^{-4} Coul/m^2 as expected. The bulk-etched electrets had charge densities near -1×10^{-4} Coul/m^2, which is significantly below the maximum limit. None of the bulk-etched electrets were used for power generation tests.

Triboelectrically charged samples (charge density shown in Figure III-15) provided initially large charge densities in excess of -5×10^{-4} Coul/m^2, but the charge half-life was on the order of minutes. Because the charge is unstable, triboelectrically charged samples were not reliable for power generation testing and were not used.
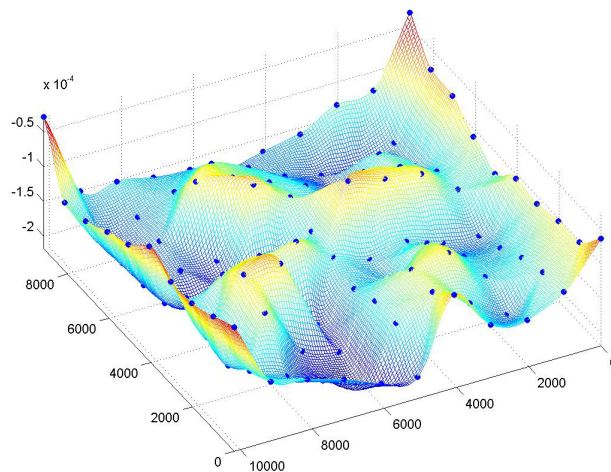
Figure III-15 Charge density measurements of a 4-pole floating metal layer electret that is triboelectrically charged

III.4.b. TESTBEDS

After fabrication of the rotor and stator it is necessary to mount them to an apparatus that can supply rotation and maintain tight tolerances for the gap distance and the alignments. Power generation experiments using the testbed involve setting the gap distance, driving the motor at different speeds, and simultaneous measurement of speed and power output. The power lead is connected to a simple op-amp, National Semiconductor LF356, in a voltage follower configuration with 10^{12} Ohm input impedance.

This high impedance allows load matching by placing different load resistors across the power and ground. Power output is measured by two different means: (a) voltage output from the amplifier is fed to an HP 54503A 500MHz Digitizing Oscilloscope to observe the waveform or (b) voltage output from the amplifier is measured in V_{RMS} with a Fluke 87III True RMS handheld multimeter. Power from the generator is simply V_{RMS}^2 / R_L .

While chasing increased power output and reliability, it was necessary to build several testbeds. The key characteristics of a testbed are rotational speed ω, angular misalignment of the rotor from the rotor axis θ_{stator} , and precision for positioning of the stator in x, y, z, ψ_{stator} and ϕ_{stator} . Methods to calibrate the testbeds will be given first followed by descriptions of the actual testbeds.

III.4.b.i. ROTATIONAL SPEED

Several methods of measuring the speed were employed to check for accuracy. A stroboscopic tachometer showed some drift from other measurement techniques, so the output waveform from the 4-pole generator was used directly by measuring $n = 4$ periods of the output signal. The motor used in testbed version 1 and version 3 is a 6-pole motor, and confirmation of speed measurements was made by connecting a secondary channel of the oscilloscope across the terminals of the motor and verifying that 6 periods of back-emf of the motor corresponded to 4 periods of the generator. Additionally, the Fluke handheld multimeter has an option to measure the frequency of an ac signal, which, as expected, reported exactly 4 times larger frequency of the power generated with a $n = 4$ generator. The oscilloscope was the primary source of speed measurements. Pulse width modulation was not a viable option to control speed since the motor used draws a current up to 30A.

In testbed version 2, the motor did not have 6 poles, but speed measurements were taken from the generator for that version.

The fourth version of the testbed was not used, but had testing proceeded it would have been necessary to measure both the speed from the motor and the speed of the generator. This is necessary because the motor would be magnetically coupled to the rotor, and synchronization cannot be guaranteed.

III.4.b.ii. ROTATIONAL ANGULAR MISALIGNMENT

The first testbed exhibited an angular misalignment of 0.46˚ for the rotor, which was measured by shining a laser pointer at the spinning rotor and measuring the radius of the reflected circle and the baseline distance as shown in Figure III-16.

Figure III-16 Proceedure for measuring angular misalignment

Because the rotor is fabricated on a glass substrate with excellent flatness, the misalignment of the rotor can be determined using a laser, the law of reflection, a ruler and simple geometry.
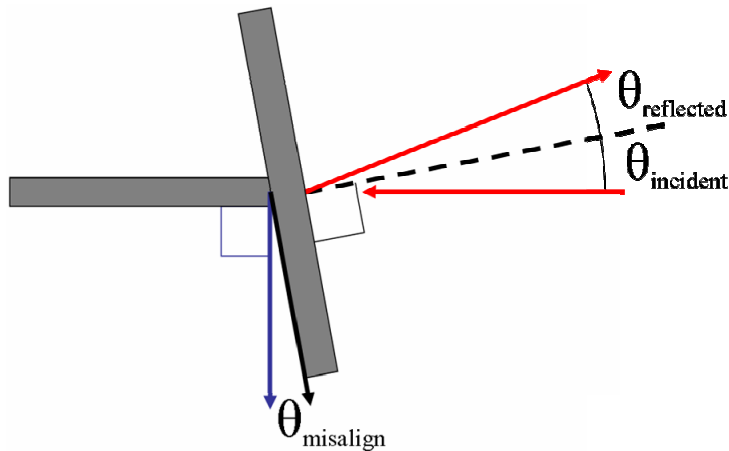
Figure III-17 Law of reflections on laser trajectory used to find angular misalignment

III.4.b.ii.1. Testbed Version 1

A 5-axis micropositioner is used for aligning the stator to the rotor. In trying to minimize the gap spacing, the stator is lightly crashed into the rotor at one point, but because of angular misalignment (measured to be 0.163˚) the far end of the rotor is at least 45.8μm away from the stator. The ground lead of the generator is the ground of the stator and the power lead is the chassis of the testbed which is electrically connected to the rotor through a bearing.
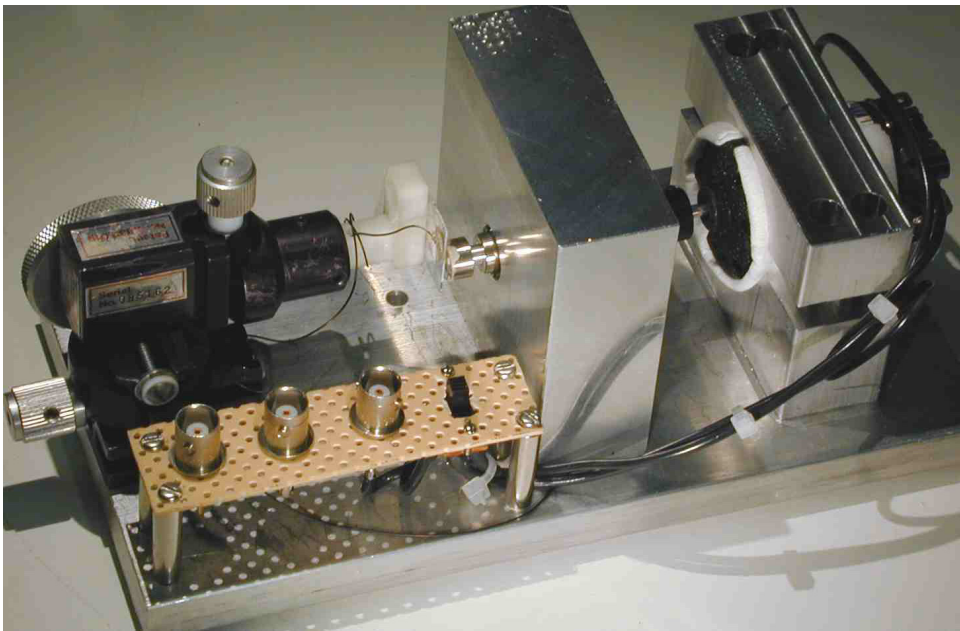
Figure III-18 Testbed with rotor and stator mounted.

III.4.b.ii.2. Testbed Version 2

In an attempt to minimize stator angular offset, a spring-loaded ball joint was designed to allow for perfect angular alignment of the stator to the rotor (when stopped) by pressing the rotor and stator together and then slowly backing-off before turning on the motor. The ball joint provides 3-axis rotation, although only 2 axes are required.
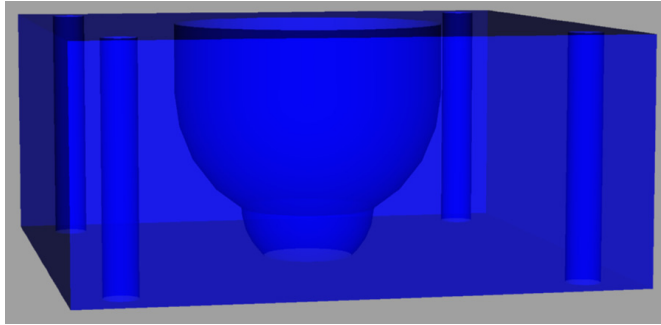
Figure III-19 Side view of ball joint
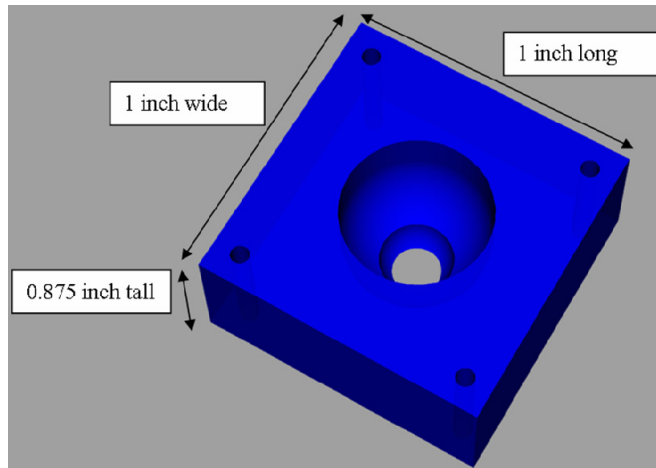
Figure III-20 Inside View of ball joint

The stators are mounted with superglue on flat aluminum plates and electrically connected to the aluminum plates with silver paste. The stator plates can be easily screwed into the spring-loaded ball-joint. A 3-axis micropositioner with 80-threads per inch (corresponding to 317.5μm/revolution) and larger knobs is used for aligning the stator to the rotor in this version. The rotor is superglued onto the motor's gear. Then silver paste is used to electrically connect the rotor to the gear, which is electrically connected to the chassis.

The powered wire is connected to the stator's metal backing plate. The ground wire is connected to the chassis at the bottom of the motor's mounting block. The ball inside the ball joint is made entirely of Teflon, which prevents electrical connection from the stator to the chassis.

The alignment process is relatively simple. With the stator slightly withdrawn and the motor off, the stator is adjusted with x and y of the 3-axis positioner so that the center of the rotor and stator are approximately aligned. Then, ψ_{stator} and ϕ_{stator} are set to zero by gently crashing the stator into the rotor a few times to allow the ball joint to settle. After the rotor and stator are parallel, the stator is backed off by approximately 100μm (~120 degrees rotation) so the motor can be turned on. The stator is then moved closer to the spinning rotor in four ~25μm increments, corresponding to 30 degree increments. The 30 degree increments continue until there is slight audible noise emanating from contact between the spinning rotor and stator. The electrical signal is then monitored while x and y adjustments are made to maximize the output power signal.

An obvious problem with this system is the lack of precision in the angular alignments ψ_{stator} and ϕ_{stator}, which are assumed to be perfect. In fact, if this system does function as well as it should, then that ψ_{stator} matches θ_{rotor}, and ϕ_{stator} is assumed to be zero. This ensures that angular misalignment, and thus gap control, has at least twice the error of θ_{rotor} alone.

In trying to minimize the gap spacing, the stator is lightly crashed into the rotor at one point, but because of angular misalignment the far end of the rotor is at least 80μm away from the stator. The ground lead of the generator is the ground of the stator and the power lead is the chassis of the testbed which is electrically connected to the rotor through a bearing.
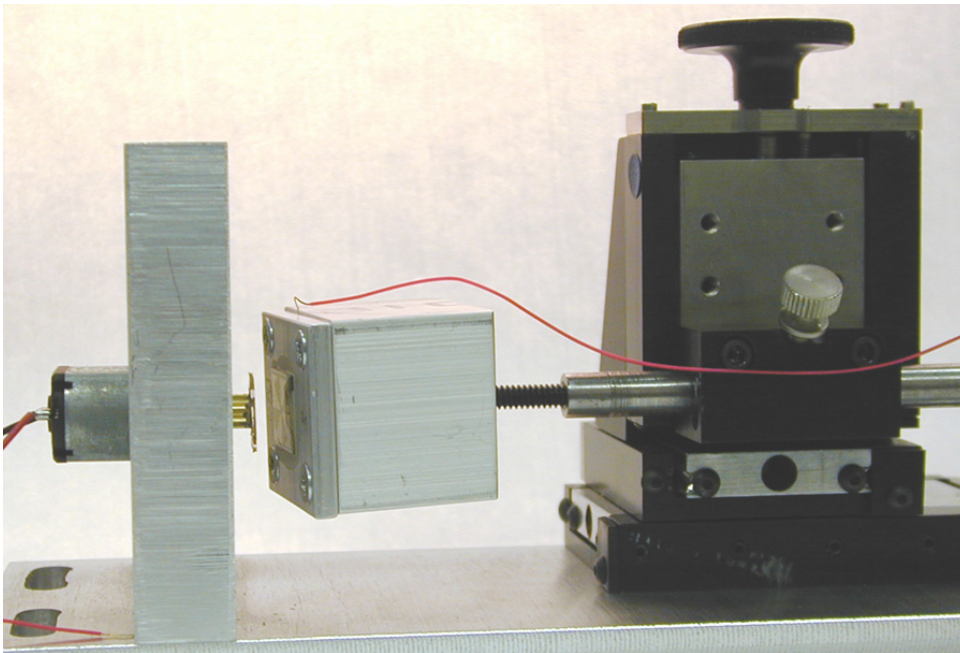

Figure III-21 Side view of testbed with rotor and stator mounted.

The major downfall that was not obvious a priori was that the motor chosen for this experiment has significant back EMF coupled into the chassis that prevents good power signals from being obtained. It is because of this reason that power measurements were never obtained from this setup.

III.4.b.ii.3. Testbed Version 3

Due to the continued problem of angular misalignment and gap control, a final testbed was developed to allow modification to the rotor angle while giving good visibility to adjust gap spacing. First, the rotor is mounted to the to the rotor mount, which has 3 screws with 80TPI pitch to allow for adjustment in ψ_{stator} and ϕ_{stator}. By turning a screw in 5degree increments, gap spacing and angular misalignment can be adjusted in 4.4μm increments. Now, the laser can be used to adjust the angular misalignment instead of just measuring it. The limits on angular alignment are now dependent on the spot size of the laser as it is reflected across a 20foot long baseline and on the flatness of the rotor after being mounted. The rotor is electrically connected to the rotor mount, which is electrically connected to the bearing. The power lead is connected to the bearing using silver paste.
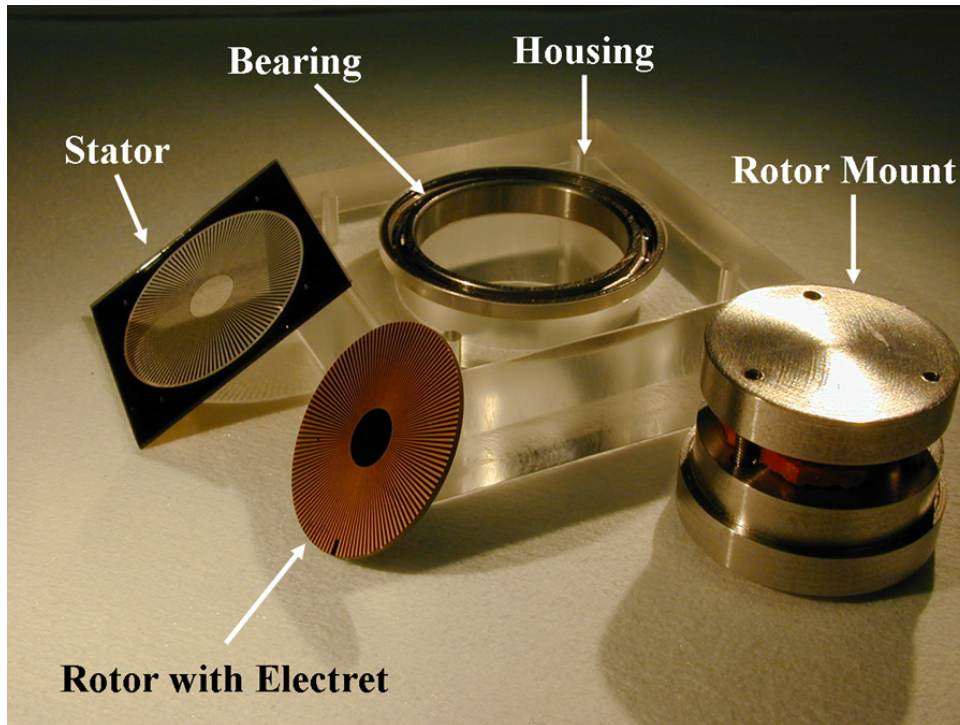
Figure III-22 Newest testbed for REPG

The stator is then glued to a flat acrylic piece (not shown), which is attached to the housing by 80TPI screws. This allows the same precision in adjusting the stator as adjusting the rotor. By visual inspection with a 10x microscope, gap distance can be set to less than 10μm.

However, the limiting piece in this setup is still the bearings. The "thin-section" bearings provided by Thin Section Bearings of America, Inc. conform to the highest standard for bearings, ABEC 9P. This means that they have a radial run-out (vibration) less that 2.54μm. However, the axial run-out is not specified because it is highly dependent on loading. Using 5lbs. of axial force should give similar run-out characteristics. At this

loading, the maximum recommended speed is 10kRPM to prevent significant wear, which is 10x slower than the intended 100kRPM. This loading will be accomplished by using magnets that will also be used to couple torque into the testbed.

Due to increased interest in the liquid electret power generator, this testbed has not been tested. Furthermore, this testbed is not appropriate for a final device design since it is costly, large, and cannot achieve the desired speeds.

III.4.c. POWER GENERATION TESTS

III.4.c.i. REPG V1.0 ON TESTBED VERSION 1

The first power generation experiments were performed using REPG V1.0 and testbed Version 1 described in Section III.4.b.ii.1. The results are shown below in Figure III-23.

Experimental Power (with different load resistors) and
Theoretical (no-stray) vs. Speed
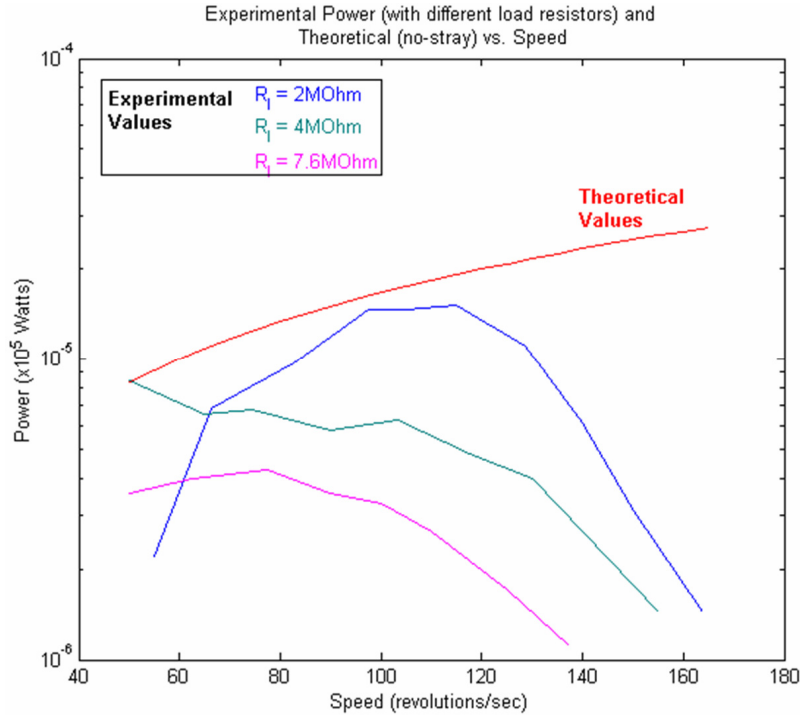
Figure III-23 Power output from 3 experimental trials using different load resistances and theoretical power of a continuously load matched system.

The experimental curve shown is a load matched curve using Equation (III.13) with a gap spacing of 60µm. This is very reasonable fit considering that the minimum spacing is zero at the crashed edge and 80µm at the far edge. The other parameters used in the theoretical values match the measured values of the generator, which are n=4, r=4mm, σ=-2.8x10-4Coulomb/m2, KTeflon=1.93, d=9µm. The noise in the experimental graphs is directly attributable to the stator being crashed into the rotor. This was, however, necessary to know the gap spacing exactly. The generator continues to perform well under this condition for the duration of the tests, despite significant wear to the surfaces.

III.4.c.ii. 32 POLE REPG V2.0

Testing of the 32 pole system was also performed on testbed version 1.
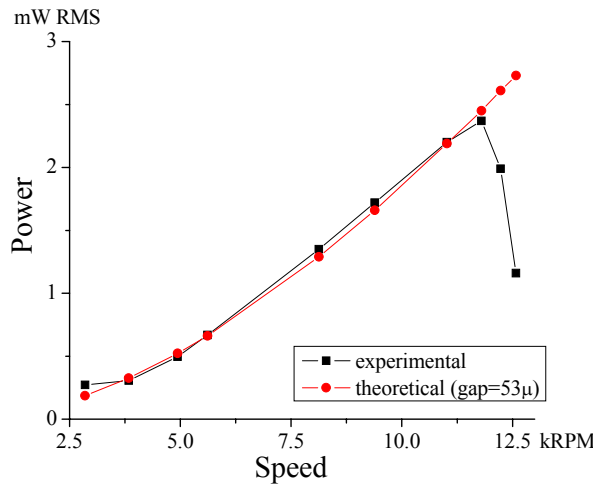
Figure III-24 Power measured and theoretical vs. rotation for the 32-pole power generator with a 600kΩ load, -5x10^{-4}C/m^2 charge implanted, 2cm diameter rotor-stator pair, and 4.25µm thick Teflon electret.

Maximum power achieved, as can be seen in Figure III-24, for the 32-pole system was 2.37mW at 11.8kRPM for a Teflon thickness of 4.25µm. Average gap spacing was unknown, but presumed to be 40µm since the rotor and stator were made to touch during the test and the angular misalignment was measured to be 0.115^0 over this 2cm diameter rotor. The decrease in power output at 12kRPM may be due to vibrations caused by the motor and the bearings, which produced significant audible noise and vibrations above 10kRPM. Fitting for the gap distance for 12.5kRPM gives a gap of 88.5µm, which is reasonable.

III.4.c.iii. 64 POLE REPG V2.0

Testing of the 64 pole system was performed on testbed version 3. Maximum power achieve was 20µW at 16.5kRPM for a Teflon thickness of 4.25µm. The decrease in power is unexpected.
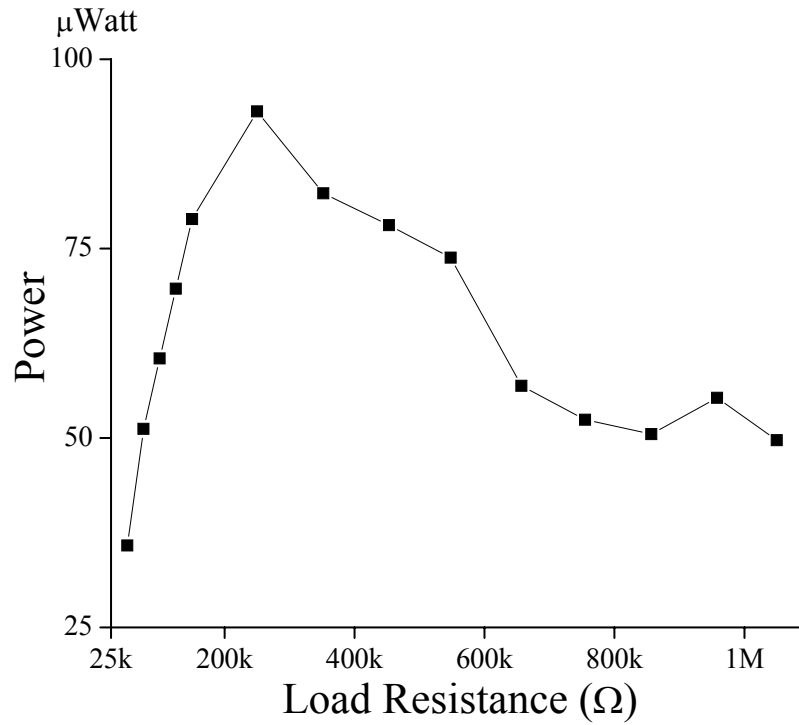
Figure III-25 Load matching test of a 64 pole generator on testbed version 3 at 2.5kRPM
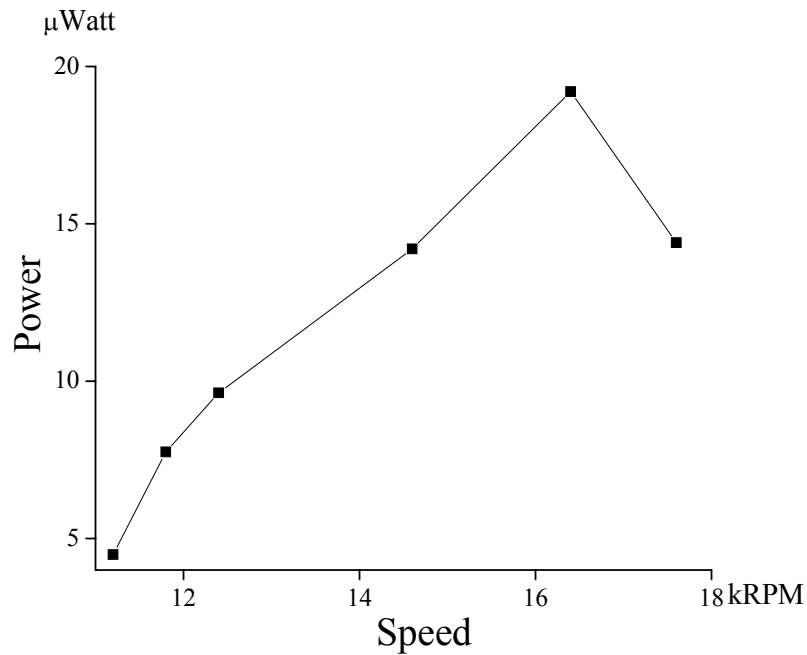
Figure III-26 Power vs. rotation for the 64-pole power generator with a 50.3kΩ load

For the graph above (Figure III-26), a similar trend to Figure III-24 is seen where the power output falls at higher RPM. In this range, the power is expected to continue to increase as f^2, however, the vibrations are known to increase significantly above 11kRPM. Further testing would need to be done to separate the gap distance effect from any other competing effect that may be decreasing the power output.

III.5. CONCLUSIONS

Uniform charge density, gap control, and dielectric thickness are the primary challenges of designing and producing an electret generator. Solutions were engineered to provide uniform charge density on thick, micromachine-compatible dielectric. A linearized theory was derived to adequately model experimental power measurements. Future work will focus on improving gap spacing, increasing the number of poles, eliminating rotor tilt, and verifying the charge distribution in the z-axis on charge implanted into a floating metal electret. A testbed-less electret generator is being designed to overcome the aforementioned difficulties by relying more heavily on the advantages of micromachining.
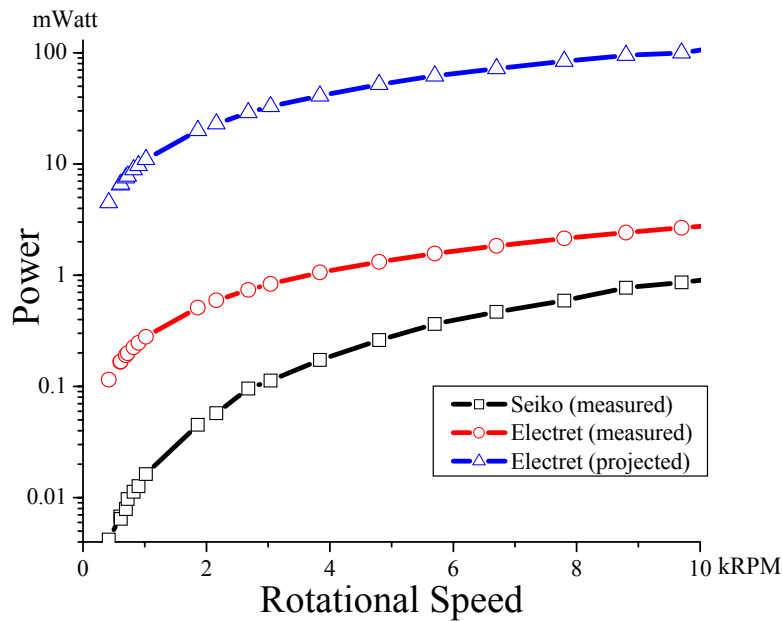
Figure III-27 Comparison of power measured from an actual Seiko watch to rotational electret power generators.

On the brighter side, the core of the results can now be extracted from the 32 pole power generator with the data taken from the Seiko watch and see that there is significant gain to be made by switching the Seiko electromagnetic power generator out for the rotary electret power generator as seen in Figure III-27.

By exploiting the micromachining techniques, an electrostatic power generator was built that produces more power output than commercial miniature electromagnetic power generators.

CHAPTER 4

IV. LIQUID ROTOR ELECTRET POWER GENERATOR

One common example in electrostatics textbooks explains the concept of work with respect to inserting a dielectric into a capacitor. Despite this, a power generator that utilizes kinetic energy to move a liquid dielectric into and out of the air gap of a capacitor has never been reported until J. Boland and Y.C. Tai published a liquid rotor electric power generator in 2004 [61].

The following story illustrates that necessity is the mother of invention. After working on the world's first micromachined rotational electret power generators for more than a year, it became clear that the key to improving the rotational power generator was in the bearings. As shown in Chapter 3, when the gap spacing between the rotor and stator is larger than d/k_{Teflon}, gap spacing is a significant hurdle towards improving power output. The idea of mounting the bearings directly between the rotor and stator seemed obvious, but bearing balls less than 0.5mm are prohibitively expensive and wear characteristics make them undesirable.

Instead of solid bearings, a fluid journal bearing, such as the gas bearings employed in high speed micro turbines, seemed a better approach to solve the gap problem. The difficulty with the rotational electret power generator system is that a single conductive contact to the rotor is required to retrieve the generated electrical current.

The proposed solution was to use a conductive liquid as a bearing, specifically mercury. The mercury would be used in the gap between the rotor and the stator by etching a conductive raceway into the rotor and stator just outside the electret material. After some reflection, it was thought that the mercury would distort the electric field and limit power generation abilities as shown in Figure IV-1.
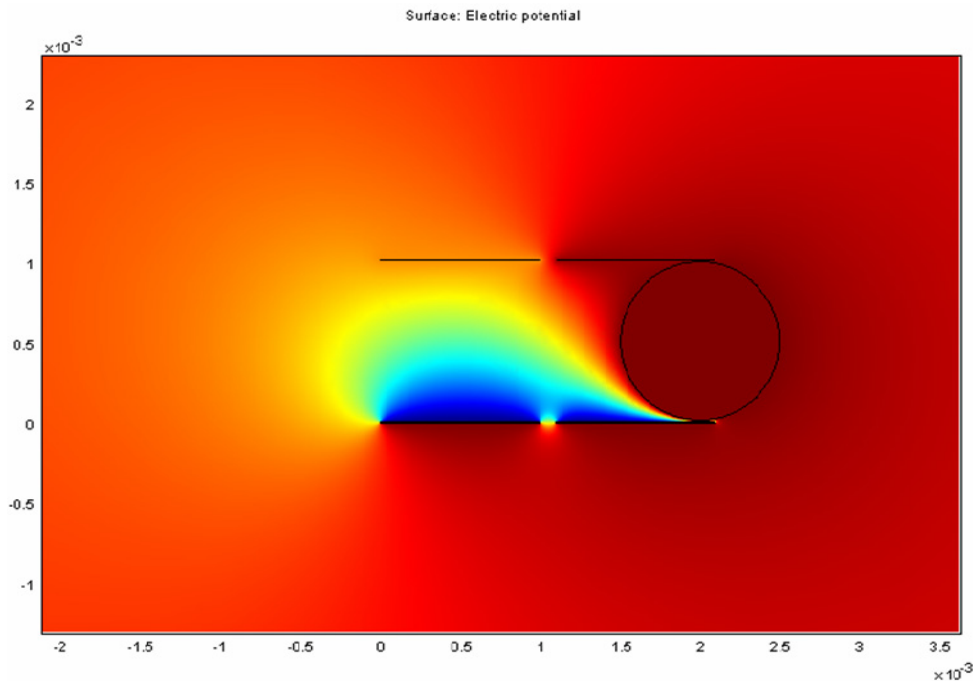
Figure IV-1 Femlab modeling of spatial potential from an electret that is modified by a sphere of mercury.

It was proposed that distinct mercury balls could be used so that the field warping due to the metal's presence could be limited. The distinction that the mercury could be divided into small volumes that might not adversely affect the electric field led to the opposing idea that small volumes of fluid could be used specifically to interrupt the electric field, which was the key to this invention.

The electret generator concept took on a new but familiar form: the generator would have a single solid geometry with no moving parts except for a fluid that will change the electric field in the gap of the capacitor. The simplicity was obvious.

Initially, water was tried as the moving fluid. The difficulty of this approach is associated with the strong electric field produced by the electret, which caused electrowetting [62]. This physical phenomenon caused water to wet and stick to Teflon, which prevented the relative motion of the liquid to the generator. To alleviate this, mercury was substituted as the moving liquid. The electrowetting effect is not noticed in mercury due to the high conductivity and a surface tension 10 times higher than water. This proved successful, and led to the successful tests that follow.

It is still desired to use liquids other than mercury to fully test the variable permittivity theory. However, in the low frequency shaking of these devices, liquid metal acts as a dielectric with infinite permittivity. The infinite permittivity allows for the gap of the capacitor to experience maximum switching, from ε_0 to ∞.

While using metals is obviously the most effective material to change the permittivity of an air gap, society has a general aversion to mercury. To attempt to make ecologically friendly devices, collections of steel beads were substituted for mercury. Not surprisingly, this arrangement also produces useful power as the beads slosh back and forth in the channel like an aggregate fluid.

IV.1. INTRODUCTION

The generator described in Chapter III converts rotational energy to electrical energy with a fixed-charge variable-area capacitor. Further exploiting the relationship

$$V(t) = \frac{Q}{C(t)},$$
(IV.1)

the work presented here explores a variable-permittivity capacitor utilizing a liquid dielectric. This produces a variable capacitance, as shown in Equation (IV.2). A device concept schematic is shown in Figure IV-2.

$$C(t) = \frac{\varepsilon(t) A}{d}$$
(IV.2)
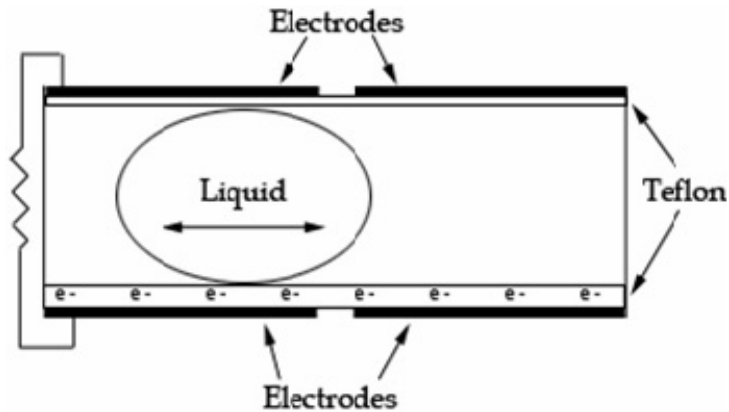
Figure IV-2. LEPG conceptual image.

The effects of a variable permittivity are explored theoretically in freshman E&M books [63], but those examples typically involve a solid dielectric. This would quickly destroy

the Teflon surface unless a mechanism is employed to maintain a gap while allowing relative motion. This causes more losses and thus consumes valuable energy. Instead of using solid dielectrics and more processing steps to create micro springs or sliders, this novel solution exploits the near-zero friction of a high contact angle liquid on the dielectric.

As mentioned previously, experiments with liquid water stalled when the liquid experienced electrowetting. Using silicone oil to prevent electrowetting would enable the use of water, but it is not clear what effect this would have on the required fixed charge since it is also used to reduce charge buildup in electrowetting devices. Mercury is a liquid at room temperature, and does not appear to suffer from electrowetting. It has a contact angle of ~150° on Teflon. Mercury, a conductive liquid metal at room temperature, is equivalent to a dielectric with infinite permittivity.

With negligible friction and heavy mass, the mercury will remain fixed as the capacitor is subjected to linear oscillatory motion. Charge that is embedded in Teflon creates a permanent electric field, and the relative motion of mercury and the chamber produces an alternating current at high voltage. The simplicity of this device allows power to be generated without the use of control circuitry, which would consume power. It is unnecessary to know the liquid's position at any point in time. Furthermore, the driving motion need not be sinusoidal. For the above reasons this new device can be used to harness random, environmental kinetic energy.

IV.2. THEORY

To model the top and bottom electrodes on the left half of the channel shown in Figure IV-2, assume a simple capacitive structure and define

$$C_1(t) = \frac{\varepsilon_{Liquid} \cdot A \cdot \alpha(t)}{G} \tag{IV.3}$$

$$C_2(t) = \frac{\varepsilon_{teflon} \cdot A \cdot \alpha(t)}{D} \tag{IV.4}$$

$$C_3(t) = \frac{\varepsilon_0 \cdot A \cdot (1 - \alpha(t))}{G} \tag{IV.5}$$

$$C_4(t) = \frac{\varepsilon_{teflon} \cdot A \cdot (1 - \alpha(t))}{D} \tag{IV.6}$$

corresponding with Figure IV-3, and use $\alpha(t)$ as a unitless quantity to describe the relative motion of the capacitors to the liquid.
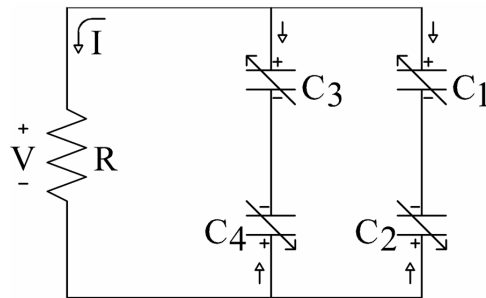
Figure IV-3. Equivalent circuit for each half of the channel.

Assuming sinusoidal motion of amplitude X_0, frequency ω, and an electrode length of L,

$$\alpha(t) = \frac{X_0}{L} \frac{\left(1 + \cos(\omega t)\right)}{2} \qquad \text{(IV.7)}$$

This equation contains normalization factors to keep the non-dimensional amplitude bounded by 0 and 1 at the extremes.
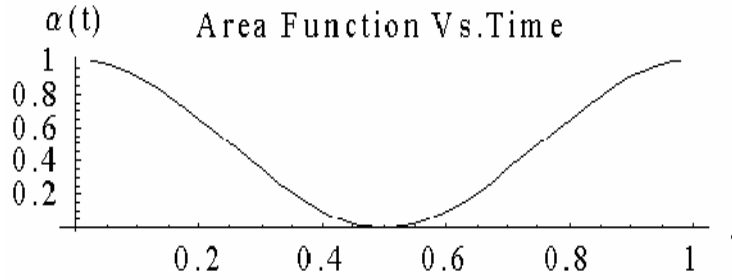
Figure IV-4 Normalized function to describe oscillations of liquid in a channel.

Kirchhoff's Voltage Law is then employed

$$V = \frac{Q_1}{C_1} - \frac{Q_2}{C_2} = \frac{Q_3}{C_3} - \frac{Q_4}{C_4} \qquad \text{(IV.8)}$$

with Q_1, Q_2, Q_3 and Q_4 corresponding to the charge stored on respective capacitors. With implanted charge ρ and capacitor area A, charge conservation states

$$Q_1 + Q_2 = \rho \cdot A \cdot \alpha(t) \qquad \text{(IV.9)}$$

$$Q_3 + Q_4 = \rho \cdot A \cdot \left(1 - \alpha(t)\right) \qquad \text{(IV.10)}$$

It follows:

$$Q_2 = \frac{-V + \rho A \, \alpha(t) \, \dfrac{1}{C_1}}{\dfrac{1}{C_1} + \dfrac{1}{C_2}} \tag{IV.11}$$

$$Q_4 = \frac{-V + \rho A \, (1-\alpha(t)) \, \dfrac{1}{C_3}}{\dfrac{1}{C_3} + \dfrac{1}{C_4}} \tag{IV.12}$$

By Kirchhoff's Current Law:

$$-\frac{V}{R} + \frac{dQ_2}{dt} + \frac{dQ_4}{dt} = 0 \tag{IV.13}$$

Taking derivatives of (IV.11) and (IV.12) and substitute them into (IV.13). After simplifying, an intractable linear first order ODE is obtained.

$$V' = \left\{ \frac{1}{\dfrac{C_1 C_2}{C_1 + C_2} + \dfrac{C_3 C_4}{C_3 + C_4}} \right\}$$
$$\cdot \left\{ -\left[\frac{1}{R} + \left(\frac{C_1 C_2}{C_1 + C_2} + \frac{C_3 C_4}{C_3 + C_4} \right)' \right] \cdot V + \left[\left(\frac{C_2}{C_1 + C_2} \right) - \left(\frac{C_4}{C_3 + C_4} \right) \right] \cdot \rho A \alpha(t)' \right\} \tag{IV.14}$$

As an aside, it is obvious that equation (IV.14) reduces to the well-known RC tank circuit when the capacitors are held constant by setting $\alpha(t) = const$.

$$V' = \frac{-1}{R\left(\dfrac{C_1 C_2}{C_1 + C_2} + \dfrac{C_3 C_4}{C_3 + C_4}\right)} \cdot V \qquad\qquad \text{(IV.15)}$$

The linear, first-order differential Equation (IV.14) does not have a useful closed-form solution. However, it can be solved numerically using built-in ODE solvers in Matlab. By setting some values for the capacitances, voltage can be solved numerically and then find the power generated by

$$P = \frac{V^2}{R} \qquad\qquad \text{(IV.16)}$$
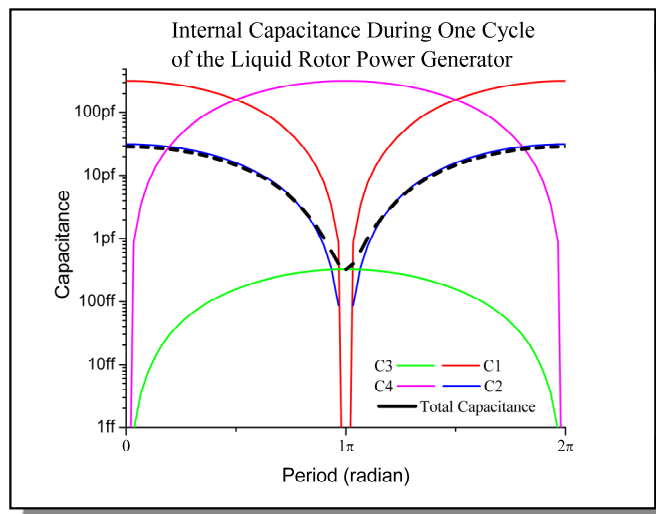
Figure IV-5 Mathematically defined capacitances over one cycle. No allowance has been made for stray capacitance.

As can be seen in Figure IV-5, the mathematical definitions of stray capacitance include unreasonably low values for capacitance, which are to blame for difficulties in getting solutions to the ODE in equation (IV.15). It is not expected that this theory be complete,

but instead the theory should give enough information to guide design of the LEPG devices.

IV.2.a. USING LIQUID METAL INSTEAD OF LIQUID DIELECTRIC

While the distortions of the electric field caused by mercury were the impetus for this new device, the first approach was to use water as moving liquid inside the capacitor. The reasoning was that water is non-toxic and changed the permittivity of the gap from the permittivity of free space, ε_0, to the permittivity of water, $80\varepsilon_0$. This significant change should be sufficient to both generate power and test the theory of variable permittivity. A third benefit is that water can be used to triboelectrically charge the Teflon electret, which would eliminate the fabrication step of implanting electrons and eliminate the worry that heat may discharge the electret. However, water electrowets Teflon in the presence of a strong electric field, and the third benefit ensures that water cannot be easily implemented in LEPG devices.

Therefore, the focus was turned back to mercury for simple reason that it will not stick to charged Teflon. The benefit of using mercury is that it provides the maximum possible change in permittivity of the air gap by effectively eliminating the gap altogether. This implies that mercury optimizes power generation for this type of device, and no other liquid can produce higher power output for the same operating parameters.

Since mercury can also be used as a low resistance path to electrically connect the top electrode to the surface of the Teflon, it can be thought of as a conductor instead of a

material to change the permittivity. In this point, mercury provides a test case to show

the equivalence of variable permittivity power generators using mercury and variable

area or variable distance power generators.

IV.3. DESIGN AND FABRICATION

IV.3.a. GENERAL CONSIDERATIONS

In designing a liquid rotor electret power generator, several questions drive the design requirements. Most geometric variables are within the designer's control, while others are dictated by materials. Understanding the limitations of materials and the relationships to the physics of this device are central for success.

IV.3.a.i. LIQUID

As learned from tests with water, liquid dielectric choice is not trivial. For small volumes of mercury, the shape of the liquid remains spherical in the presence of ordinary gravity. Therefore, the height (h) and width (w) of the channel is chosen to be equal to the diameter (ϕ) of the mercury droplet and a channel length (l) that is twice the diameter. When a collection of small beads is used instead of mercury, it may be possible to reduce the height of the channel. As long as the height of the channel is a factor of ten larger than the electret thickness (d), lowering the height of the channel can give better power per volume characteristics for the resulting device.

Furthermore, choice of liquid in combination with desired operating frequency may have consequences in the designed geometry for the cavity. For example, is has been observed in high-speed video that beads can get stuck in 90degree corners at 60Hz shaking frequency and 1mm peak-peak displacement. Another example is that mercury can have

difficulty occupying corners at low accelerations, which prevents part of the cavity from producing useful power. While rounded channels may give better performance characteristics for a single device, rectangular cavities provide for denser packing of cavities on a single chip.

IV.3.a.ii. CAVITY MATERIAL

To minimize parasitic capacitance, a low-k dielectric material is chosen to define the height of the air gap and to contain the moving liquid. This material will be called the spacer. Furthermore, the spacer should be able to form a good seal to contain the liquid and provide enough strength to withstand the impact of the liquid with the walls. Thus, the spacer material is not only a function of the liquid dielectric choice but also the maximum impact energy, which can be determined from the mass of the liquid and high-speed photography (to determine impact speed and deformation of liquid). In some versions of the LEPG devices, the silicone elastomer Sylgard 184 from Dow Corning is used as the spacer material. This materials is transparent, castable silicone, also known as poly(dimethylsiloxane) or PDMS, with good sealing properties and k=2.65. Several disadvantages exist such as poor rigidity and difficulty in removing the material from a mold without it tearing.

Teflon PTFE (k=2) has also been used as a spacer material, but the limitations are that it is a difficult plastic to machine and also difficult to mold due to the high melting point (327˚C) of the material and the high viscosity of the melted PTFE. Ongoing work is

using Teflon PFA for an injected molded spacer, which has lower melting point, better flow characteristics, and higher purity that PTFE.

IV.3.a.iii. ELECTRET

The electret should be simpler in terms of design consideration, but it must not be overlooked. Obviously, the material for the electret should store the maximum amount of charge with a long lifetime. The maximum output voltage of the finished device is related to the difference in voltage from the implanted charge to the ground electrode (distance $(d - \Delta)$) and the voltage from the charge to the top of the dielectric (distance Δ), as can be verified by simple scaling laws.

$$V_{max} \propto \frac{\sigma}{k_{Teflon}\varepsilon_0}(d - 2\Delta) \qquad \text{(IV.17)}$$

Thicker dielectric, d, will produce higher output voltage, but there is much experimental data indicating that stored charge, σ, is decreased in both maximum quantity and lifetime with thicker dielectrics. Storing charge near the surface (small Δ) implies lower acceleration energies should be used to implant the charge[reference], which affects all variable in the implantation process. Storing charge near the surface may make it more vulnerable to decay by conduction while the lower implantation energies may actually cause more damage to the dielectric.

At this point, it is also necessary to realize that maximum current (Equation (IV.18)) flowing through the external circuit is proportional to implanted charge. Therefore, a decrease in stored charge has a squared effect on power output.

$$I_{max} \propto \sigma A f \tag{IV.18}$$

$$P_{max} \propto V_{max} I_{max} \tag{IV.19}$$

$$P_{max} \propto \frac{A f \sigma^2}{k_{Teflon} \varepsilon_0}(d - 2\Delta) \tag{IV.20}$$

The following table aids in optimizing the design process.

Variable	Increase or decrease?	State of the art	Limitations	Other relationships
σ (charge)	Increase	$5\times10^{-4} \text{C/m}^2$	Breakdown field, material choice. σ decreases as d increases.	$\dfrac{P_{max}}{volume} \propto \sigma^2$
h (height)	Decrease	10x d	Decreasing lowers peak-to-peak voltage swing	$\dfrac{P_{max}}{volume} \propto \dfrac{(d-2\Delta)}{h+d}$
w,l (width, length)	Increase relative to dead space	1mm-5mm	Allowed volume, target frequency	Optimum length decreases for increasing frequency
f (frequency)	Increase	120Hz	Wall strength and sealing. Can easily exceed surface tension of mercury.	$\dfrac{P_{max}}{volume} \propto f$
d (Electret thickness)	Increase	100μm	σ decreases as d increases. Destabilizes implanted charge.	$\dfrac{P_{max}}{volume} \propto \dfrac{(d-2\Delta)}{h+d}$
k_{Teflon} (permittivity electret)	Decrease	1.93	Already lowest known dielectric	$\dfrac{P_{max}}{volume} \propto \dfrac{1}{k_{Teflon}\varepsilon_0}$
Δ (implantation depth)	Decrease	1μm	Decreasing Δ destabilizes charge	Necessitates re-optimization of implantation process

Table IV-1. Design considerations for LEPG

IV.3.b. FABRICATION

IV.3.b.i. LEPG V1.0: QUICK AND DIRTY

The first LEPG process was a very quick and dirty attempt to see if a measurable signal can be detected from the device using water as the liquid dielectric. A picture of the capacitive plates, each 1cm x 1cm made of thermally evaporated aluminum. On top of one of the electrodes is a 4μm layer of Teflon AF 1601-s 7% solids. This layer is applied through spin coating, baked, and then implanted with charge in the back lighted thyratron. The spacer was cut by hand from a 2mm thick sheet of Teflon PTFE.
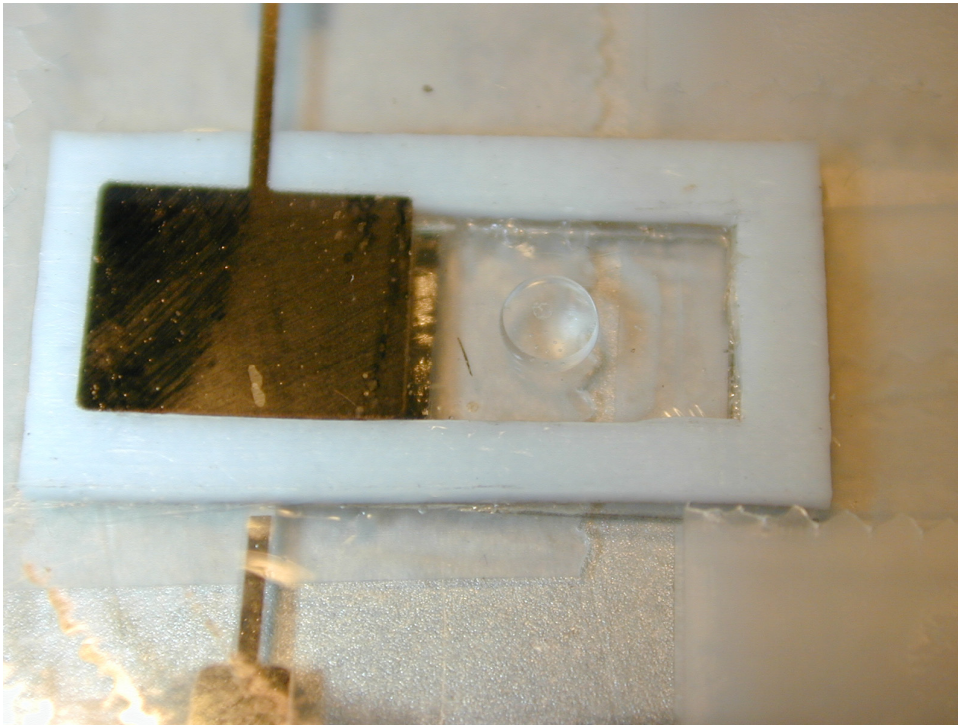
Figure IV-6 LEPG with a small droplet of water in the channel.

The Teflon wetted the surface and would not move. A second trial was performed without charging the Teflon. In this case, the water would shake in the channel until it had triboelectrically charged the Teflon. At that point, all shaking would halt.

Substituting mercury for water worked instantly. Using a LF356 op-amp as a voltage buffer, a voltage signal of +/- 15Volts was observed for the first trials of mercury in a charged Teflon-air gap capacitor.

IV.3.b.ii. LEPG V2.0: PDMS MOLD AND PROCESS REFINEMENTS

A second fabrication process of the LEPG is shown in Figure IV-7. Glass plates with patterned metal are the starting capacitor electrodes.
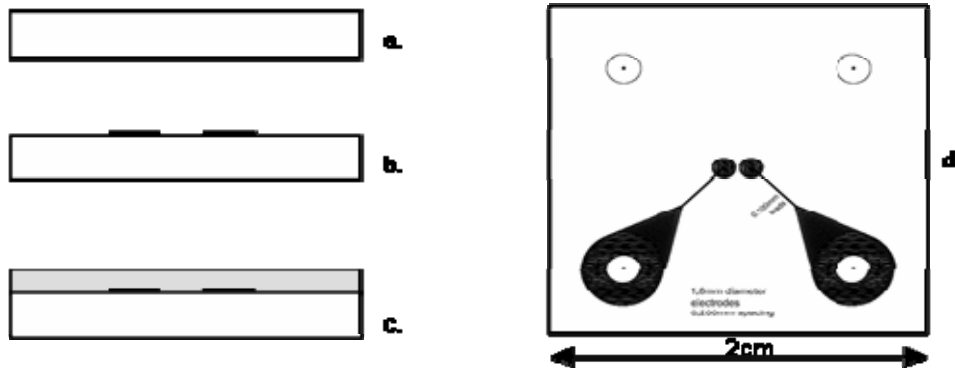
Figure IV-7 Process Flow a. deposit metal on glass substrate b. pattern metal c. spin-on Teflon AF d. mask design used.

An 8μm thick Teflon AF is spun onto the bottom plate, and 0.5μm Teflon onto the top plate [4]. The Teflon AF layer on the bottom plate is then implanted with electrons from a back-lighted thyratron to form the electret [7]. The spacer (which also provides the liquid chamber) is made by casting Sylgard 184 PDMS onto a CNC-machined mold as seen in Figure IV-8 and bonded to the bottom plate with epoxy.
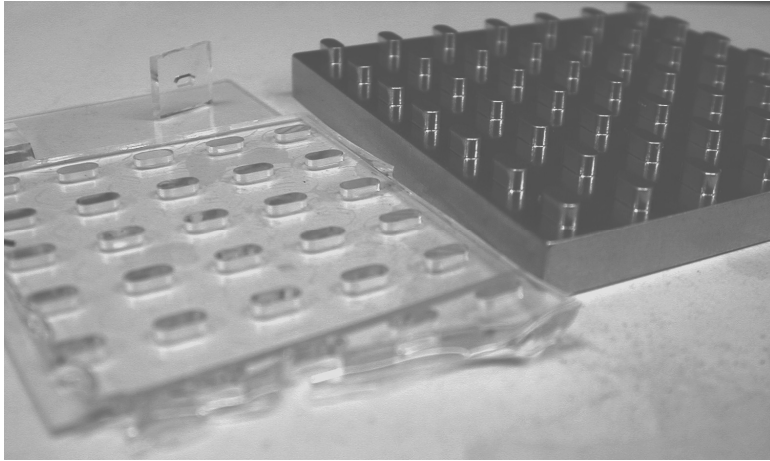
Figure IV-8 Mold Master for Sylgard 184 and peeled PDMS.

For this demonstration, a liquid mercury droplet is used to partially fill the chamber on the bottom electrode. The top electrode plate is then bonded to the spacer to finish the device (Figure IV-9). Cavity dimensions for Device 3 are W=2.3mm, L=4.812mm, and H=2.3mm for a droplet of 50µL. Cavity dimensions for Device g are W=3.5mm, L=9.4mm, H=4.45mm for a droplet about 600µL.

Figure IV-9 Assembled LPG Device. Clear epoxy binds the top plate to the bottom plate and prevents the mercury from leaking.

IV.3.c. LEPG V3.0: MULTIPLE CHANNELS ON SINGLE CHIP

Fabrication of arrays of LEPG channels is very similar to the fabrication of a single channel as described in the previous section. Glass plates are patterned with metal to form capacitor electrodes (Figure IV-11).
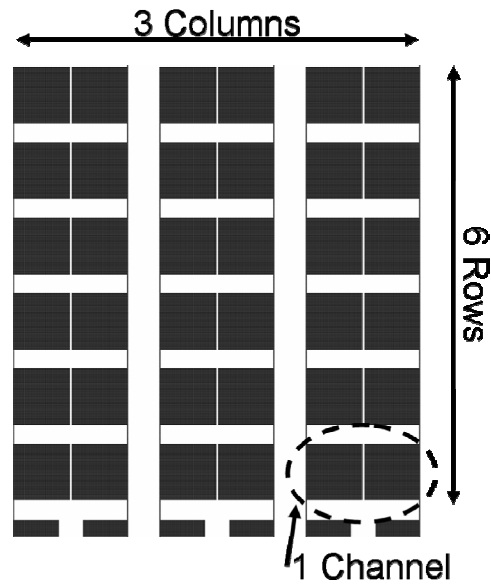
Figure IV-10 Electrode pattern for 6x3 cavities with 2 top and 2 bottom electrodes per cavity.

A 25 μm thick film of Teflon FEP is glued to the bottom plate using Teflon AF, which does not provide good adhesion. A 0.5 μm Teflon AF thin film is spun on the top plate to protect the top electrodes from the mercury. The Teflon PTFE layer on the bottom plate is then implanted with electrons from a Welty handheld ion generator to form the electret. The surface voltage was measured to be -850 V before the power generation trials. The spacer (which also defines the liquid chamber) is made by casting Sylgard 184 PDMS

onto a CNC-machined mold.   Either liquid mercury droplets or an aggregate of steel beads [64] is used to fill half the chamber on the bottom electrode plate.
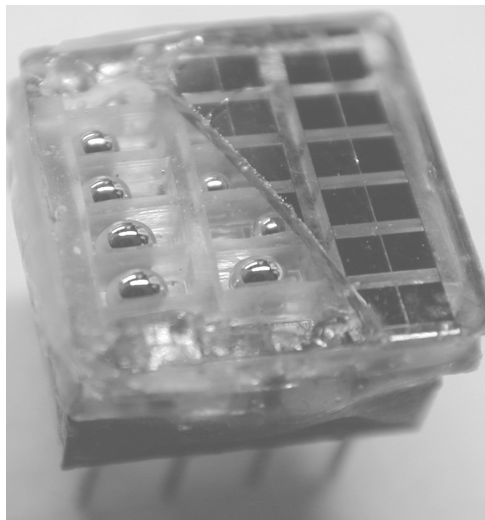
Figure IV-11 Assembled LEPG device with cutaway to reveal bottom electrodes.

The top electrode plate is then placed on the spacer to finish the device (Figure IV-11). The final device is then sealed in clear epoxy to provide structural support as well as guard against leakage. Cavity dimensions are W = 1 mm, L = 2 mm, and H = 1 mm with a droplet volume of 1 μL, with 3 columns of 6 cavities per die.

IV.4. EXPERIMENTAL DETAILS

Power generation experiments are performed on a Labworks Inc. ET-139 electrodynamic shaker (Figure IV-12) driven sinusoidally by a HP33120A function generator through a Labworks Inc. PA-141 power amplifier. Acceleration is measured using an Endevco 256HX-10 accelerometer. Displacement is acquired by double integration of the acceleration waveform. The shaking frequency can be varied from 20 to 100Hz, and the displacement can be varied from 0 to 5 mm peak-to-peak. The LEPG's output voltage across a load resistor is measured with a National Semiconductor LF356N op-amp used as a 10^{12} Ohm impedance voltage buffer. Both acceleration and generator voltage waveforms are averaged over 256 samples on an HP oscilloscope and captured to computer by IntuiLink software over GPIB.

Figure IV-12 Test setup for LEPG mounted on shaker

IV.4.a. DATA

With the top electrodes replaced by a glass slide, high-speed video clearly shows the motion of the channels and the mercury droplets within. Shaking at low amplitudes and above 20Hz with the channels perpendicular to gravity, the mercury droplets remain fixed in space while the channels move about them. By increasing t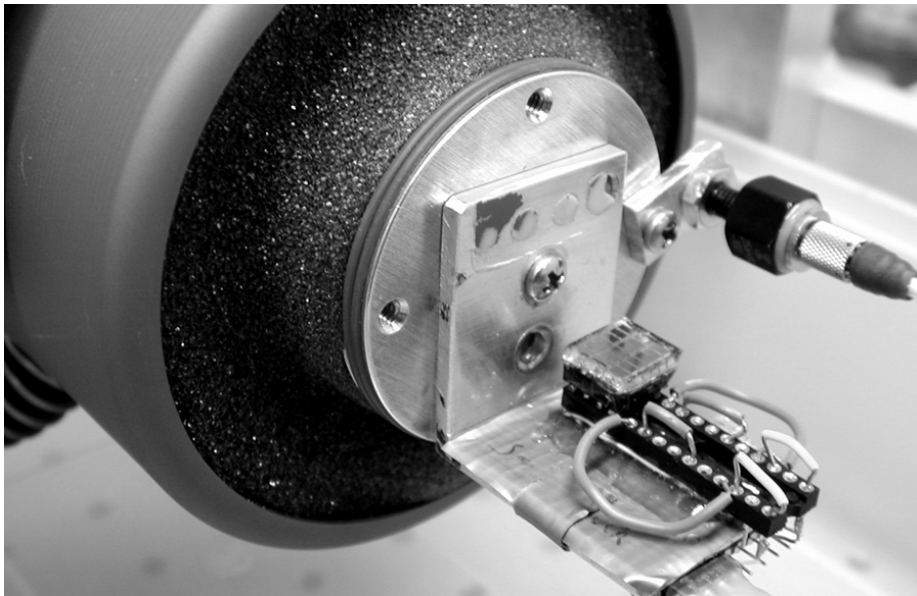he amplitude to at least half the channel length, the droplets' centers of mass are well synchronized but no longer stationary. Impacts with the ends of the cavities impart energy to the mercury droplets that is converted into deformation of the surface as shown in Figure IV-15. When the walls and the droplets have zero relative velocity, the energy of surface deformation is transferred back into kinetic energy of the droplets. This process increases the relative motion of the droplets, and is reflected in the output waveforms as phase lag (Figure IV-18) and larger currents with reduced duty cycle. The increase in power output in this overdriving mode is smaller than the increase in input energy. While overdriving the amplitude ensures synchronization, it is rarely the case that the channels are perfectly perpendicular to gravity, and overdriving may be unnecessary. Replacing the mercury with aggregates of steel beads demonstrates no phase lag and also benefits from overdriving [9].

IV.4.a.i. REPLACING MERCURY WITH STEEL BEADS

A collection of small diameter beads can flow much in the same way a liquid can. Using this effect, the mercury in the LEPG can be replaced with a collection of small beads. The beads used had a mean diameter of 280μm, but a large variance over the set of beads

used. Furthermore, the shape of the beads are not necessarily spherical. This is because the beads used in the experiments are originally sold as sand-blasting media, which is many orders of magnitude cheaper than purchasing individual bearing balls.
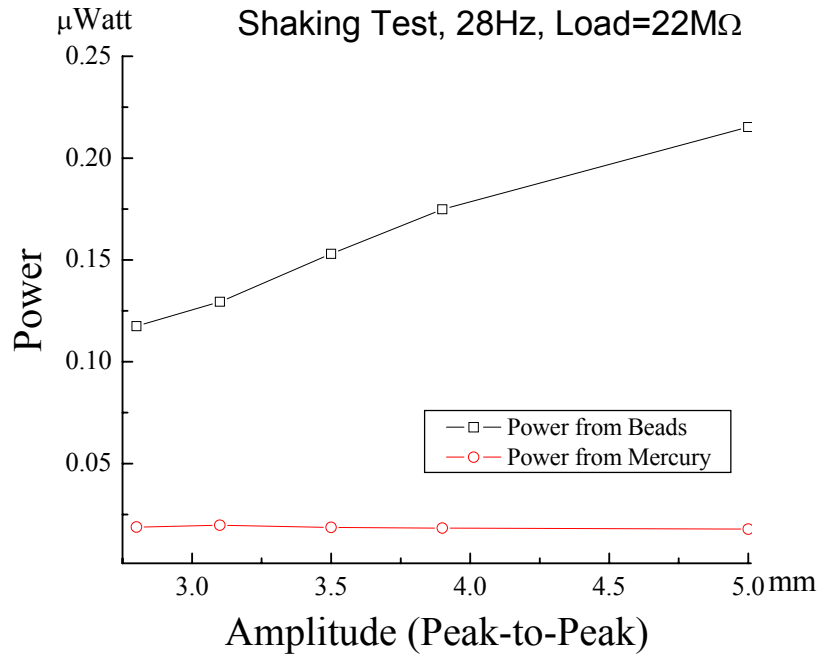
Figure IV-13 Power generated in LPG V2.1 with 100μm Teflon PTFE

This result is not intuitive. It is expected that mercury can generate higher power output in Figure IV-13 because it can completely occupy the gap of the LEPG and the completely evacuate it, whereas the motion of the beads prevent them from moving perfectly in unison. Two observations that may be important: a. the steal beads used were originally purposed for sand blasting media and they obviously cause some wear (and perhaps triboelectricity) on the channel, and b. the beads net motion is almost stationary as can be seen from high speed video, which is what the theory originally calls

for while the mercury absorbs and re-releases impact energy from collisions with the walls.

Figure IV-14 Still-frame position 1 taken at 2000fps while shaking at 60Hz and 1 mm peak to peak.

Figure IV-15 Still-frames position 2 taken at 2000fps while shaking at 60Hz and 1 mm peak to peak.

IV.4.a.ii. PARALLEL ARRAYS

By design, the arrayed devices are organized in 3 columns, where every column contains 6 devices in parallel (Figure IV-2 and Figure IV-10). Each device in the array contains an electrode pair on each half of the channel. For the purposes of this test, only the electrodes on the left side of the channels are tested. Data is taken from 1, 2, or 3 columns in parallel (Figure IV-16). Data shows power output scaling linearly with number of devices in parallel. Testing smaller arrays with 4 and 5 devices per column produced similar results.
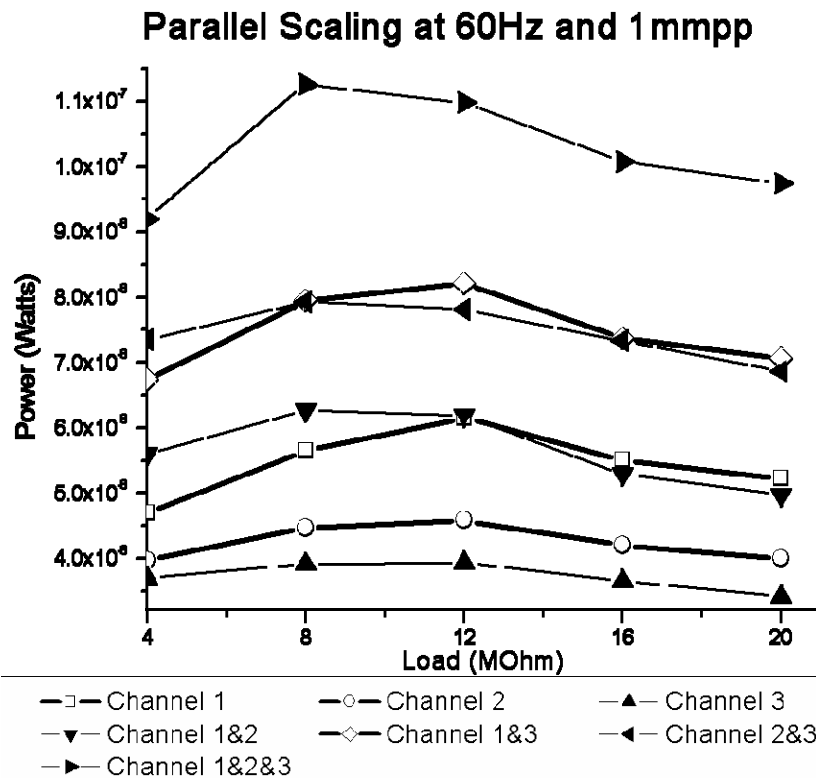
Figure IV-16 Experimental values for parallel channels shaking of 2.58 mm peak-to-peak at 60Hz.

IV.4.a.iii. SERIAL ARRAYS

After tests demonstrated the linear scaling of parallel arrays, the same columns of 6 electrodes are used, but this time the electrodes between the columns were connected serially.
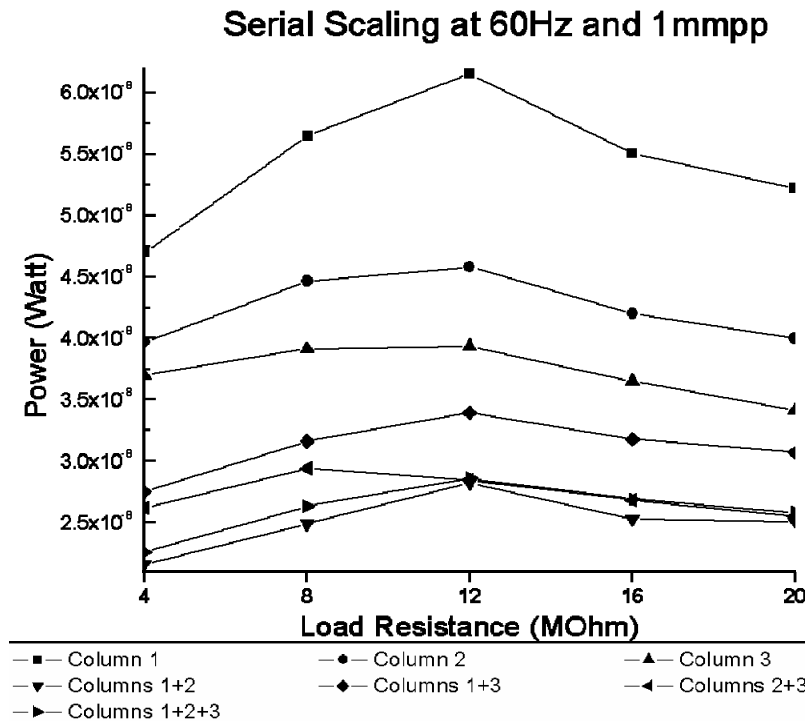
Figure IV-17 Experimental values for serial columns shaking at 1 mm peak-to-peak at 60Hz.

The relationship is anything but linear in this case, and any columns in serial produce less power output than single columns. The waveforms are shown in Figure IV-18, which shows voltage vs. time for each column and combinations of those columns. These results imply complicated interactions between columns, probably related to slight phase

differences and feedback effects. Testing with 4 and 5 electrode columns produced similar results.
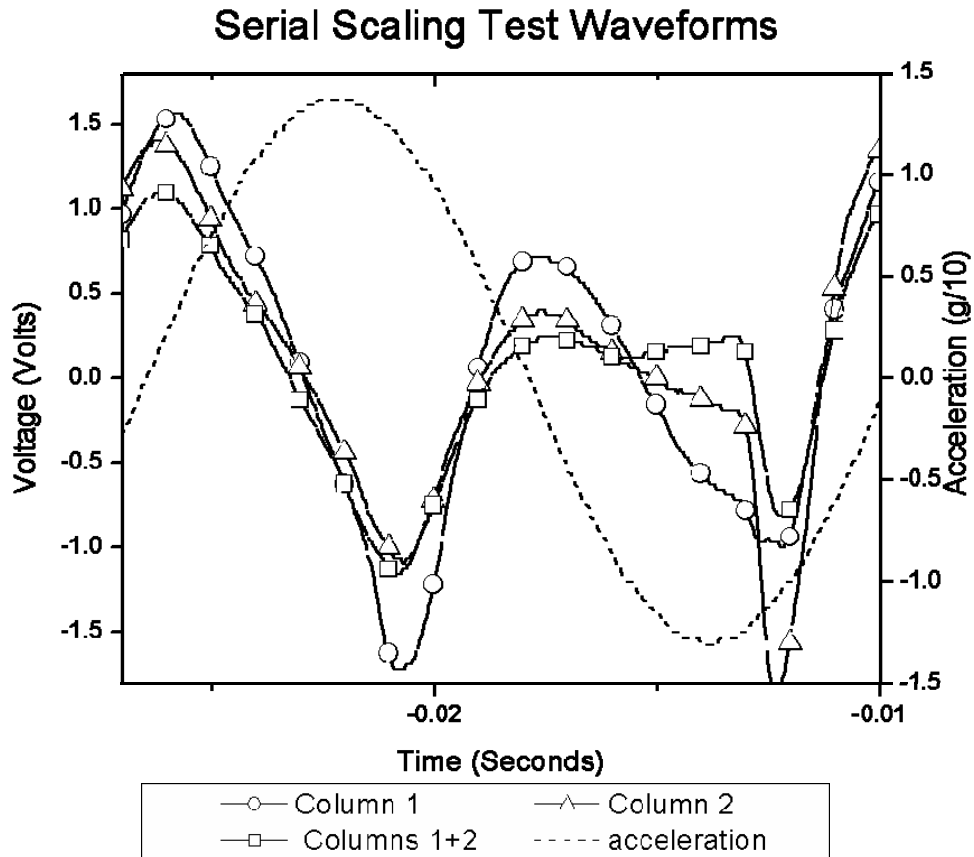
Figure IV-18 Experimental values for shaking at 2.58 mm peak-to-peak at 60 Hz and Rl of 4 MOhm.

IV.4.a.iv. NON-OBVIOUS ELECTRICAL CONNECTIONS

Different combinations of connections between electrodes on the LEPG devices were tested on LEPG V3.0 with beads and with mercury as shown in Figure IV-19.
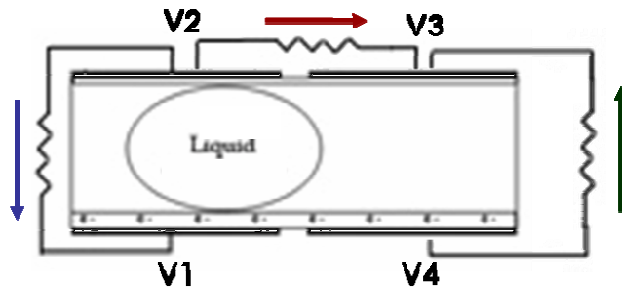
Figure IV-19 Diagram showing all connections across LEPG

Power output was, on average, lowest when the top and bottom electrodes directly across from each other were tested, which implies that the original design is neglecting a large effect—most likely the influence of nearby electrodes. The highest power was obtained when there were three resistors connected at the same time, most likely related to charge flow between all four electrodes.
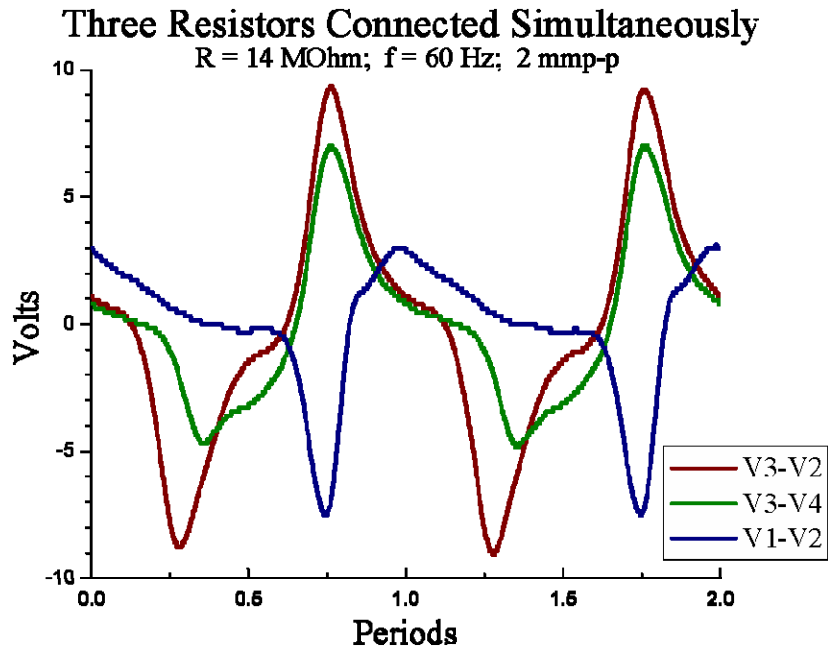
Figure IV-20 Voltage waveforms with resistors connected across V3-V4, V1-V2, and V2-V3 on an LEPG device shaking at f = 60 Hz, displacement = 2 mm p-p, R = 14 MOhm for all three resistors.

Careful examination of Figure IV-19 reveals that the V1-V2 and V3-V4 signals are inverted and reversed in time. The V3-V2 signal is the largest signal and perhaps the most useful for power generation because of its near sinusoidal nature and larger voltage. This test was not part of the original design, but it yields new and exciting data that may be used to construct more efficient devices in the future.
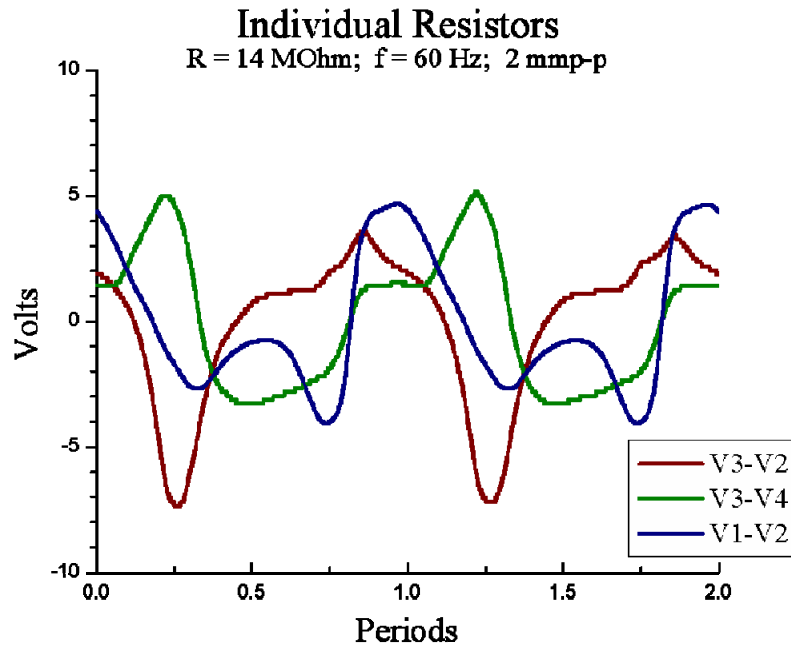
Figure IV-21 Waveforms from same connections as above in Figure IV-19 except only one resistor is connected at any time.

Figure IV-21 shows that the V3-V2 signal is less significant if charge is not allowed to flow around the entire system when the V1-V2 and V3-V4 resistors are removed. What this suggests is that neighboring electrodes have significant impact on each other and that the system needs further modeling where all four electrodes are considered to be part of the same system.

IV.5. CONCLUSIONS

A new class of power generation device was developed: the liquid-rotor electret power generator. Although simple in concept, this device had not been possible in the past because the lack of good electret technology and precise methods for fabrication and assembly had not been applied to this area. Instead of fighting the change in permittivity that mercury would induce into the electric field, this effect was exploited to create a new type of power generation device. One of the major advantages of this device is the lack of friction, which causes significant losses in microscale devices [65, 66].

A theory was developed from linearized equations, but it is impossible to implement without numerical calculations. A simpler theory was developed to explain the scaling principles of the device for practical purposes.

This work demonstrates the ability to connect many LEPG devices in parallel, and the difficulty with serially connected LEPG devices. Devices in parallel allow for increased power output, and also allow for the possibility of creating further miniaturized and embedded power systems.

The improved LEPG is a promising, economical method to harvest power from vibrational environments to power remote sensing devices. Steel beads can approximate a fluid and produce more power than mercury. However, wear characteristics need further exploration to prove the long-term viability of this approach. Future work will attempt to coat the beads with parylene or other soft polymers to prevent the beads from wearing the channels.

Evidence presented here warrants further study and modeling to describe the power generated with varying the configuration of connections. These results suggest that optimal electrode design has not yet been attained. Furthermore, since two, coplanar electrodes generated the most power, it may be possible to reduce the number of electrodes and produce a simpler device.

CHAPTER 5

V. CONCLUSIONS AND FUTURE WORK

Under the direction of Yu-Chong Tai, I set out to produce a rotary electret power generator (REPG) utilizing micromachining techniques. Along the way I improved some processes, extended electret processing capabilities, built the world's first micromachined rotary electret power generator, and built the world's first liquid rotor electret power generator (LEPG).

V.1. ROTARY ELECTRET POWER GENERATOR

Although this project is part of a larger project to generate electricity from fossil fuels, the devices that have been presented in this work will make excellent energy harvesters. Comparing the power output of the Seiko Kinetic watch generator, the rotary electret generator not only produces more power but produces more power proportionally at low RPMs that the Seiko electromagnetic generator. What this implies is that the rotary electret generator has the distinct advantage of generating usable electricity from small motions.

In contrast to the electromagnetic generator, the rotary electret generator is inherently a high voltage power generator. The electromagnetic power generator produces less than 1.4Vpp from rest until 8800RPM, which implies that it cannot be used with a simple bridge rectifier for most of the motions it is attempting to harvest. This leads to more

complicated circuitry and more inefficiencies, whereas the 32-pole rotary power generator produces 16Volts peak to peak at the slow speed of 1900RPM.
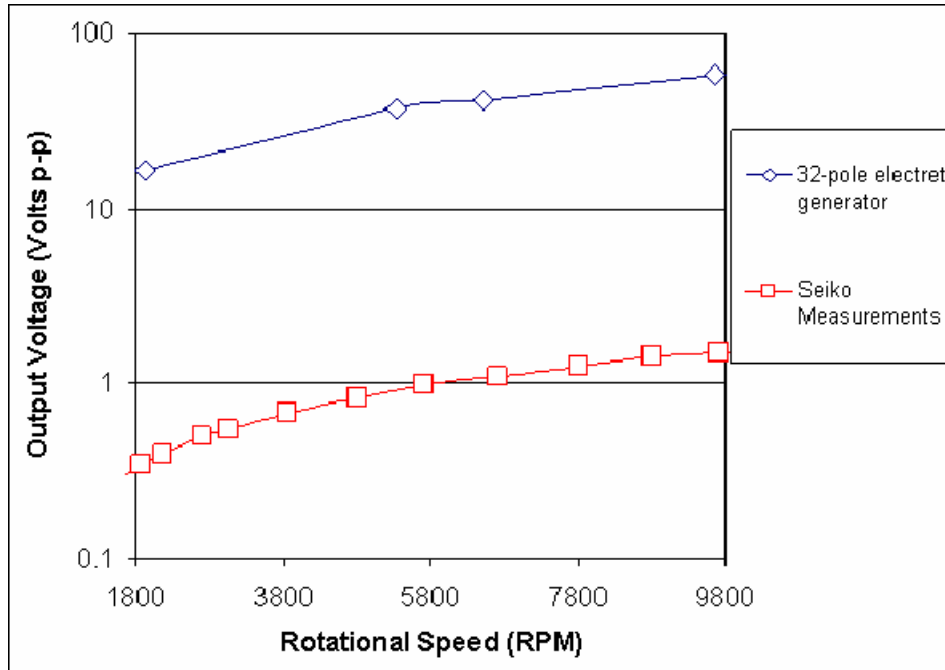
Figure V-1 Comparison of Seiko's Kinetic electromagnetic power generator to the REPG

While these comparisons are promising, much work is left to perfect the REPG. Table III-1 illustrates the design parameters left to optimize. It was found that gap distance is very difficult to control when using commercial bearings. Therefore, a micromachine compatible solution is necessary to improve this aspect, which would give large gains in power generated. A fluid bearing is still the most promising approach, and a possible design is shown in Figure V-2 and Figure V-3. In this design, distinct droplets of mercury or a ring of mercury is made to wet the rotor or stator while other part makes

physical and electrical contact to the mercury without wetting. Micromachined magnets can be used to couple axial torque into the generator to cause rotation as well as to apply force to draw the rotor closer to the stator.
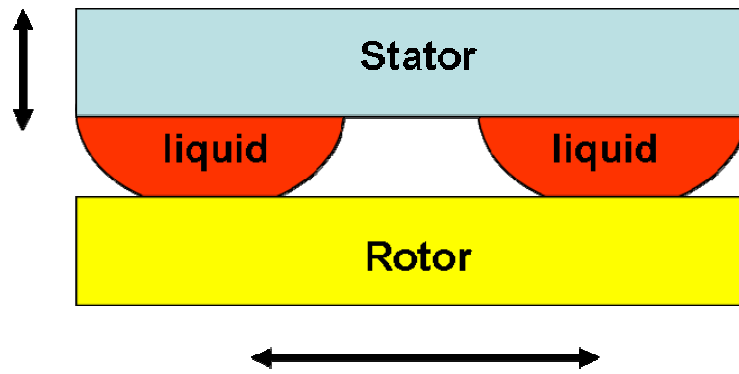
Figure V-2 Liquid bearing concept for gap control in REPG.
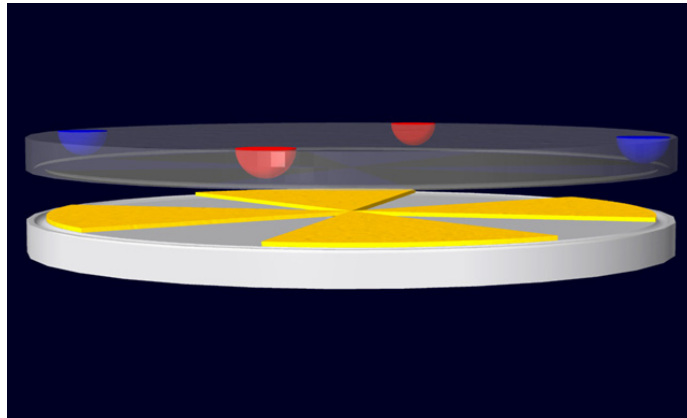
Figure V-3 Micromachined magnets (red is north pole up, blue is south pole up) are used to apply force and couple torque into the REPG.

The gap distance criterion can be slightly relaxed by a factor of $\dfrac{d}{k_{Teflon}}$ if thickness of the electret is increased. This may be accomplished by layered polymers, injection molded

polymers or inorganic dielectrics such as spin-on glass, or other polymer molding/deposition steps. The dangers in increasing the thickness of the electret are two-fold: a) the dimensions of the electrodes may violate the infinite plane approximation causing significant parasitic capacitance and b) the storage of charge in an electret is inversely proportional to its thickness. Danger b) is alleviated if the electret is composed of a layered structure.

The REPG is inherently a low current power generator, with current being proportional to the area of the generator. This low current drawback can cause difficulty if the generator is used to charge a storage device with large leakage current. The low current is also a difficulty when trying to build a custom ASIC in silicon because silicon diodes have leakage currents on the order of microampere (from a conversation with an engineer at International Rectifier Custom Solutions department). The simple solutions to produce more current are: operate at higher rotational speeds; increase the number of poles; implant more charge; and have a larger disk. The first three are feasible areas of improvement, but the last is a design constraint.

Operating at higher frequency has not proved viable to date, which is curious. It is probably that there is a significant source of parasitic capacitance in the testbeds and circuitry used to date. By inverting Equation (III.12), maximum power should occur when

$$f = \frac{1}{\varepsilon_0 \, n \, \pi \, r^2 \, R_{load}} \left(\frac{d}{K_{teflon}} + g \right) \tag{IV.21}$$

Plugging in typical values leads to Figure V-4, which was generated by calculating the theoretical power output of a rotary generator as given by equations (III.10) and (III.11), using the typical values of for a 32 pole generator with 1cm radius, 4μm thick Teflon layer, -5x10^{-4} C/m^2 charge implanted, and a Teflon permittivity of 1.93.
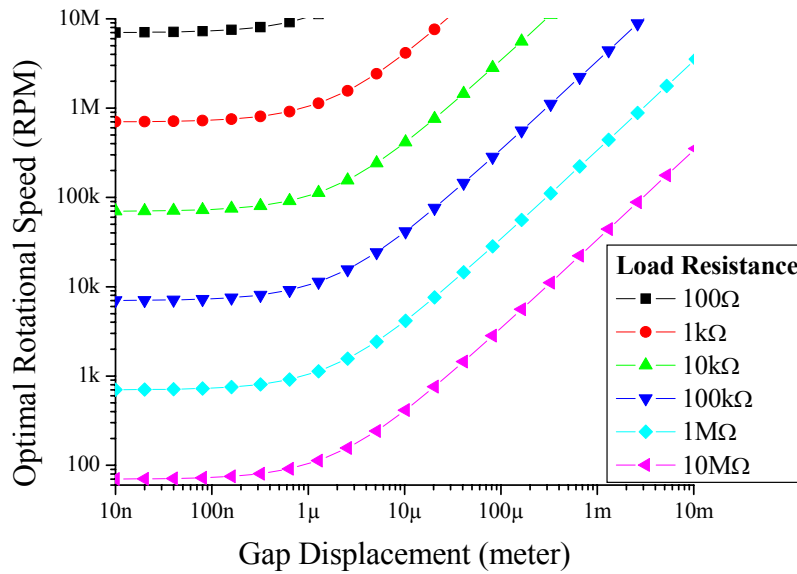
Figure V-4 Theoretical plot of rotational speed versus gap displacement showing that higher rotational speeds are necessary when gap distance is large.

Examination of the theoretical plot in Figure V-4 shows that spinning a rotational generator at higher speeds will allow for a lower load resistance to be used. This is due to the current increase at higher speeds (Equation (III.10)), which causes a lower internal impedance (Z) of the generator.

$$Z = \frac{1}{j\,\omega\,C} \tag{IV.22}$$

Where j is used to represent the imaginary phase of the capacitance. When using a resistor to load match, the load resistance should be equal to the real part of Z.

It can also be seen that the knee in the rotational speed curve corresponds to the thickness of the electret divided by the dielectric constant. This confirms the analysis of the gap spacing in section III.3.a.iii.

When compared to Figure III-25, this indicates that not everything in the test was ideal. It is possible that a significant external capacitance is present, which has caused significant difficulties in measuring power for the liquid-rotor power generators. Furthermore, significant shaking of the testbed at higher rotational rates cause significantly larger vibrations in the chassis and these vibrations can cause misalignment and gap separation.

Going back to electrical current production, future REPG devices may have stacked geometries such as the Wimhurst Machine shown in Figure V-5.
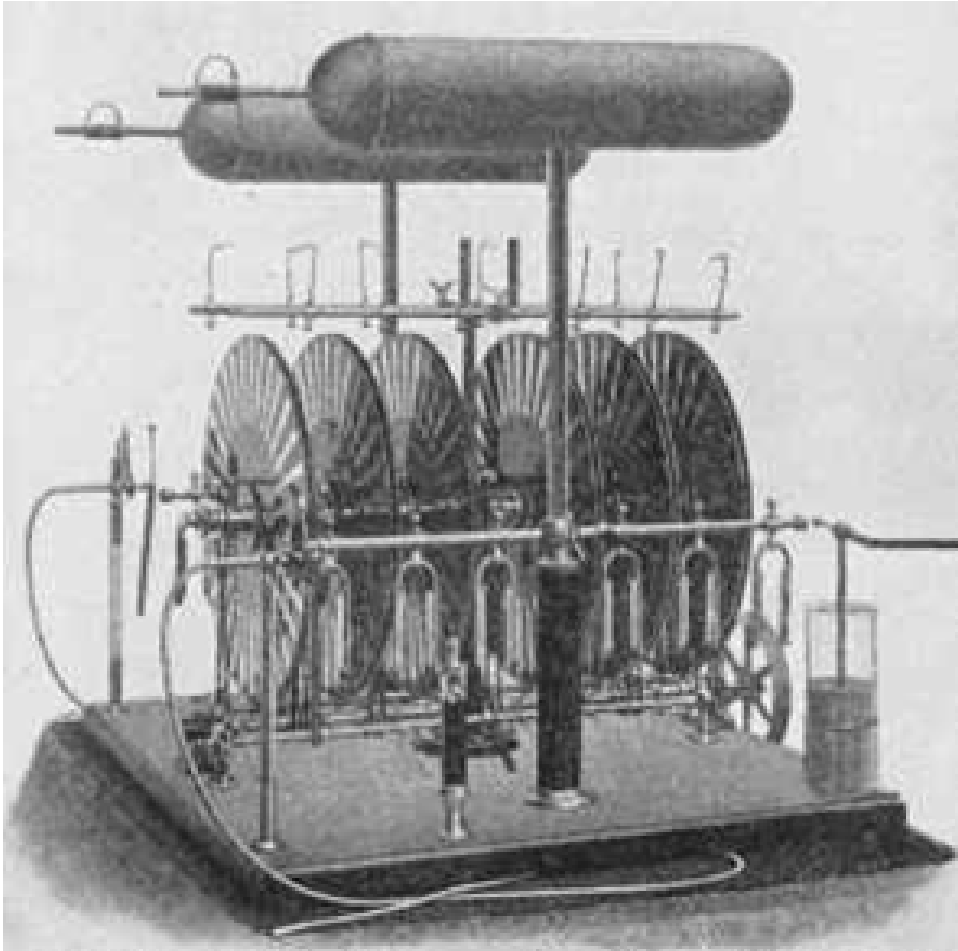
Figure V-5 A Wimshurst machine used to generate electricity from electrostatics and triboelectricity.

Finally, the fight with leakage current in storage elements is reliant on start-of-the-art technology, which is still lacking. Preliminary tests show that the majority of capacitor types have leakage currents on the order of microamperes, which is on the order of the current produced by the power generator.
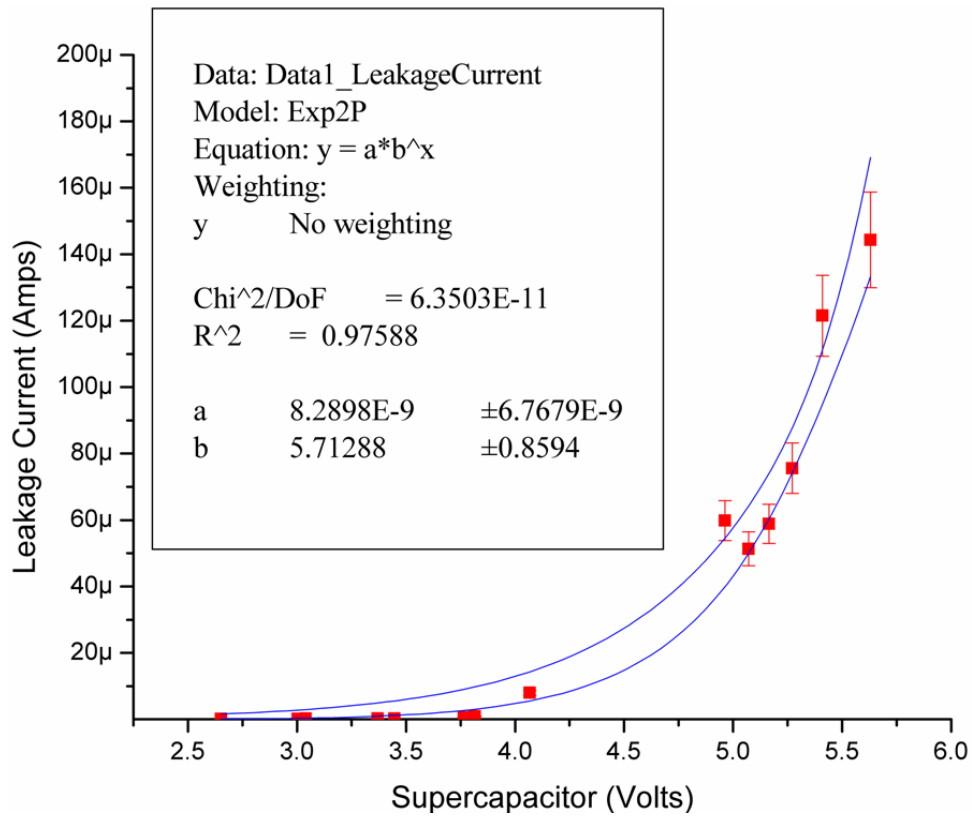
Figure V-6 Decay curve of charge 1farad supercapacitor due to leakage current alone.

V.2. LIQUID ROTOR ELECTRET POWER GENERATOR

The LEPG was born in the Caltech Micromachining Laboratory and has survived infancy. Now, it needs to grow. The weaknesses of the LEPG are similar to the REPG, except the LEPG operates at much lower frequency. This is also a strength for energy scavenging applications, but it exacerbates the difficulties of leakage current and low current output.

By Equation (I.4), the figure of merit for the 0.1cc LEPG shaking at 60Hz, 1mmpp, with a mass of 74mg (assuming the liquid remains still and the cavity shakes around it) is $N_{LEH} = 25 \big/ cc$. This number is magnitudes lower than competing devices, which can partly be explained by the lack of information given in the literature on competing devices and the generous assumptions made, while the rest of the deficiency is due to a non-optimized design. This work focused on exploring the relationships between variables and scaling laws, which allows for future optimization of power generation from the LEPG.

The next set of experiments should be aimed at exploring the power output as the load resistance in matched to the other parameters of the LEPG. This is challenging because there is no closed form criteria for load resistance, so a theory ought to be developed to handle this. Very simple relations can be used, such as $I_{max} = 2 \, \sigma \, A \, f$ (for short circuit current) and $V_{max} = \dfrac{\sigma \, d}{2 \, \varepsilon_{Teflon}}$ (for open circuit voltage), but these ought to be developed a bit further and tested for accuracy.

After load matching experiments are performed, the LEPG ought to be scaled in parallel into the 3rd dimension by stacking 2-dimensional arrays. When a LEPG generator system is proven sufficiently reliable, efficiency tests need to be performed to characterize how much of the mechanical energy is absorbed into the generator and how much of the absorbed energy is converted to electrical power.

Finally, a system should be built to take power generated from a LEPG system and charge a storage device that in turn is the power source for some useful electronic function [11, 31, 67].

Chapter 6

VI. References

[1]   *D. L. Anderson, Discovery of the Electron: The Development of the Atomic Concept of Electricity (1964).*

[2]   *E. T. Whittaker, History of Theories of Aether and Electricity (1954, repr. 1987).*

[3]   *M. Kaufman and J. A. Wilson, Basic Electricity (1973).*

[4]   *W. T. Scott, The Physics of Electricity and Magnetism (2d ed. 1966).*

[5]   S. Roundy, P. K. Wright, and J. Rabaey, "A study of low level vibrations as a power source for wireless sensor nodes," *Computer Communications*, 26 (11), pp. 1131-1144, 2002.

[6]   Mercury-Containing and Rechargeable Battery Management Act, 42 U.S.C. § 14301 (1996)

[7]   J. M. Kahn, R. H. Katz, and K. S. J. Pister, "Emerging challenges: Mobile networking for "Smart Dust"," *Journal of Communications and Networks*, 2 (3), pp. 188-196, 2000.

[8]   "http://www.dust-inc.com."

[9]   S. Roundy, P. K. Wright, and J. M. Rabaey, *Energy Scavenging for Wireless Sensor Networks*

with Special Focus on Vibrations: Kluwer Academic Publishers, 2003.

[10]   S. Roundy, E. Leland, J. Baker, E. Carleton, E. Reilly, E. Lai, B. Otis, J. Rabaey, P. Wright, and V. Sundararajan, "Improving power output for vibration-based energy scavengers," *Pervasive Computing, IEEE*, 4 (1), pp. 28-36, 2005.

[11]   R. Amirtharajah and A. P. Chandrakasan, "Self-powered signal processing using vibration-based power generation," *Ieee Journal of Solid-State Circuits*, 33 (5), pp. 687-695, 1998.

[12]   C. B. Williams, C. Shearwood, M. A. Harradine, P. H. Mellor, T. S. Birch, and R. B. Yates, "Development of an electromagnetic micro-generator," *Iee Proceedings-Circuits Devices and Systems*, 148 (6), pp. 337-342, 2001.

[13]   P. D. Mitcheson, T. C. Green, E. M. Yeatman, and A. S. Holmes, "Architectures for vibration-driven micropower generators," *Journal of Microelectromechanical Systems*, 13 (3), pp. 429-440, 2004.

[14]   C. B. Williams and R. B. Yates, "Analysis of a micro-electric generator for microsystems," *Sensors and Actuators a-Physical*, 52 (1-3), pp. 8-11, 1996.

[15] S. P. Beeby, M. J. Tudor, E. Koukharenko, N. M. White, T. O'Donnell, C. Saha, S. Kulkarni, and S. Roy, "Micromachined Silicon Generator for Harvesting Power from Vibrations," presented at The Fourth International Workshop on Micro and Nanotechnology for Power Generation and Energy Conversion Applications, Kyoto, Japan, 2004.

[16] P. Limited, "PMG0100 Evaluation Model," P. Limited, Ed. Southampton, UK, 2005.

[17] P. Limited, "Power output vs acceleration in g at 100 Hz," P. Limited, Ed. Southampton, UK, 2005.

[18] N. Shenck and J. Paradiso, "Energy scavenging with shoe-mounted piezoelectrics," *IEEE Micro*, 21 (3), pp. 30-42, 2001.

[19] P. Glynne-Jones, S. P. Beeby, and N. M. White, "Towards a piezoelectric vibration-powered microgenerator," *Iee Proceedings-Science Measurement and Technology*, 148 (2), pp. 68-72, 2001.

[20] M. Ichiki, K. Ashida, and T. Kitahara, "Characterization of piezoelectric lead zirconate titanate from the viewpoint of transducer and power generator properties," *Japanese Journal of Applied Physics Part 1-Regular Papers Short Notes & Review Papers*, 41 (11B), pp. 7080-7083, 2002.

[21] M. Ichiki, K. Ashida, T. Kitahara, and M. Tanaka, "Piezoelectric transducer properties and its application to the micro power generator," *Ferroelectrics*, 273 2615-2620, 2002.

[22] F. Lu, H. P. Lee, and S. P. Lim, "Modeling and analysis of micro piezoelectric power generators for micro-electromechanical-systems applications," *Smart Materials & Structures*, 13 (1), pp. 57-63, 2004.

[23] E. Reilly, E. Carleton, S. Roundy, and P. Wright, "Vibrational energy scavenging via thin film piezoelectric ceramics," *Advanced Materials for Energy Conversion II Symposium. TMS.*, 2004.

[24] H. A. Sodano, G. Park, and D. J. Inman, "Estimation of electric charge output for piezoelectric energy harvesting," *Strain*, 40 (2), pp. 49-58, 2004.

[25] Z. Xia, S. Ma, X. Qiu, Y. Wu, and F. Wang, "The measurement of piezoelectric coefficient for PP cellular electret and the improvement of its piezoelectricity," in *Journal of Electrostatics*: Elsevier B.V., 2003, pp. 57–69.

[26] J. Hillenbrand, "High-sensitivity piezoelectric microphones based on stacked cellular polymer films," 3267, 2004.

[27] A. Mellinger, F. C. Gonzalez, and R. Gerhard-Multhaupt, "Ultraviolet-induced discharge currents and reduction of the piezoelectric coefficient in cellular polypropylene films," *Applied Physics Letters*, 82 (2), pp. 254-256, 2003.

[28] A. Mellinger, F. C. Gonzalez, and R. Gerhard-Multhaupt, "Photostimulated discharge in electret polymers: an alternative approach for investigating deep

traps," *Ieee Transactions on Dielectrics and Electrical Insulation*, 11 (2), pp. 218-226, 2004.

[29]   A. Mellinger, M. Wegener, W. Wirges, and R. Gerhard-Multhaupt, "Thermally stable dynamic piezoelectricity in sandwich films of porous and nonporous amorphous fluoropolymer," *Applied Physics Letters*, 79 (12), pp. 1852-1854, 2001.

[30]   S. Boland. "Sol-Gel Synthesis of Highly Oriented Lead Barium Titanate and Lanthanum Nickelate Thin Films for High Strain Sensor and Actuator Applications." Ph.D., California Institute of Technology, 2005.

[31]   S. Roundy, B. P. Otis, Y.-H. Chee, J. M. Rabaey, and P. Wright, "A 1.9GHz RF Transmit Beacon using Environmentally Scavenged Energy," presented at ISPLED 2003, Seoul, Korea, 2003.

[32]   S. Priya, C.-T. Chen, D. Fye, and J. Zahnd, "piezoelectric windmill: a novel solution to remote sensing," *japanese journal of applied physics*, 44 (3), pp. L104-L107, 2004.

[33]   P. D. Mitcheson, P. Miao, B. H. Stark, E. M. Yeatman, A. S. Holmes, and T. C. Green, "MEMS electrostatic micropower generator for low frequency operation," *Sensors and Actuators A:Physical*, 115 (2-3), pp. 523-529, 2004.

[34]   S. Roundy and P. K. Wright, "Micro-electrostatic vibration-to-electricity converters," presented at ASME International Mechanical Engineering Congress & Exposition, New Orleans, Louisiana, 2002.

[35]   R. S. Muller and R. T. Howe, "Technologies for microdynamic devices," *Nanotechnology*, 1 8, 1990.

[36]   K. Y. Park, C. W. Lee, H. S. Jang, Y. Oh, and B. Ha, "Capacitive type surface-micromachined silicon accelerometer with stiffness tuning capability," *Sensors and Actuators a-Physical*, 73 (1-2), pp. 109-116, 1999.

[37]   B. Q. Li, D. R. Lu, and W. Y. Wang, "Micromachined accelerometer with area-changed capacitance," *Mechatronics*, 11 (7), pp. 811-819, 2001.

[38]   W. Hsieh. "MEMS Thin Film Teflon Electret Condenser Microphones." Ph.D Dissertation, California Institute of Technology, 2001.

[39]   R. Gerhard-Multhaupt, B. Gross, and G. M. Sessler, "Recent Progress in Electret Research," *Topics in Applied Physics*, 33 383-431, 1987.

[40]   V. I. Arkhipov, A. I. Rudenko, and G. M. Sessler, "Space-Charge Distribution in Electron-Beam Charged Dielectrics," *JOURNAL OF PHYSICS D-APPLIED PHYSICS*, 24 (5), pp. 731-737, 1991.

[41]   G. F. L. Ferreira and M. T. Figueiredo, "Corona Charging of Electrets - Models and Results," *Ieee Transactions on Electrical Insulation*, 27 (4), pp. 719-738, 1992.

[42]   T. Y. Hsu. "A Novel Electron Beam Source Based on the Back-Lighted Thyratron." 1992.

[43]   K. Frank, E. Dewald, C. Bickes, U. Ernst, M. Iberler, J. Meier, U. Prucker, A. Rainer, M. Schlaug, J. Schwab, J. Urban, W. Weisser, and D. H. H. Hoffmann, "Scientific and technological progress of pseudospark devices," *IEEE TRANSACTIONS ON PLASMA SCIENCE*, 27 (4), pp. 1008-1020, 1999.

[44]   J. A. Malecki, "Linear decay of charge in electrets," *Physical Review B*, 59 (15), pp. 9954-9960, 1999.

[45]   M. G. Broadhurst, G. T. Davis, R. Gerhard-Multhaupt, B. Gross, S. Mascarenhas, G. M. Sessler, J. van Turnhout, and J. E. West, "Electrets," vol. 1, G. M. Sessler, Ed., 3 ed. Morgan Hill, California: Laplacian Press, 1998, pp. 453.

[46]   D. A. Berkley, "Computer simulation of charge dynamics in electron-irradiated polymer foils," *JOURNAL OF APPLIED PHYSICS*, 50 (5), pp. 3447-3453, 1979.

[47]   A. Palov, H. Fujii, and S. Hiro, "Theoretical investigation of charge-up dynamics in Teflon film induced by electron beam," *Japanese Journal of Applied Physics Part 1-Regular Papers Short Notes & Review Papers*, 38 (12A), pp. 6777-6781, 1999.

[48]   A. Palov, H. Fujii, and S. Hiro, "Monte Carlo simulation of 1 eV-35 keV electron scattering in teflon," *Japanese Journal of Applied Physics Part 1-Regular Papers Short Notes & Review Papers*, 37 (11), pp. 6170-6176, 1998.

[49]   S. Hiro, H. Fujii, and A. Palov, "Theoretical investigation of total secondary electron yield for Teflon," *Japanese Journal of Applied Physics Part 1-Regular Papers Short Notes & Review Papers*, 37 (7), pp. 4162-4163, 1998.

[50]   A. Mellinger, R. Singh, M. Wegener, W. Wirges, R. Gerhard-Multhaupt, and S. B. Lang, "Three-dimensional mapping of polarization profiles with thermal pulses," *Applied Physics Letters*, 86 (8), pp. -, 2005.

[51]   J. S. Boland and Y. C. Tai, "Method and resulting device for fabricating electret materials on bulk substrates," Y. C. Tai, Ed., 2003 (filed).

[52]   O. D. Jefimenko and D. K. Walker, "Electrostatic Current Generator Having a Disk Electret as an Active Element," *Ieee Transactions on Industry Applications*, 14 (6), pp. 537-540, 1978.

[53]   Y. Tada, "Theoretical Characteristics of Generalized Electret Generator, Using Polymer Film Electrets," *Ieee Transactions on Electrical Insulation*, 21 (3), pp. 457-464, 1986.

[54]   V. G. Nazarov, *Elektrichestvo*, 7 (60), pp., 1954.

[55]   Y. Tada, "Experimental Characteristics of Electret Generator, Using Polymer Film Electrets," *Japanese Journal of Applied Physics Part 1-Regular Papers Short Notes & Review Papers*, 31 (3), pp. 846-851, 1992.

[56]   Y. Arakawa, Y. Suzuki, and N. Kasagi, "Micro Seismic Power Generator Using Electret Polymer Film," presented at The Fourth International Workshop on Micro and Nanotechnology for Power Generation and Energy Conversion Applications, Kyoto, Japan, 2004.

[57]   Boyce and D. Prima, *Differential Equations*.

[58]   W. H. Hsieh, T.-J. Yao, and Y.-C. Tai, "A High Performance MEMS Thin-Film Teflon Electret Microphone," presented at The 10th International Conference on Solid-State Sensors and Actuators, Sendai, Japan, 1999.

[59]   W. Hsieh, T. Hsu, and Y. Tai, "A Micromachined Thin-Film Teflon Electret Microphone," presented at TRANSDUCERS '97, Solid-State Sensors and Actuators, Chicago; IL, 1997 Jun.

[60]   Y. Tada, "Improvement of Conventional Electret Motors," *Ieee Transactions on Electrical Insulation*, 28 (3), pp. 402-410, 1993.

[61]   J. Boland and Y. C. Tai, "Liquid-rotor electret micropower generator," presented at the Solid State Sensor and Actuator Workshop, Hilton Head Island, South Carolina, 2004.

[62]   H. Moon, S. Cho, R. Garrell, and C. Kim, "Low voltage electrowetting-on-dielectric," *JOURNAL OF APPLIED PHYSICS*, 92 (7), pp. 4080-4087, 2002.

[63]   D. J. Griffiths, *Introduction to Electrodynamics*, Second ed. Upper Saddle River: Prentice Hall, 1989.

[64]   J. S. Boland, J. D. M. Messenger, and Y.-C. Tai, "Alternative Designs of Liquid Rotor Electret Power Generator Systems," presented at The Fourth International Workshop on Micro and Nanotechnology for Power Generation and Energy Conversion Applications, Kyoto, Japan, 2004.

[65]   L. S. Tavrow, S. F. Bart, and J. H. Lang, "Operational characteristics of microfabricated electric motors," presented at Int. Conf. on Solid-State Sensors and Actuators, San Francisco, CA, 1991.

[66]   R. Feynman, "Infinitesimal Machines," *J. MEMS*, 2 (1), pp. 4-14, 1993.

[67]   D. Duggirala, H. Li, A. M. Pappu, Z. Fu, A. Apsel, and A. Lal, "Radioisotope micropower generator for CMOS self-powered sensor systems," presented at the Fourth International Workshop on Micro and Nanotechnology for Power Generation and Energy Conversion Applications, Kyoto, Japan, 2004.